Modelling and Analysis of Fault Ride Through Techniques in a Power Network with Type 4 Wind Generation

A Thesis submitted to the Faculty of Graduate Studies of
The University of Manitoba
in partial fulfillment of the requirements of the degree of

Master of Science

by

Pravakar Soumya Shilpi

UNIVERSITY
OF MANITOBA

**DEPARTMENT OF ELECTRICAL AND COMPUTER
ENGINEERING**

**UNIVERSITY OF MANITOBA
WINNIPEG, MANITOBA**

ACKNOWLEDGEMENTS

ABSTRACT

The increasing penetration of renewable energy sources, particularly wind power, necessitates the development of efficient control strategies and system stability improvements. This thesis presents a comprehensive investigation into the modelling and analyzing the fault ride-through techniques in Type 4 wind generators. The Type 4 wind generator, which incorporates a permanent magnet synchronous generator (PMSG), has emerged as a promising solution for renewable energy generation. The objective is to investigate the transient behaviour of the wind generator and develop strategies to incorporate its fault ride-through capabilities. Various control strategies are examined, including maximum power point tracking, dc chopper control, and active and reactive power control. Electromagnetic simulations (EMT) simulation studies and validations will be conducted to evaluate the performance of these control strategies under different operating conditions. Today, renewable energy systems, including wind generators, are expected to meet the same reliability standards as traditional power systems. IEEE Standard 1547-2018 suggests that the wind generator must maintain its connection to the grid during minor faults or disturbances within the specified voltage limits. The Type 4 wind generator consists of a fully controlled back-to-back configuration-based voltage source converter; the abilities of the converter can be used to detect the severity of the disturbance and react accordingly. This thesis implements the low and high-voltage ride-through and the frequency ride-through capabilities of the Type 4 wind generator as per the IEEE Std 1547-2018. Lastly, the thesis presents a novel approach that utilizes a dc chopper-based active power modulation technique. The effectiveness of this technique in damping power system oscillations and reducing the rise in frequency variations during some contingencies is investigated in a power network with Type 4 wind generators.

Keywords: Type 4 wind generators, dc chopper, MPPT, Fault ride-through capabilities, LVRT, FRT, Active Power Modulation, Frequency stability

Acronyms

PMSG   Permanent Magnet Synchronous Generator

EMT   Electromagnetic Transients

IEEE   Institute of Electrical and Electronics Engineers

dc   Direct Current

MPPT   Maximum Power Point Tracking

LVRT   Low - Voltage Ride Through

HVRT   High- Voltage Ride Through

FRT   Frequency Ride Through

IEA   International Energy Agency

VSC   Voltage Source Converter

BTB   Back to Back

ac   Alternating Current

MMC   modular multilevel converters

IGBT   Insulated Gate Bipolar Transistor

TSR   Tip Speed Ratio

GBR   Gear Box Ratio

P   Active Power

Q   Reactive Power

SPWM   Sinusoidal Pulse Width Modulation

RPM   Rotation per minute

PSF   Power Signal Feedback Control

HCS   Hill-Climb Search Control

GSC   Grid Side Converter

MSC   Machine Side Converter

DCC   Decoupled Current Controller

PLL   Phase Locked Loop

VCO   Voltage Controlled Oscillator

EPS   Electric Power System

DER   Distributed Energy Resource

PCC   Point of Common Coupling

SCR   Short Circuit Ratio

Contents

List of Figures

List of Tables

Chapter 1

Introduction

1.1 Background

Renewable energy sources (RES), such as wind, solar, hydro, tidal, wave, and biomass, have significantly contributed to conventional power systems in recent decades. This shift towards renewable energy is driven by various factors, including the need to reduce carbon emissions, combat global warming, address environmental concerns, and mitigate the depletion of fossil fuel resources. One notable example is wind energy conversion systems, which have become increasingly prevalent in many regions. According to the International Energy Agency (IEA), the proportion of renewable energy sources in the global power generation mix is projected to increase from 29% to 35% by 2025. The majority, exceeding 70%, of this growth is anticipated to be contributed by China, Southeast Asia, and India [2]. This chapter provides an overview of wind generator technology types and the need for grid codes.

1.2 Types of Wind Energy Conversion System

Over the years, wind energy has manifested in various applications, such as propelling sailboats to electrical and mechanical usage like mining salts, pumping water, and grinding flour. In 1887, a wind generator produced the first electric generation in Scotland [3]. wind generator design's electrical and mechanical aspects have developed over the years, providing solutions for reducing carbon footprints and meeting increasing demand and supply. wind generators can be classified based on various factors. The first category is based on blade orientation, where the wind generators

can be categorized into horizontal and vertical-axis. Horizontal-axis wind generators are more suited to areas with strong winds. In contrast, vertical-axis wind generators can better accommodate the intermittent nature of wind. Other factors, such as geographic location (onshore wind generators/offshore wind generators) and wind speed, can also influence the design of the tower structure and thus impact the wind power output.[4]
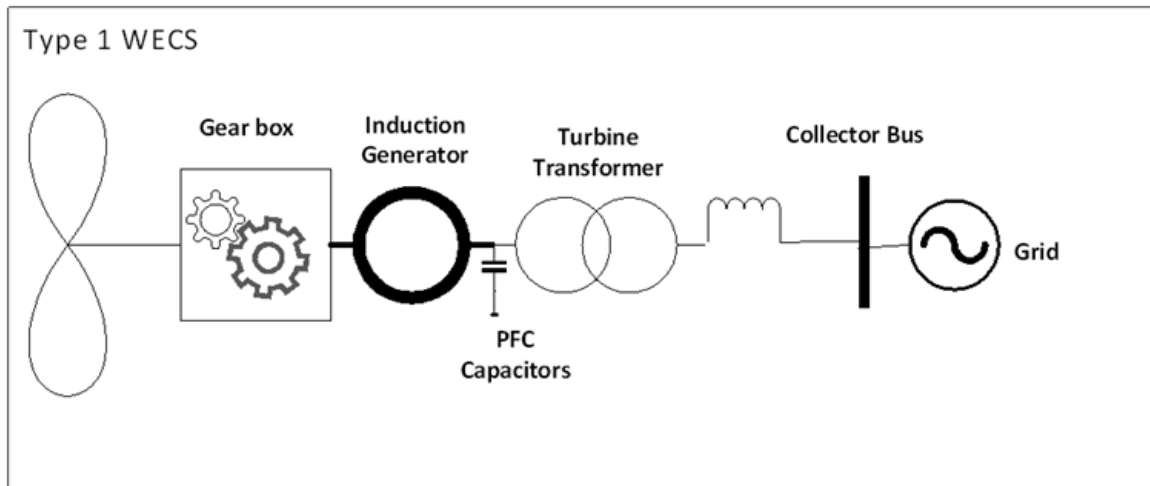
Figure 1.1: Type 1 Wind Energy Conversion System

Wind generators have undergone significant developments in generation, control, operation, and connection to the grid. Wind energy conversion systems are classified as fixed or variable-speed wind generators based on the turbine's rotational speed. Fixed-speed wind generators have a simple and reliable structure with mechanical controllers such as pitch control and no power electronics converter control [4] [5]. Examples of fixed-speed wind generators include the Type 1 wind generator, which is essentially a Squirrel-cage Induction Generator (as shown in Figure 1.1), and Type 2 wind generators, which use a wound rotor induction generator with the addition of a variable resistor in the stator circuit (as shown in Figure 1.2). The electrical grid frequency determines the turbine's rotational speed in both types. It should be noted that the induction generator consistently consumes reactive power from the grid to establish air gap magnetic flux. To address this, switched capacitor banks are commonly used for reactive compensation. Fixed-speed wind generators utilize mechanical controls like pitch control and mechanical brakes to manage power generation and adapt to external disruptions. However, fixed-speed wind generators are

directly connected to the grid, leading to limited control of active and reactive power flows and ac-voltage, high starting current, and low-voltage ride-through capabilities.
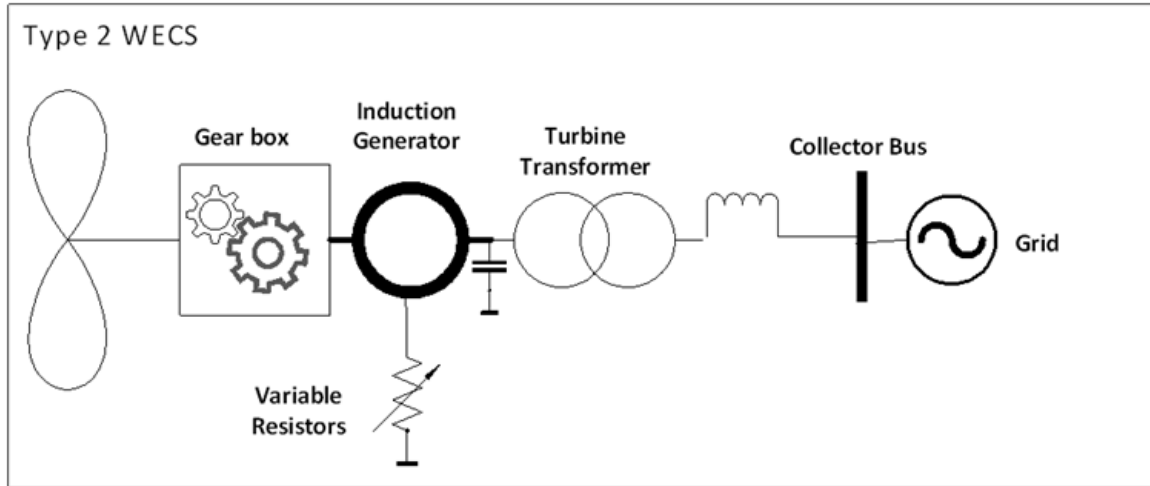
Figure 1.2: Type 2 Wind Energy Conversion System
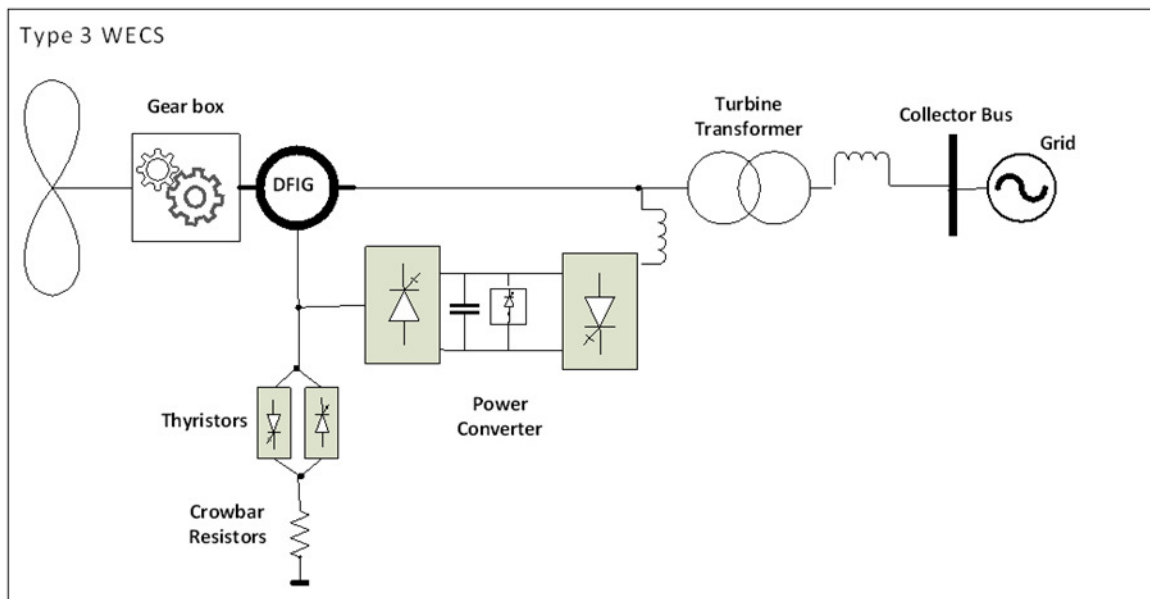
Figure 1.3: Type 3 Wind Energy Conversion System

Variable speed wind generators are efficient, reliable and have partially/fully controlled active and reactive power capabilities. The double-fed induction generator-based wind generator (Type 3 wind generator) is shown in Figure 1.3, and the permanent magnet synchronous generator (PMSG) based wind generator (Type 4 wind generator Figure 1.4) comes under this category [6] [7].

The control of the rotor circuit in the Type 3 wind generator and back-to-back (BTB) converter in PMSG is based on a power electronics converter. Type 3 wind generator uses a converter rated at 30% of the generation rating of the turbine, whereas PMSG-based wind generator uses 100% rated power converters. As a result, both types of wind generators can provide reactive power support during turbulence [8], thus maintaining the voltage. The converter also helps maintain the synchronization between the generator and grid when there is a change in wind generator speed by controlling the rotor voltages and currents in Type 3 wind generators and providing isolation via BTB converter in Type 4 wind generators.
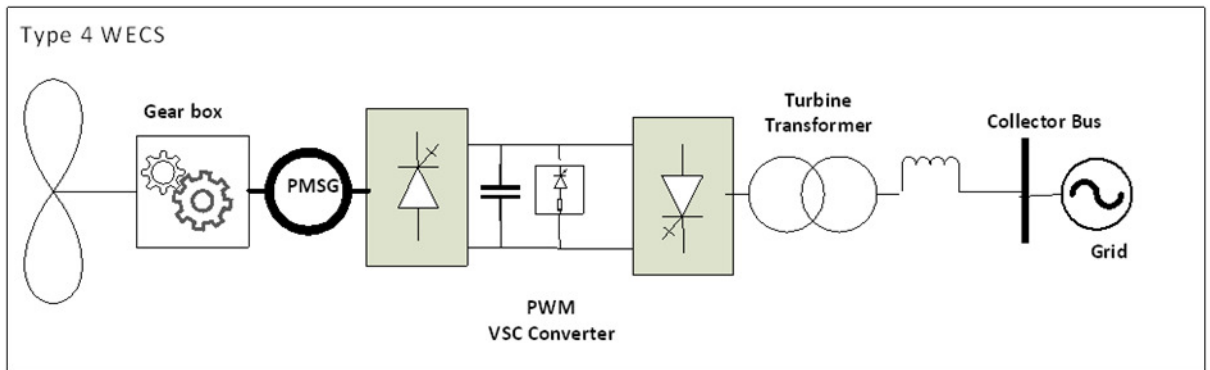
Figure 1.4: Type 4 Wind Energy Conversion System

The converter types (Grid following or Grid forming), turbine topology, control characteristics, reactive power assistance and voltage ride-through capabilities via power electronics converter have proved to be the basis of future trends. In a Type 4 wind generator, the generator is connected via a back-to-back converter to the grid, leading to machine isolation during contingencies and, thus, less mechanical stress on the rotor. To aid wind generators' operation, maintenance, and integration into the grid due to the high penetration of renewable sources, control structures like mechanical control such as pitch control, active power and reactive power control, maximum power point techniques, and dc chopper are implemented [9] [10]. The variable-speed wind generator does not need an external reactive power compensation device. In this thesis, a PMSG-based wind generator (Type 4 wind generator), one of the variable speed wind generators, is used to study the application of IEEE Std 1547-2018 for fault ride-through.

4

1.3 Grid Codes

Converter-interfaced generation significantly impacts power system generation. The increasing penetration of RES equipped with power electronics converters has led to tremendous research on integrated systems stability, control, and dynamics. Handling system frequency and voltage has become critical, and IEEE Std 1547-2018 provides a uniform standard. Grid codes are the rules manufacturers and system operators follow at various levels to maintain smooth operating conditions. They are constantly revised and updated based on changes in technology. Individual grid codes are specific to each utility and may modify the settings within the guidelines listed in the Standard.

In the past, renewable energy generation was considered an auxiliary supplement to traditional power systems. Traditional systems heavily relied on generators, speed governors, and voltage regulators to manage dynamics and active and reactive power. As a result, when contingencies arose, renewable energy systems were promptly disconnected from the grid. However, the increasing electricity demand, the need to reduce carbon footprint, and growing environmental concerns have led to greater integration of renewable energy systems into the existing power grid. The performance standards of renewable energy systems, such as wind generators, are now expected to be as reliable as those of the existing electric power system. The IEEE Std 1547-2018 helps to provide suggestions for requirements and performance criteria for power generation systems, which include the acceptable range of grid frequency or voltage deviations, the duration for which the system should remain connected during faults, etc.

IEEE Std 1547-2018 [1] is the recommended IEEE standard that utilities can use to design specific grid codes. According to IEEE Std 1547-2018, the wind generators must remain connected to the grid during minor faults or disturbances, such as voltage reductions that fall within limits specified by the standard. This is known as low voltage ride-through (LVRT), allowing for faster recovery after the disturbance has passed. However, the wind generator is disconnected when there are severe contingencies, such as a total voltage collapse, to prevent damage to the turbine or the grid. The turbine control system must detect the disturbance's severity and respond appropriately by remaining connected or disconnecting from the grid. Similarly, some events, such as short circuits, sudden load changes, or the disconnection of large power plants from the grid, can cause disturbances in the system's grid frequency. The grid

frequency may deviate from its normal operating range. The wind generators are connected to the grid through power electronic converters, which can be sensitive to frequency changes. So, the frequency ride-through capabilities include control mechanisms that allow wind generators to adjust their output power to ride through the frequency disturbances. Therefore, the ride-through operation of renewable energy systems is mandatory during abnormal conditions because it ensures frequency and voltage maintenance and continuous energy flow. In this thesis, the assumed grid code directly implements the IEEE Std 1547-2018 [1] with default values for settings for implementing fault ride-through capabilities in wind energy conversion systems.

1.4   Thesis Objectives

The main objective of this thesis is:

- Developing and studying the modelling of Voltage source converter and converter control operation on an electromagnetic transient (EMT) program. PSCAD was chosen as the EMT program.

- Implementation of Type 4 Wind Energy Conversation system in PSCAD: Studying the controller behaviour and fault behaviour of Type 4 wind generator. Modelling and studying different components of the turbine.

- Assessing the fault ride through performance and chopper operation in different SCR conditions, the advantage of LVRT mechanism in the weak grid.

- Implementing a frequency ride through a mechanism based on IEEE 1547 grid code in a Type 4 wind generator and studying advantages of wind generator active power modulation during grid frequency change on grid frequency stability.

- Designing and implementing a special damping controller in the DC chopper controller in a Type 4 wind generator for fast active power reduction to reduce the change in frequency and damps the frequency oscillations.

1.5   Thesis Organization

After the introduction in Chapter 1, Chapter 2 briefly describes wind aerodynamics in designing wind generators in electromagnetic simulations. It also explains the different control mechanisms in a Voltage source converter (VSC) based back-to-back converter, including active/reactive power control, dc-link voltage control, decoupled control, etc. It also explains the dc link chopper controller and maximum power point technique (MPPT) and its advantages.

Chapter 3 studies the Type 4 wind generator transient behaviour and fault behaviour using the PSCAD test case. Converter control of the machine side converter and grid side converter is observed. Simulations are carried out to confirm the results of the existing literature. The impact of additional features like Tip speed ratio (MPPT technique) and DC chopper in parallel to the dc link are also observed.

Chapter 4 outlines the voltage ride-through (VRT) and frequency ride-through(FRT) techniques. The fault ride-through techniques are implemented as dictated in IEEE Std 1547-2018 [1] .

Chapter 5 briefly explains the need for frequency stability in a power system and studies the impact of the dc chopper with a damping controller on fast frequency recovery. Case studies are provided to verify the results of this method, followed by Chapter 6, which presents a summary of the conclusions and suggestions for future works.

Chapter 2

Analysis and Control of Type 4 PMSG based wind generator

This chapter overviews the basic mechanical and electrical subsystems and the control mechanism of a permanent magnet synchronous generator (PMSG) based wind generator, also known as a Type 4 wind generator. This system is a popular full-scale converter-based wind energy system. The focus of this thesis is on the PMSG-based wind generator. The PMSG-based wind generator includes a wind generator, which converts the kinetic energy of wind into mechanical energy, and a PMSG, which converts the mechanical energy into electrical energy. The PMSG is connected to a full-scale power converter (i.e., with the total rating of the PMSG), which controls the flow of electrical energy between the PMSG and the electrical grid. The power converter can be operated in a grid-connected mode, which feeds the electrical energy generated by the PMSG into the grid, or in a standalone mode, where it supplies power to a local load.

The control mechanism of the PMSG-based wind generator involves two main control loops: the active power control loop and the reactive power control loop. The active power control loop regulates the electrical power output of the wind generator, which is influenced by wind speed and other environmental factors. This thesis implements a speed controller which regulates the active power flow of the wind generator. The speed control loop is responsible for maintaining a constant rotor speed of the wind generator, which is necessary to ensure that the generator produces the desired electrical power output. The reactive power control loop helps to maintain the respective ac voltage at ac side of the converter.

In summary, this chapter provides a basic understanding of the mechanical and electrical subsystems and the control mechanism of a PMSG-based wind generator. This information is helpful for further investigation into the performance and implementation of fault ride-through capability in wind generation systems.

2.1 Introduction

Full-scale converter-based wind energy conversion systems utilize various ac generator types, such as permanent magnet synchronous generators, self-excited induction generators, and synchronous generators for wind energy conversion. The primary feature of fully scaled wind generators is a full-rated back-to-back converter connecting the generator and the grid [11] [12]. The back-to-back converter configuration is an ac/dc/ac converter system that comprises a machine-side converter, a dc link, and a grid-side converter. The machine-side converter rectifies the output from PMSG and inverts it back to the grid-side converter while receiving dc support from the capacitor. Complete control over the back-to-back converters assists in achieving flexible connections with the grid and enhancing fault ride-through ability during contingencies[13][14]. The presence of a dc link capacitor in a full-scale power converter aids in decoupling the grid, providing better operation of the PMSG-based wind generator(Type 4) [15] [16].

Type 4 wind generator systems are becoming very popular due to their ease of control and more reliable operation. Synchronous generators used in Type 4 are of the permanent magnet type, so the field winding typically present in generators is absent. As a result, the generator's volume and mass are also reduced. The absence of exciting winding and slip rings on the rotor leads to higher efficiency and more straightforward control (i.e. no exciter control). It ensures safer and more reliable operation than the generator with a field winding. Type 4 wind generators can have fault ride-through capabilities and provide improved reactive power contribution [17].

An electromagnetic transient (EMT) simulation model is developed on the PSCAD program to demonstrate the Type 4 wind generator operation. The Type 4 wind generator's typical structure includes a PMSG-based turbine model with a gearbox and a back-to-back converter with a machine-side converter, grid-side converter, and dc link in between, as shown in Figure 2.1. More advanced topologies, i.e. modular multilevel converters (MMC), are possible. This thesis uses the typical two-level voltage

source converter often used for low-voltage applications such as ac grids connected to a PMSG. The voltage source converter can be based on Insulated Gate Bipolar Transistor (IGBT) or Gate Turn-Off Thyristor (GTO). The stability of a grid-connected wind power plant based on a Type 4 wind generator is analyzed against a test wind generator example.
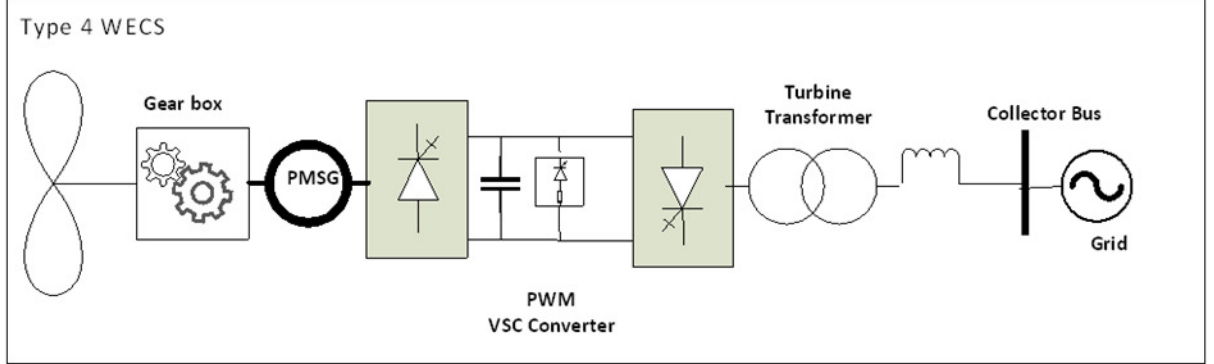
Figure 2.1: Example of a typical Fully controlled Wind Energy Conversion System

2.2 Understanding the Mechanical Aspects of Wind Energy Generation

Wind energy is one of the renewable sources, with a global power capacity of over 743 GW as of 2022, and has reduced 1.1 billion tons of carbon emissions. However, wind energy is variable and intermittent, and its availability depends on various factors such as time, height, weather conditions, and temperature. A wind generator consists of blades hinged to a rotor hub, a nacelle frame containing the gearbox connecting low and high-speed shafts, a yaw control system, a rotor mechanical brake, a generator, and a power electronics converter system for connecting to the grid. The turbine blades capture the kinetic energy of the wind and transfer this energy into the rotary motion of the generator via a shaft [18] [19]. The generator converts this mechanical energy into electrical energy. The wind energy availability E_{wind} can be expressed as Equation 2.1

$$E_{wind} = \frac{1}{2}mV_w{}^2 \tag{2.1}$$

where m is the air mass flowing at wind speed V_w.

The wind energy with the air mass (m) flowing at wind speed V_w, air density ρ, and the area swept by the blades A over a specific period t leads to Equation 2.2.

$$E_{wind} = \frac{1}{2}\rho A t V_w{}^3 \tag{2.2}$$

The available power in the wind is calculated as

$$P_{wind} = \frac{E_{wind}}{t} \tag{2.3}$$

Based on the wind speed and area swept by the rotating turbine blades, the total available power is given as

$$P_{wind} = \frac{1}{2}\rho A V_w{}^3 \tag{2.4}$$

The power coefficient (C_p) is often regarded as the efficiency of the wind generator. This thesis uses Equation 2.5 [20] [21] for modelling the wind generator.

$$C_p = \frac{4}{9} - (\frac{\beta}{60}) * \sin(\frac{0.5 * \pi * 20(TSR - 3)}{150 - 3 * \beta}) - (2 * \frac{\beta}{1087} * (TSR - 3)) \tag{2.5}$$

$$P = \frac{1}{2}\rho A V_w{}^3 C_p(\beta, TSR) \tag{2.6}$$

Where TSR ($= \frac{r\omega}{V_w}$) is the tip speed ratio defined as the ratio of the rotor's speed at the tip of the blade and the wind speed, where r is the radius of the turbine and ω is the rotational speed of the turbine.

The theoretical maximum power (also known as the Betz limit) that the wind generator can extract is 59.3% as obtained in Equation 2.7 with $\rho = 1.225$ (kg/m^3) A = 7854 m^2), and so $C_p \leq 0.593$.

$$P_{max} = P_{Betz} = \frac{1}{2}\rho A V_w{}^3(0.593) \tag{2.7}$$

The power curve is characteristic of wind generators, showing the output power produced by wind generators at different wind speeds. Figure 2.2 shows the theoretical power curve where at the cut-in wind speed of (3 m/s), the active power begins rising and gets curtailed to zero at the cut-off speed of (12 m/s). No output power is produced below cut-in wind speed since the developed torque cannot cause effective blade rotation. Typically, the range for cut-in wind speed is between 2 m/s to 5 m/s,

which allows the turbine to overcome the static friction and losses and generate a minimum amount of power.

For speeds greater than the rated speed, constant power is maintained using aerodynamic control, like controlling the pitch angle of the turbine blades. The power curve depends on the geographical conditions, wind generator technology and structure. Cut-off wind speed value is assigned as per the mechanical design and material of the respective wind generator to avoid damages due to high-speed wind striking and creating turbulence as a protection scheme.
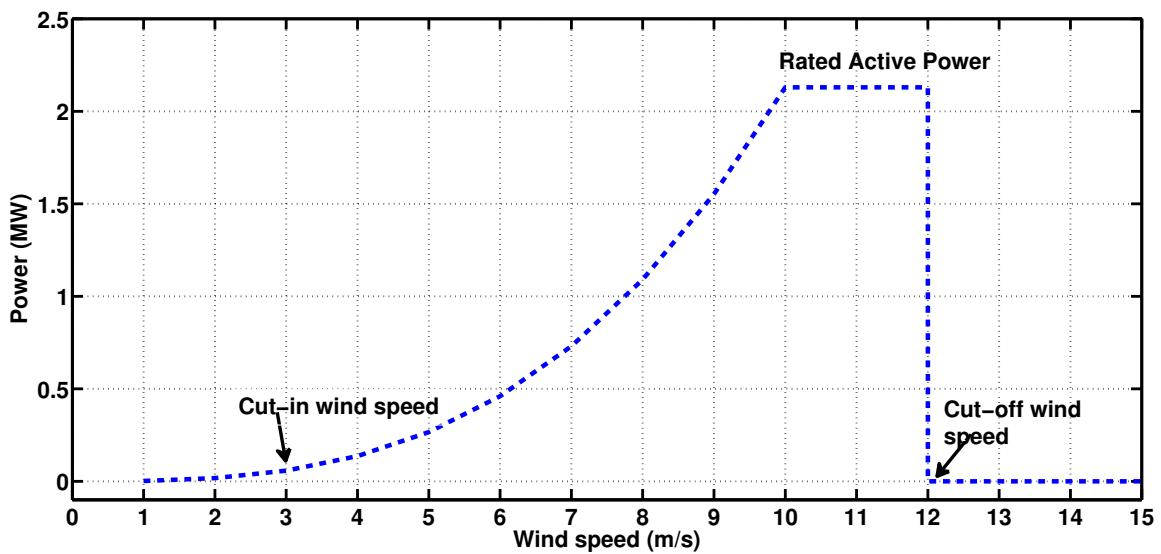
Figure 2.2: Theoretical Power Curve (Power vs Wind Speed)

2.3 Electrical Design and Operation of wind generators for Power Generation

The Type 4-PMSG-based wind generator used in the thesis employs a gearbox, a permanent magnet synchronous generator (PMSG), and a power controller system. The PMSG has permanent magnets in the rotor to create the excitation field. When the wind hits the wind generator blades with speed V_w, they start rotating and convert the mechanical energy in the wind into kinetic rotational energy of the PMSG rotor. The rotor poles then produce a rotating magnetic field at the same electrical speed

as the high-speed shaft, generating a voltage of electrical frequency of f, as shown in Equation 2.8.

$$Frequency(f) = \frac{P}{2}\frac{N}{60} \tag{2.8}$$

'P' represents the number of poles, 'N' is the mechanical speed (number of rotor revolutions per minute), and 'f' is the frequency of the generated ac voltage, whose value is typically 50 Hz or 60 Hz depending on the grid.

A gearbox helps to convert the low-speed shaft speed of the rotating turbine blades into the high-speed rotation required for generating the PMSG voltage frequency. Gearboxes require regular maintenance due to sudden load variations that can lead to wear and tear. The gearbox ratio (GBR) can be expressed numerically as:

$$GBR = \frac{Generator\ speed(rpm)}{Turbine\ speed(rpm)} \tag{2.9}$$

To run the Type 4 wind generator efficiently, the PMSG must be set to a particular rotational speed to provide maximum power at the respective wind speed. When the PMSG is connected directly to the ac grid, it tries to follow the frequency variation of the grid. However, a direct connection to the ac grid can hinder the goal of achieving maximum power transmission. One way to overcome this challenge is to interface the PMSG to the ac grid using an asynchronous back-to-back (BTB) voltage source converter. This connection allows the generator frequency to be different from the ac grid frequency, enabling the PMSG to operate at its optimal speed. The control system of BTB converters will be explained in detail in subsequent sections[22] [23].

2.4 Basic Operating Principles of VSC based Back-to-Back Converter and its Waveform Generation

The voltage source converter is connected in inverter mode to the 3-phase ac ideal source via a 3-phase transformer [24] [25] as shown in Figure 2.3. The dc side system is not shown, but there would be another converter as discussed in Section 2.5. Active power (P) flows from the converter to the ac network in inverter operation. A positive sign is assigned to 'P.' Equations 2.10 and 2.11 are the mathematical representation of the active and reactive power, respectively. The phase shift between the converter
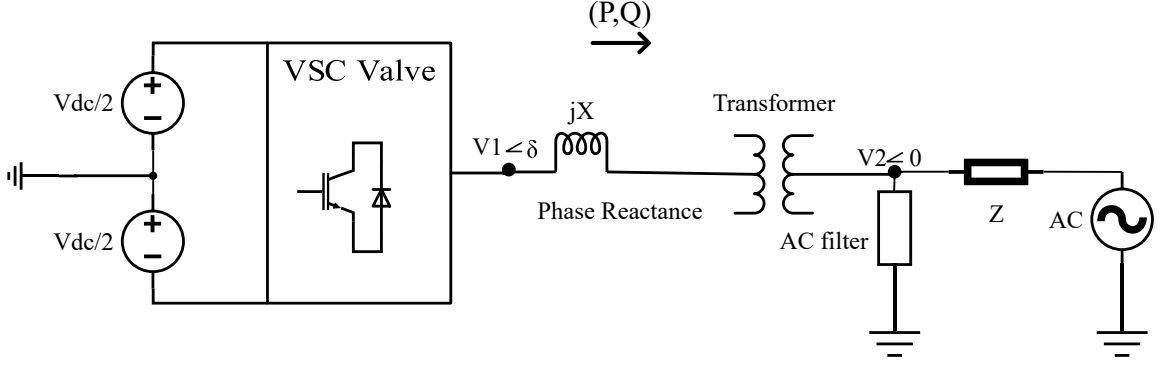
Figure 2.3: A typical configuration of VSC converter terminal

ac bus voltage (V_1) and the ac source fundamental voltages (V_2) of both sides of the transformer and the phase reactance is mainly responsible for active power flow. A positive reactive power (Q) means that the magnitude difference $|V_1| - |V_2|$ is positive, and the converter has a leading power factor. Similarly, $|V_1| - |V_2|$ is negative for a negative value of Q. The VSC's control system controls the magnitude and phase angle of converter output ac voltage (V_1). If the resistance of the transformer is ignored and taking into account the direction of power flow as in Figure 2.3, the 3-phase active power and reactive power (in pu) are expressed as :

$$P = \frac{V_1 . V_2}{X} . \sin(\delta) \tag{2.10}$$

$$Q = \frac{V_2^2}{X} - \frac{V_1 . V_2}{X} . \cos(\delta) \tag{2.11}$$

where: δ is the phase angle between the fundamental voltages of V_1 and V_2, V_1 fundamental voltage at the converter ac side, V_2 fundamental voltage at the source side and X is the combined inductance of the transformer and the phase reactor.

The sinusoidal pulse width modulation (SPWM) technique generates the converter's ac side voltage, assuming a two-level converter topology, as shown in Figure 2.4. This technique also helps in eliminating low-order harmonics in ac voltage forms.

Consider one phase arm (say phase 'a') of the three-phase converter in Figure 2.4. In SPWM, a high-frequency carrier signal (triangular waveform) is compared with the desired sinusoidal modulating signal. If the modulating signal is larger than the triangular wave, the output phase voltage Va(t) is switched to the positive dc bus voltage, and if it is smaller, it is switched to the negative dc bus, as shown in Figure

2.5. Depending on the triangular carrier signal's frequency, the converter output 'Va(t)' (square waveform) consists of high-frequency harmonics and the fundamental component. A high-pass filter is usually added downstream from the converter to reduce the harmonic content of the current entering the ac network. The modulation signals for phases (b) and (c) are 120 degrees and -120 degrees displaced in phase from that of phase (a), respectively, to produce a three-phase balanced waveform [26].
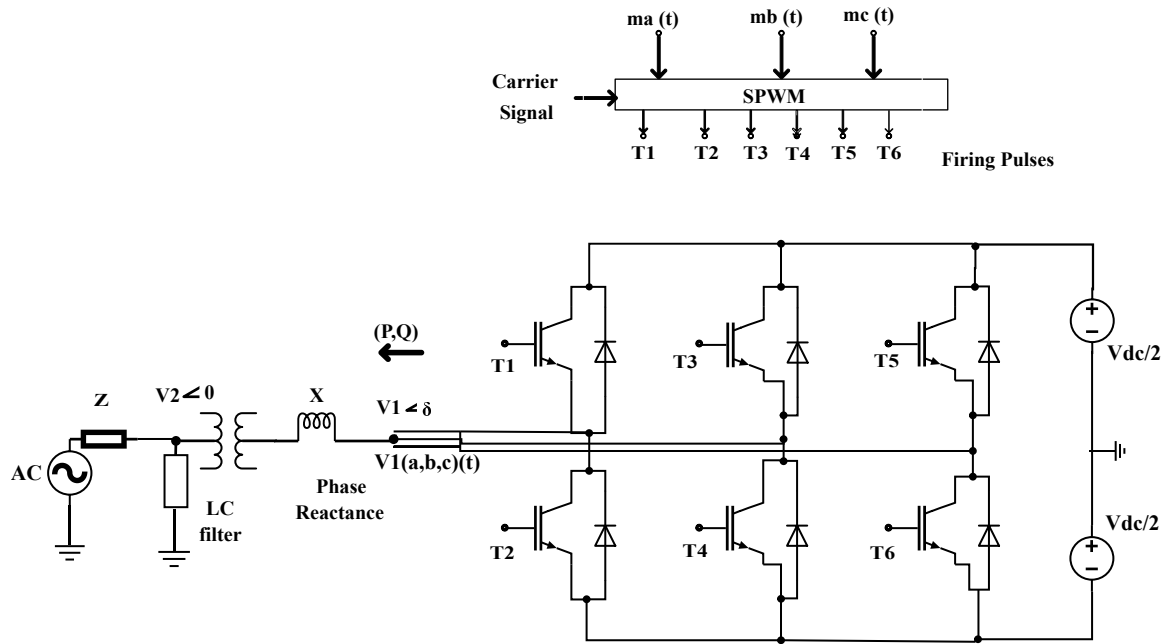
Figure 2.4: Two-level IGBT valve bridge
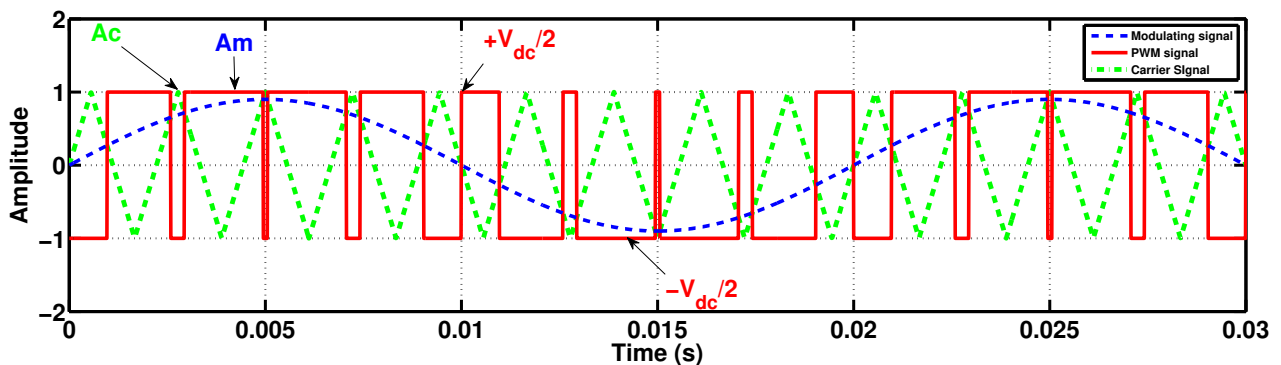
Figure 2.5: Bipolar SPWM wave forms

The converter is connected to the grid via a transformer. The transformer provides

15

electrical isolation between the dc and ac sides and matches the ac grid voltage to the converter's internal voltage. The modulation index ($m = \frac{A_m}{A_c}$) is the ratio of the peak magnitude of the sinusoidal modulating signal (A_m) and peak magnitude of the high-frequency triangular carrier signal (A_c). 'm' is kept between the linear modulation range of $[0, 1]$. The fundamental frequency component $V_1(t)$ of the converter output voltage is given by equation 2.12

$$V_1(t) = m\frac{V_{dc}}{2}\sin(\omega t + \delta) \tag{2.12}$$

where: 'δ' is the V_1 phase angle relative to ac voltage V_2, 'V_{dc}' is the dc voltage between the positive pole and the negative pole of the dc link, and 'ω' is the fundamental angular frequency.

The amplitude of the converter's output voltage and the corresponding reactive power can be controlled by adjusting the modulation index (m). Similarly, the active power output can be regulated by changing the phase angle of the modulating signal (δ). It is essential to maintain m at or below unity ($m \leq 1$) to ensure the proper functioning of SPWM. If m exceeds 1, the triangle wave will miss many crossings with the modulating signal, and the magnitude of the output signal will no longer be linearly proportional to m. Additionally, when the ac side is connected to an external ac source, it is crucial to ensure that the magnitude of the ac bus voltage, V_m, does not exceed the dc link voltage ($\frac{V_{dc}}{2}$), as this can result in uncontrolled conduction due to the diode connected in anti-parallel to the IGBT transistor turning on.

In Type 4 wind generators, a back-to-back VSC converter arrangement is commonly used, with one VSC acting as a rectifier to convert the variable frequency wind generator voltage to the dc bus voltage and the other acting as an inverter to convert the dc voltage to the ac grid at the nominal frequency. The three-phase two-level VSC bridge is the most straightforward switching configuration that produces an ac square waveform from a dc source. The phase reactor limits the short-circuit current and affects the active and reactive power flows into the network, as given by equations 2.10, 2.11 and 2.12.

2.5 Modelling and Simulation of Type 4 Wind Generators

This thesis develops models for Type 4 wind generators that provide fault ride-through capability based on IEEE Std 1547-2018 [1] during contingencies. Fault ride-through means that the wind generator can remain connected to the grid during faults that cause a drop in ac voltage above the disconnection threshold, allowing for a quicker recovery of the system than disconnection. However, during the fault period, specific control measures may need to be implemented to ensure a healthy resumption of power transfer [27] [28].

A Type 4 wind generator includes a generator connected to the ac grid through a back-to-back voltage source converter (VSC) arrangement via a dc link, as shown in Figure 2.6.
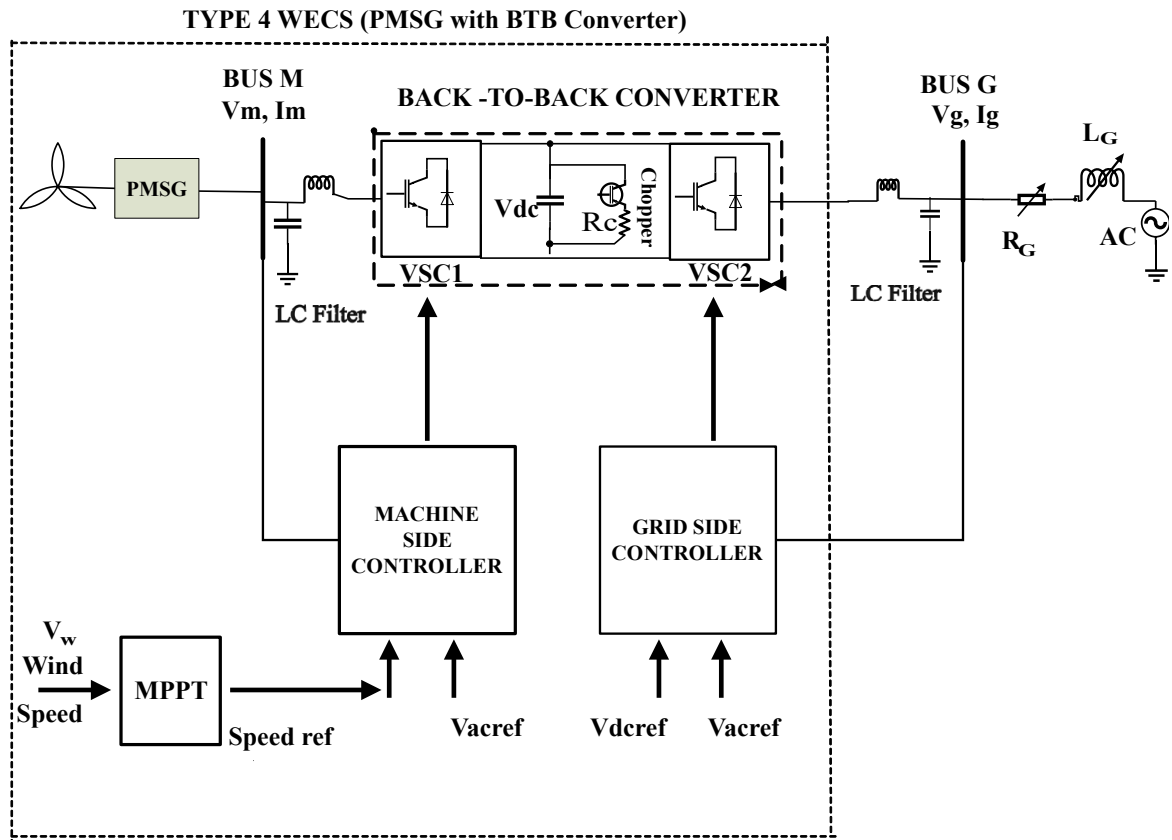
Figure 2.6: Modelling of Type 4 PMSG-based Wind Energy Conversion System

The permanent magnet synchronous generator (PSMG) produces a variable frequency voltage proportional to the windmill's rotation per minute (RPM). The machine side converter (VSC 1) is a rectifier to convert this variable frequency ac voltage into dc voltage. The grid side converter (VSC 2) acts as an inverter and injects power into the ac grid by converting dc voltage back to ac at the grid frequency. As wind energy is intermittent and variable, the maximum power that can be extracted from the windmill depends on wind speed, and there is an optimal wind generator speed for a given wind speed. The back-to-back power train permits the interconnection of two ac systems with different frequencies. The dc link capacitor between the rectifier and inverter is a temporary energy storage that manages active power differences and maintains an active power balance in normal conditions. The capacitor helps limit dc voltage variation and filters high-frequency dc link voltage harmonics. A dc chopper (i.e., discharging switch) is often connected across the capacitor as a protective device during faults on the ac grid, which can result in the capacitor overcharging as the output power drops due to the fault. This protective measure acts as an energy dump to dissipate excess energy safely [29]. The LC filters are used to filter out ac side's higher-order harmonics at both MSC and GSC.

The following sections of the thesis discuss the controller used in voltage source converters, the dc chopper, and maximum power point tracking methods to achieve maximum efficiency at a specific wind speed.

2.5.1 Dc Link Chopper

The dc Chopper consists of IGBT controlled resistor. It protects the converter by dissipating dc link overvoltage caused by a decrease in active power flow resulting from disturbances in the grid [30] [31]. The chopper is triggered by a hysteresis controller, activated when the voltage across the capacitor reaches an upper threshold ($V_{dc\ upper}$) and turns off when it falls below a lower threshold ($V_{dc\ lower}$). This action helps maintain the dc voltage between the upper and lower thresholds and protects the capacitor from overvoltage while dissipating excess power in the resistor. The chopper's resistance value is determined based on equation 2.13, where $P_{chopper}$ is the maximum power absorbed by the dc chopper; it is generally the same as the rating of the wind generator. Depending on the overvoltage and hysteresis thresholds, the chopper switch is turned on for a period T_{on} and off for a period T_{off}. Depending on

the T_{on} and T_{off} duration, the effective resistance R_{eff} across the capacitor can be calculated using equation 2.14.

$$R_c = \frac{V_{(dc\ upper)}^2}{P_{Chopper}} \quad (2.13)$$

$$R_{eff} = R_c \cdot \frac{T_{on}}{T_{on} + T_{off}} \quad (2.14)$$

2.5.2 Maximum Power Point Tracking (MPPT)

Wind energy is an intermittent energy source; the maximum power available depends upon various factors like air density, turbine blade area, pitch angle, power coefficient and, most importantly, wind speed. The maximum power that can be extracted from the wind varies with each wind speed value. Maximizing the wind's power content and making the converter and control schemes more efficient and cost-effective is essential. A maximum power point tracking (MPPT) controller tracks the peak power point concerning wind speed [32].

MPPT control techniques can be divided into two categories: direct power control and indirect power control. Direct power control does not require mechanical sensors or any prior information. Examples include perturb and observe algorithm, which alters the operating point of the wind generator, such as the pitch angle of the blade, by a small amount and then observes how this change affects the power output. One of the advantages of this algorithm is its simplicity, as it only requires basic measurements of the turbine's power output and wind speed. However, it also has certain disadvantages, such as slow response times, susceptibility to rapid changes in wind speed, and power output fluctuations.

Indirect power control is simple, uses information like wind speed, torque estimation or power curve to collect the data and find the maximum power point, and includes methods such as power signal feedback (PSF) control, hill-climb search (HCS) control and tip speed ratio (TSR) control [33].

PSF control requires maximum power curves of wind generators obtained from simulations or field data to generate optimum power reference with rotor speed as input. PSF control can keep the power output constant, regardless of wind conditions, and can be helpful for large-rated wind generators. Hill Climb Search uses a control algorithm continuously tracking out for maximum power point. It is the most flexible

algorithm which accommodates the power–speed relation. In this method, the turbine continually adjusts the operating point in response to changes in wind speed and direction. TSR control involves adjusting the operating factors, such as the pitch angle of the wind generator or the rotor speed, to maintain the optimal tip speed ratio, which is the ratio of the blade tips's speed to the wind speed. This method is commonly used in small wind generators. Ultimately, the choice of control method depends on the particular wind generator design and operational environment. While TSR control may be more straightforward and cheaper, it may not perform optimally in variable wind conditions. In contrast, PSF and HCS control may provide better results but come at a higher cost and complexity [33] [34].

This thesis uses Tip speed control for maximum power point tracking operation. In Section 2.2, the Tip speed ratio was defined as $TSR = \frac{r\omega}{V_w}$, where V_w is the wind speed (m/s), and ω is the rotor speed and r the blade's radius (m). In the TSR control, a table look-up approach determines the optimum tip speed ratio for maximum power at a given wind speed (Appendix A). This TSR optimum value is used to control the generator speed.

2.5.3 Control of the VSC based Back-to-Back Converter

The VSC back-to-back (BTB) system consists of a rectifier which converts an ac signal to a dc signal, a dc link capacitor, and an inverter which converts a dc signal to an ac signal. These are connected in the back-to-back configuration as shown in Figure 2.6 and allow smooth power transmission between two different ac frequency systems. Each converter controls its generated voltage to achieve necessary active and reactive powers. As stated in Equation 2.10 and Equation 2.11 suggest, the converter generated voltage's phase angle δ and magnitude $|V|$ can be used to control active (i.e. active) and reactive power outputs respectively by generating different values of respective complex parts of the converter current ($i_a = i_{active} + ji_{reactive}$) [35] [36].

There are different ways of controlling the phase angle (δ) and the magnitude of converter voltage (m), mainly direct and vector control. In direct control, the modulation index (m) and the phase angle (δ) are directly regulated by PI controllers, where m is responsible for setting the desired voltage magnitude of the converter's ac voltage (V_c), consequently responsible for reactive power flow and phase angle (δ) is responsible for setting the active power flow. Direct control leads to coupled interactions, which means that a change in power order causes a transient change in

reactive power and vice-versa. There is also no way to limit over-current explicitly. To address the dependability issue, vector control may be used to control the active and reactive currents in each VSC. The controller provides a decoupled response, meaning P can be independently changed without affecting Q and vice versa [37] [38] [39]. Additionally, over-current is prevented using an open-loop approach by limiting the d and q current orders to safe values. Each converter has an outer controller tailored to achieve a specific objective, which will be explained later.

2.5.3.1 Outer Loop Controller

The outer controllers are used to achieve the broader system level objective, such as the dc voltage control, the ac voltage control, the active power control, and the reactive power control. So, as shown in Figure 2.6 in the vector control, outer controllers provide the reference values for the inner current controllers.

(a) Grid Side Controller

Figure 2.7 shows the grid side converter (GSC) control of the Type 4 wind generator. The GSC Controller uses a dc voltage controller to regulate the active power flow and an ac voltage controller to regulate the reactive power flow. The dc voltage controller maintains the desired dc voltage level across the dc link capacitor by regulating the q-axis current reference, denoted as i_{qref}. The dc voltage reference v_{dcref} is compared to the measured and filtered dc voltage $v_{dc(measured)}$ across the capacitor.

The proportional-integral (PI) controller helps regulate the error and generates an order for i_{qref}. A phase-locked loop tracks the voltage phase at the point of common coupling (Bus-G in Figure 2.6) and uses it as a timing reference for the firing pulses. The PLL will be explained in detail in subsequent sections. The ac voltage controller compares the measured ac voltage ($v_{ac(measured)}$) with the reference ac voltage (v_{acref}), and a PI controller generates the active current reference, denoted as i_{dref}, for the inner control loop. The outputs of the dc voltage controller's i_{qref} and the ac voltage controller's i_{dref} are input to the decoupled current controller, which generates the required q-axis and d-axis voltage references, denoted as v_{qref} and v_{dref}. These references are then converted to abc coordinates, and firing pulses are generated using SPWM, as described in Section 2.4

21
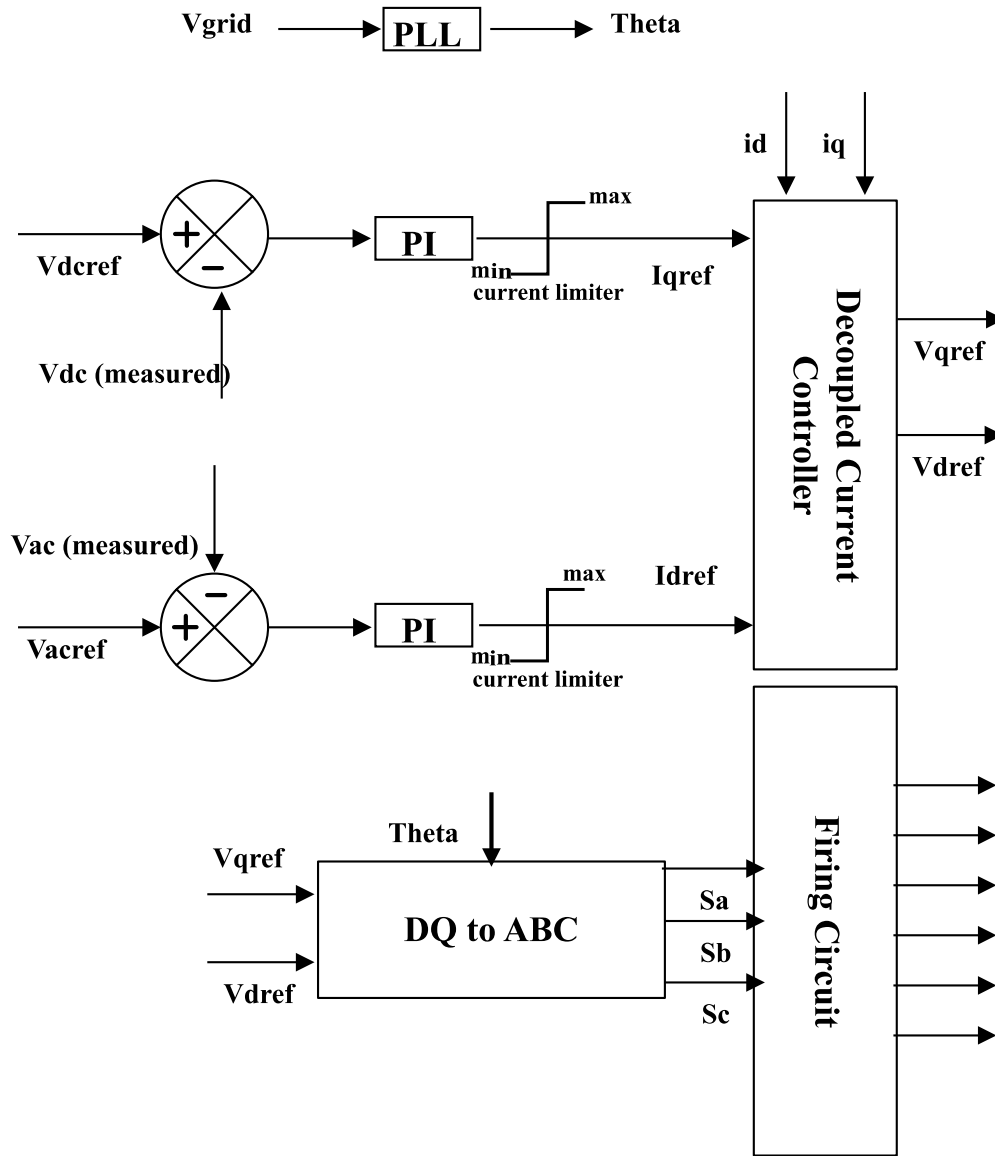
Figure 2.7: Grid side converter vector control

(b) Machine Side Controller

The machine side converter controls its ac side voltage and the wind generator speed (w_{ref}). The speed w_{ref} is controlled by increasing or decreasing the power drawn from the generator, and this is achieved through the component (i_{qref}), which is responsible for the active power. The ac voltage v_{acref} at BUS-M in Figure 2.6 is controlled via the reactive current reference i_{dref}. Figure 2.8 illustrates the above control strategy.
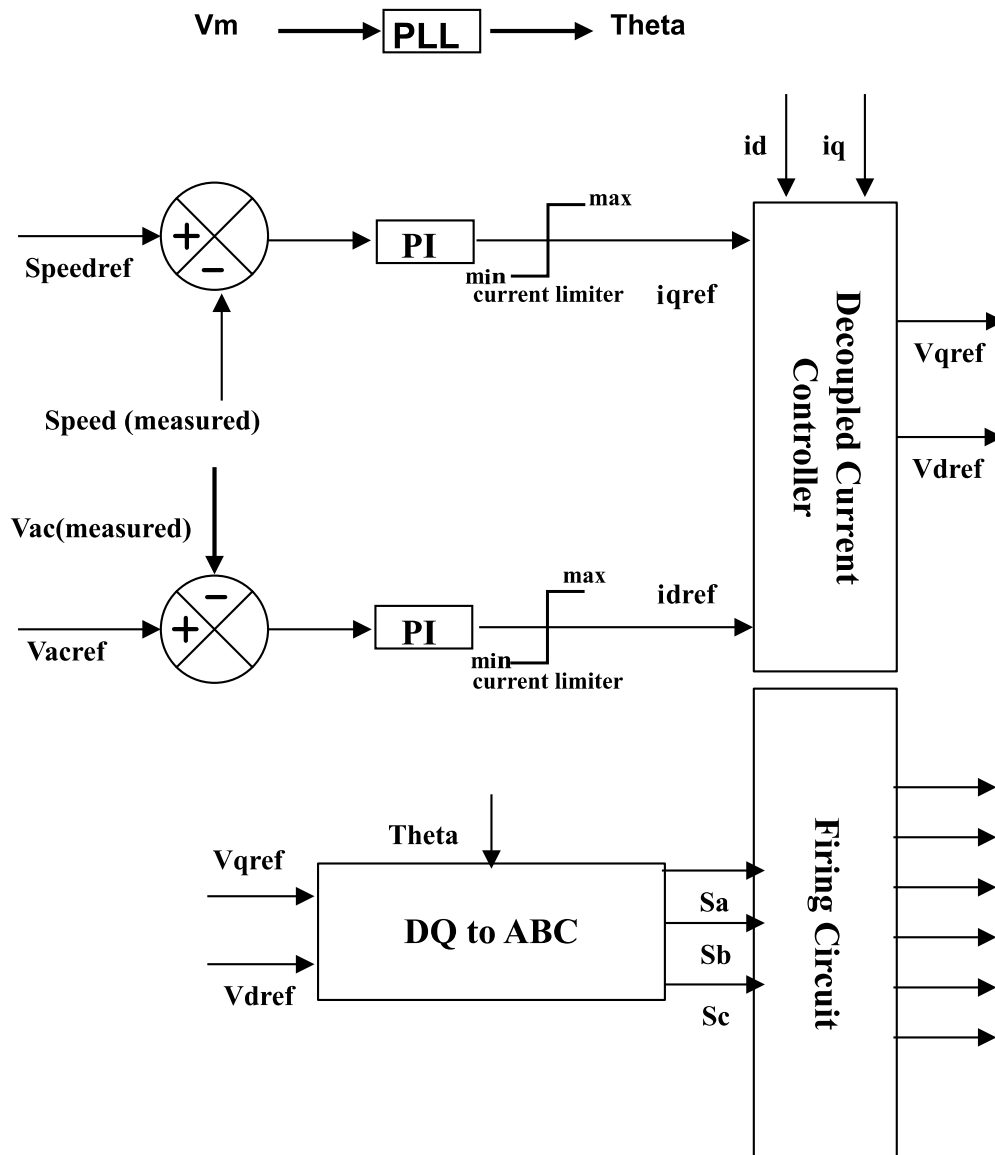
Figure 2.8: Machine side converter vector control

2.5.3.2 Decoupled Inner Current Controller

Figure 2.9 shows a single-line diagram of the ac grid system and ac converter system connected via the resistor (R) and reactor (L) representing the converter transformer and the phase reactor.

The voltage and current relationship in three-phase instantaneous form is expressed as
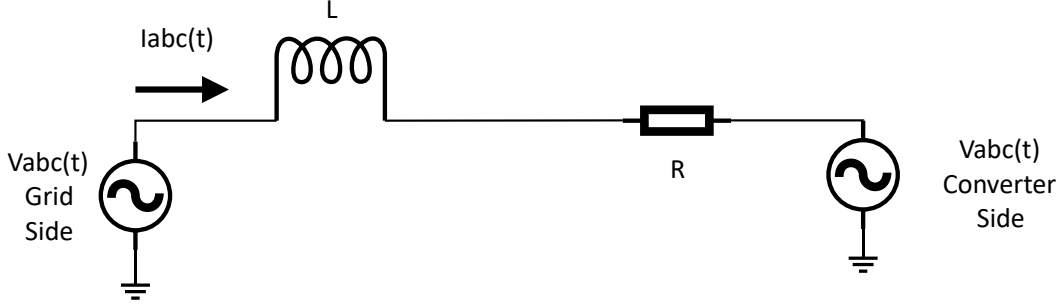
Figure 2.9: Single-line diagram of Converter ac side connected to an ac grid system

$$\frac{d}{dt} \cdot \begin{bmatrix} i_a \\ i_b \\ i_c \end{bmatrix} = \frac{-R}{L} \cdot \begin{bmatrix} i_a \\ i_b \\ i_c \end{bmatrix} + \frac{1}{L} \cdot \left(\begin{bmatrix} v_a^g \\ v_b^g \\ v_c^g \end{bmatrix} - \begin{bmatrix} v_a^c \\ v_b^c \\ v_c^c \end{bmatrix} \right) \tag{2.15}$$

In equation 2.15, $v_{abc}^g = [v_a^g, v_b^g, v_c^g]$ and $v_{abc}^c = [v_a^c, v_b^c, v_c^c]$ represent three-phase voltage at grid bus and the converter terminal respectively. Park's transformation shown in equation 2.16, is applied to the ABC-frame in equations 2.15 and converted to a synchronously rotating dq reference frame, as shown in equations 2.17 [40]. The angle θ is in phase with the positive sequence of the fundamental frequency ac waveform v_{abc}^g and is generated using a phase-locked-loop (PLL) to the system voltages v_{abc}^g.

$$\frac{d}{dt} \cdot \begin{bmatrix} i_a \\ i_b \\ i_c \end{bmatrix} = \sqrt{\frac{2}{3}} \begin{bmatrix} \cos(\theta) & \sin(\theta) & \frac{1}{\sqrt{2}} \\ \cos(\theta - 120) & \sin(\theta - 120) & \frac{1}{\sqrt{2}} \\ \cos(\theta + 120) & \sin(\theta + 120) & \frac{1}{\sqrt{2}} \end{bmatrix} \cdot \begin{bmatrix} i_d \\ i_q \\ i_0 \end{bmatrix} \tag{2.16}$$

$$\frac{d}{dt} \cdot \begin{bmatrix} i_d \\ i_q \\ i_0 \end{bmatrix} = \frac{-R}{L} \cdot \begin{bmatrix} i_d \\ i_q \\ i_0 \end{bmatrix} + \begin{bmatrix} 0 & -\omega & 0 \\ \omega & 0 & 0 \\ 0 & 0 & 0 \end{bmatrix} \cdot \begin{bmatrix} i_d \\ i_q \\ i_0 \end{bmatrix} + \frac{1}{L} \cdot \left(\begin{bmatrix} v_d^g \\ v_q^g \\ v_0^g \end{bmatrix} - \begin{bmatrix} v_d^c \\ v_q^c \\ v_0^c \end{bmatrix} \right) \tag{2.17}$$

Equation 2.18, which is the Laplace transformation of Equation 2.17, clearly shows that the dq system is coupled due to off-diagonal terms in transfer function $G(s)$. The converter output voltages are v_d^c and v_q^c, and each affects both i_d and i_q. Equation 2.17 can be rewritten as Equation 2.19, decoupled in nature.

$$\begin{bmatrix} I_d(s) \\ I_q(s) \end{bmatrix} = \underbrace{\begin{bmatrix} R + Ls & \omega L \\ -\omega L & R + Ls \end{bmatrix}^{-1}}_{G(s)} \cdot \begin{bmatrix} v_d^g(s) - v_d^c(s) \\ v_q^g(s) - v_q^c(s) \end{bmatrix} \tag{2.18}$$

24

$$L.\frac{d}{dt}\begin{bmatrix} i_d \\ i_q \end{bmatrix} = -R.\begin{bmatrix} i_d \\ i_q \end{bmatrix} + \frac{1}{L}.\begin{bmatrix} \overbrace{v_d^g(s) - v_d^c(s) - \omega L i_q}^{v_d'} \\ \underbrace{v_q^g(s) - v_q^c(s) + \omega L i_q}_{v_q'} \end{bmatrix} \tag{2.19}$$
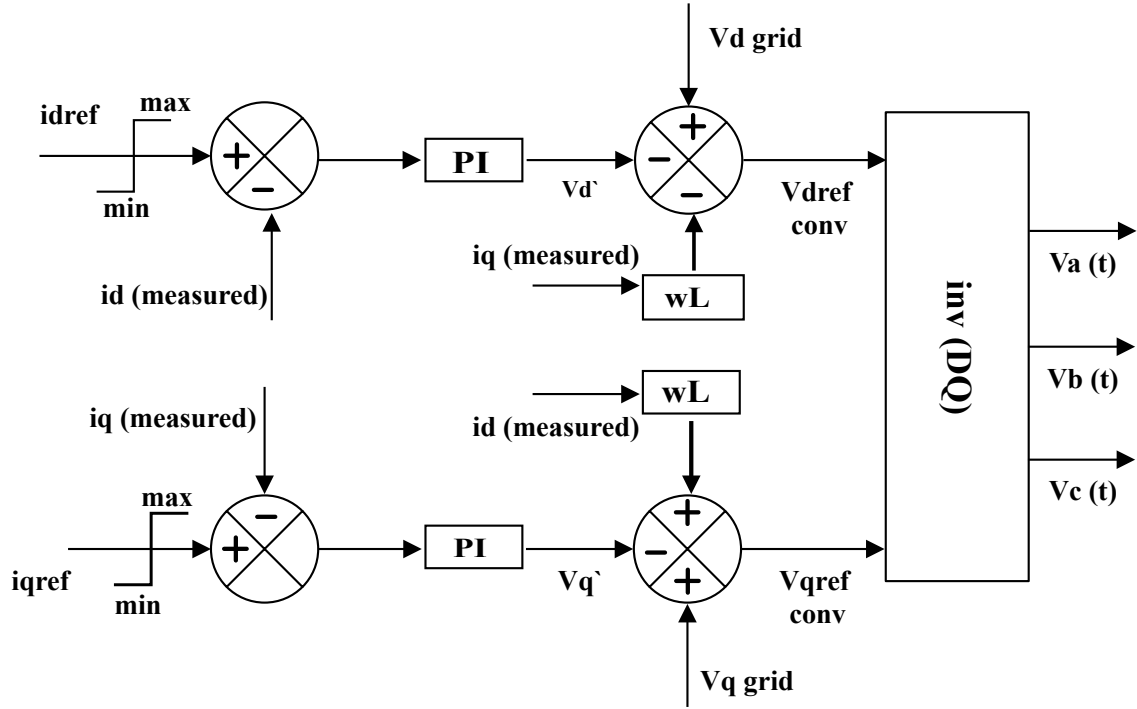
Figure 2.10: Decoupled current controller (inner controller)

A PI controller generates the intermediate control signals v_d' and v_q' as given in Equation 2.19. Note that v_d' only affects i_d and v_q' only i_q, so decoupled control is possible. The actual v_d^c and v_q^c voltages for the VSC can be generated from v_d' and v_q' using the control system shown in Figure 2.10. The references for phase a, b and c voltages (v_a, v_b, v_c) can be generated by using the inverse Park's transform on v_d^c and v_q^c. Sinusoidal PWM can generate the firing pulses to achieve the given output voltage. This inner controller is common to both machine-side converters and grid-side converters. The current magnitude can be limited in the open loop by limiting values of i_{dref} and i_{qref} so that the magnitude of the current, i.e. $\sqrt{(i_{dref}^2) + (i_{qref}^2)}$ does not exceed the rated current value.

2.5.4 Phase Locked Loop

The Phase Locked Loop (PLL) provides a reference phase angle for the ac voltage input at Bus M and Bus G, as depicted in Figure 2.6. The operation of converters heavily relies on accurately tracking the phase angle at Bus M and Bus G. This reference angle, denoted as θ, is utilized for Park transformation matrices (Equation 2.16) and is also used as a reference for generating firing pulses for the converter switch.
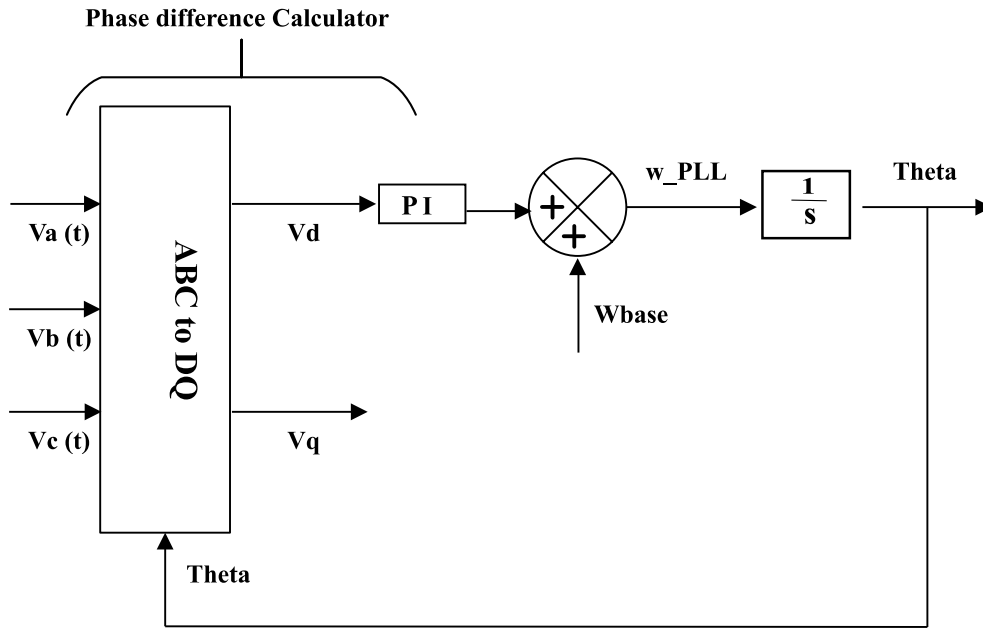
Figure 2.11: Phase Locked Loop controller

Figure 2.11 demonstrates the operation of dq-based PLL [37]. The PLL consists of a voltage-controlled oscillator (VCO) that adjusts its output frequency based on the input reference signal. The phase difference between the ac voltage and the output of the PLL, represented by θ, is fed to a PI controller that aims to minimize this phase difference to synchronize θ with the ac voltage. The input to the VCO is adjusted using the output of the PI controller, ensuring that θ remains synchronized with the ac voltage. The phase detector mechanism shown in the figure, utilizing the dq transform as phase angle $= (tan^{-}1(\frac{v_d}{v_q}))$, which results in zero average phase error when θ is in sync with phase a of the positive sequence component of the ac voltage [41].

To facilitate the frequency locking process of the filtered ac voltage, a "lock-in range" value is included in the control system. This value represents the expected steady-state value of controller ω_{base}, which equals $2\pi f$ where 'f' is the nominal operating grid frequency. This value makes it easier to lock the frequency of the filtered ac voltage and reduces the controller's effort. The PLL aids in generating modulating signals for the firing circuit, which uses the sinusoidal Pulse Width Modulation (PWM) technique to trigger the IGBT valves precisely.

2.5.5 Overall BTB VSC Vector Control

In this chapter, we have explained the mechanical and electrical aspects of wind power generation. We have discussed the control methods used for regulating voltage and power in an ac electrical system using Voltage Source Converters (VSCs). VSCs are electronic devices that convert dc power to ac power with variable voltage and frequency.

Various control methods have been employed to regulate voltage and power in an ac electrical system using VSCs, including direct and indirect control. These control methods involve generating current references to regulate the output voltage and power of the VSC. The direct control method modulates the amplitude and phase of the VSC output voltage to control the reactive and active power, respectively. However, it has a disadvantage, as changing the reactive current results in a transient change in active power. Additionally, direct control does not limit the converter's current, which could lead to overcurrent and damage.

On the other hand, the indirect control method involves generating d and q current references and using a decoupled control strategy. This strategy ensures decoupled control of active power (P) and reactive power (Q), and over-current is avoided by limiting the magnitudes of i_{dref} and i_{qref}. Indirect control is the approach used in this thesis.

To prevent over-speeding of the generator and overvoltage in the dc link capacitor during ac side faults or contingencies, a chopper is often placed between the two back-to-back converters (BTBs). The overall VSC vector control is shown in Figure 2.12.
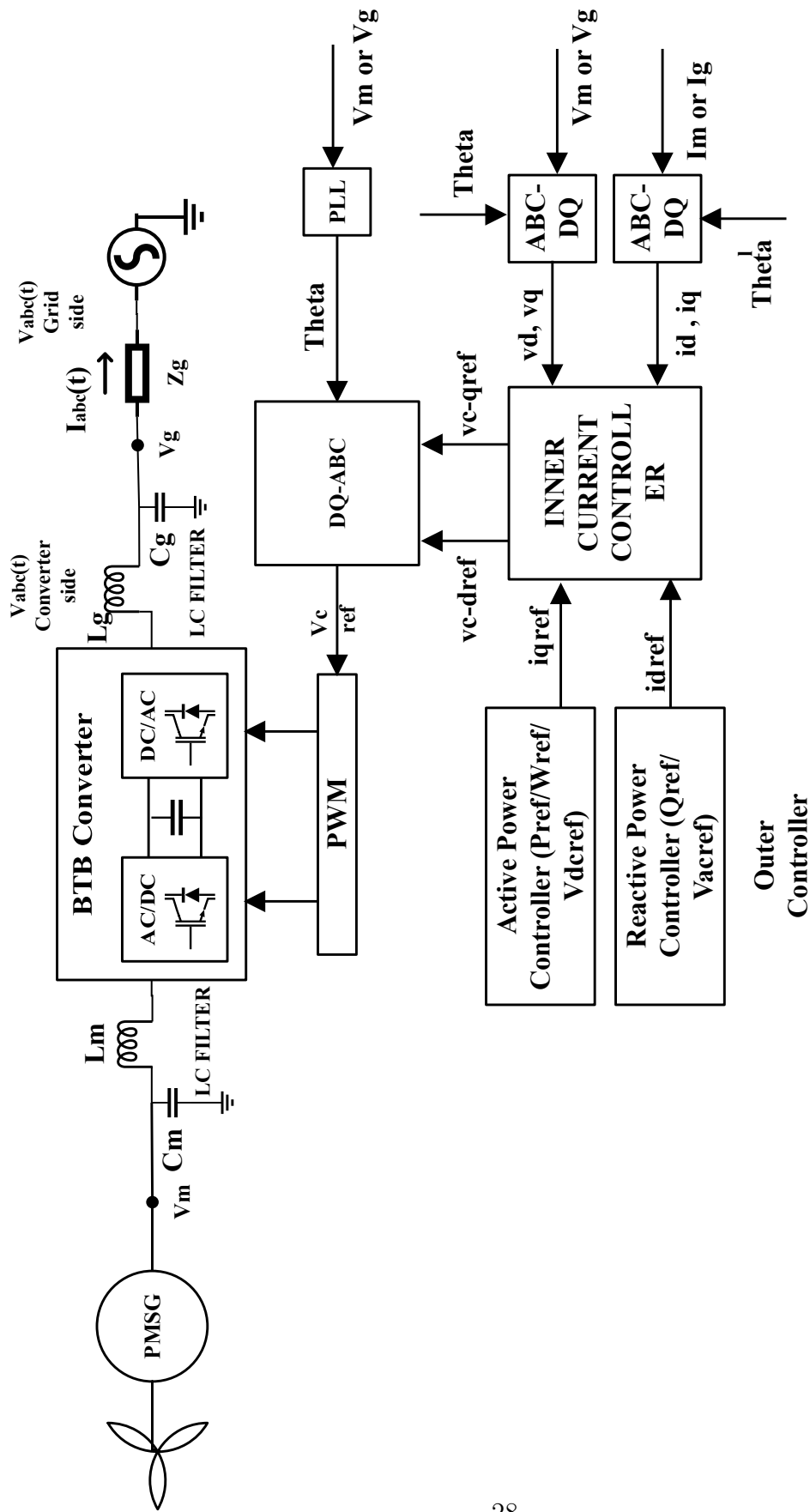
Figure 2.12: VSC-based BTB control structure with inner and outer controllers

Chapter 3

Transient behaviour of Type 4 PMSG based Wind generator

This chapter analyzes the system behaviour and control mechanism of the PMSG-based wind generators, which are Type 4 wind generators. The analysis is done without fault ride-through techniques to focus solely on the normal operating behaviour of the wind generator. In the upcoming chapters, the analysis and findings presented in this chapter will serve as the foundation for implementing fault ride-through mechanisms for PMSG-based wind generators. The techniques will be based on the IEEE Std 1547-2018 (IEEE 1547) [1] for distributed energy resources, which outlines the requirements for grid-connected distributed energy resources. In addition to fault ride-through techniques in Chapter 4, chapter 5 will also focus on developing a new control approach for power oscillation damping in PMSG-based wind generators. The following sections describe the operational behaviour of the maximum power point tracking (MPPT) controller, dc chopper, and inner and outer current control loops under different conditions, such as sudden changes in demand, faults, or changes in the generator's operating conditions.

3.1 Wind Generator Test System to Investigate Controller Response and Fault Behaviour

The system in Figure 3.1 will be used as the test system. The system is implemented on the PSCAD, one of the EMT simulators. The components, such as the BTB converter and chopper, are briefly described in Chapter 2, from sections 2.5.1 to 2.5.3.

The performance of a 2 MW wind plant is observed. A voltage source behind a series-connected impedance represents the grid. The back-to-back converter configuration includes the voltage source converter's controllers and the dc chopper (as discussed in Chapter 2). The controller parameters for both the inner and outer loop controllers, regulating active power flow and reactive power flow for the rectifier and inverter sides, are provided in Table 3.1. The network transformer is rated at 20 MVA, 11 kV/69 kV and has a 10% leakage reactance.

Type 4 Wind Generator
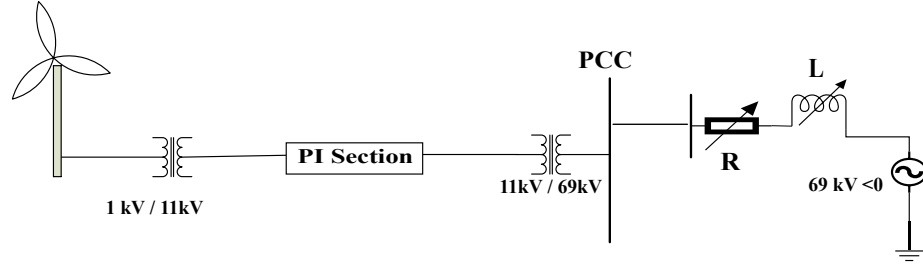
Figure 3.1: PMSG-based wind generator connected to the grid

Table 3.1: The wind generator parameters (K_p:Proportional Constant, T_i:Integral Time Constant)

MSC Controller	ac Voltage controller : Kp=1 pu/pu, Ti=0.1 pu/pu-sec
	Speed Controller : Kp=2 pu/pu, Ti=0.07 pu/pu-sec
	PLL parameter : Kp=50 pu/pu, Ti=0.002 pu/pu-sec
GSC Controller	ac Voltage controller : Kp=0.66 , Ti=30.23 pu/pu-sec
	dc link Voltage Controller : Kp=0.321 , Ti=0.1097 pu/pu-sec
	PLL parameter : Kp=50 , Ti=0.002 pu/pu-sec

3.2   Maximum Power Point Tracking (MPPT)

Wind generators generate electricity from wind energy, which depends on wind speed. As the wind speed changes, the turbine's power output also changes, and the turbine's power curve is non-linear. MPPT, or Maximum Power Point Tracking, is a method employed in wind generators to obtain the wind generator's power output. This is accomplished by tracing the wind generator's maximum power point (MPP), the location on the power curve where the output power peaks for a specific wind speed. The types of MPP techniques are mentioned in Chapter 2, Section 2.5.2. Without

MPPT, wind generators might not operate at their maximum power output level, resulting in lower efficiency and energy production. By utilizing MPPT, the wind generator can operate at its maximum power point, which can help to optimize its performance and increase energy generation.
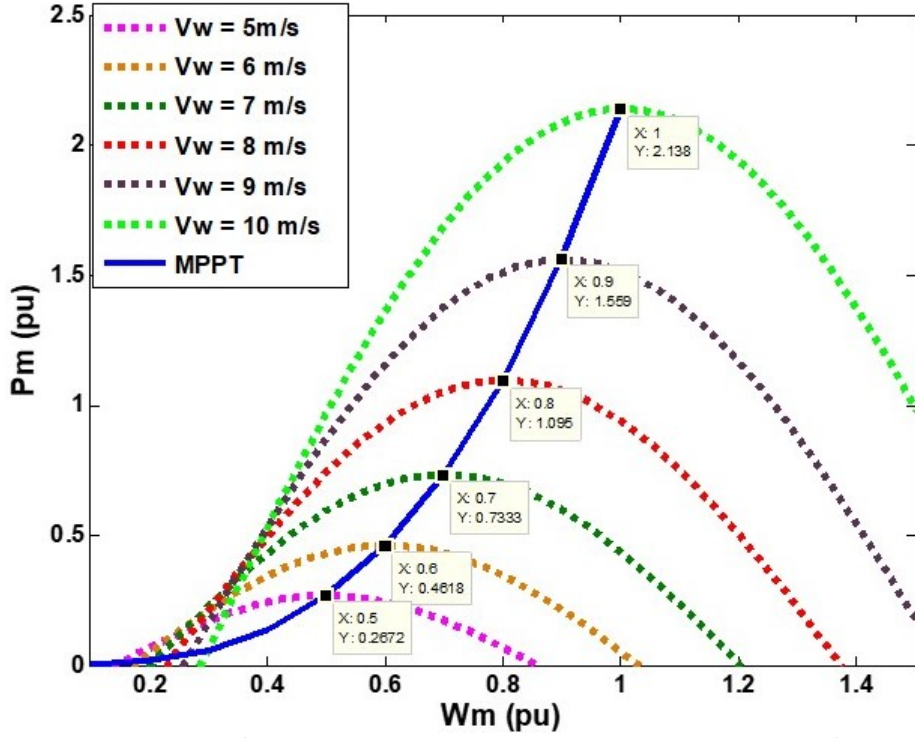
Figure 3.2: MPPT tracking maximum power point in respective turbine angular speed

Figure 3.2 shows the multiple curve plot for the wind generator output power at different turbine speeds. Those curves are obtained using the wind generator characteristic equation in Equations 3.1 and 3.2. Equation 3.3 represents the mathematical expression for the maximum power obtained using the TSR method. Each curve corresponds to a particular wind speed. The peak of each curve represents the maximum output power points. These points are joined to get the MPPT curve as shown in Figure 3.2.

$$TSR_{opt} = w_{opt} \frac{R}{V_w} \tag{3.1}$$

$$C_p = \frac{4}{9} - (\frac{\beta}{60})\sin(\frac{0.5\pi 20(TSR_{opt} - 3)}{150 - 3\beta}) - (2\frac{\beta}{1087}(TSR_{opt} - 3)) \tag{3.2}$$

31
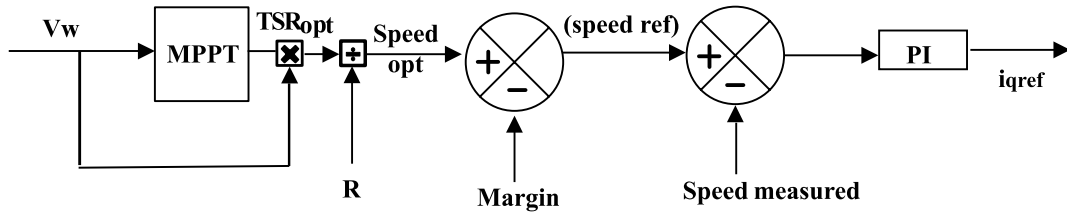
Figure 3.3: Tip speed ratio calculation and Control

$$P_{max} = \frac{1}{2}\rho AV^3 C_p(\beta, TSR_{opt})$$ (3.3)

This thesis uses a Tip-Speed Ratio (TSR) based MPPT algorithm. A MATLAB
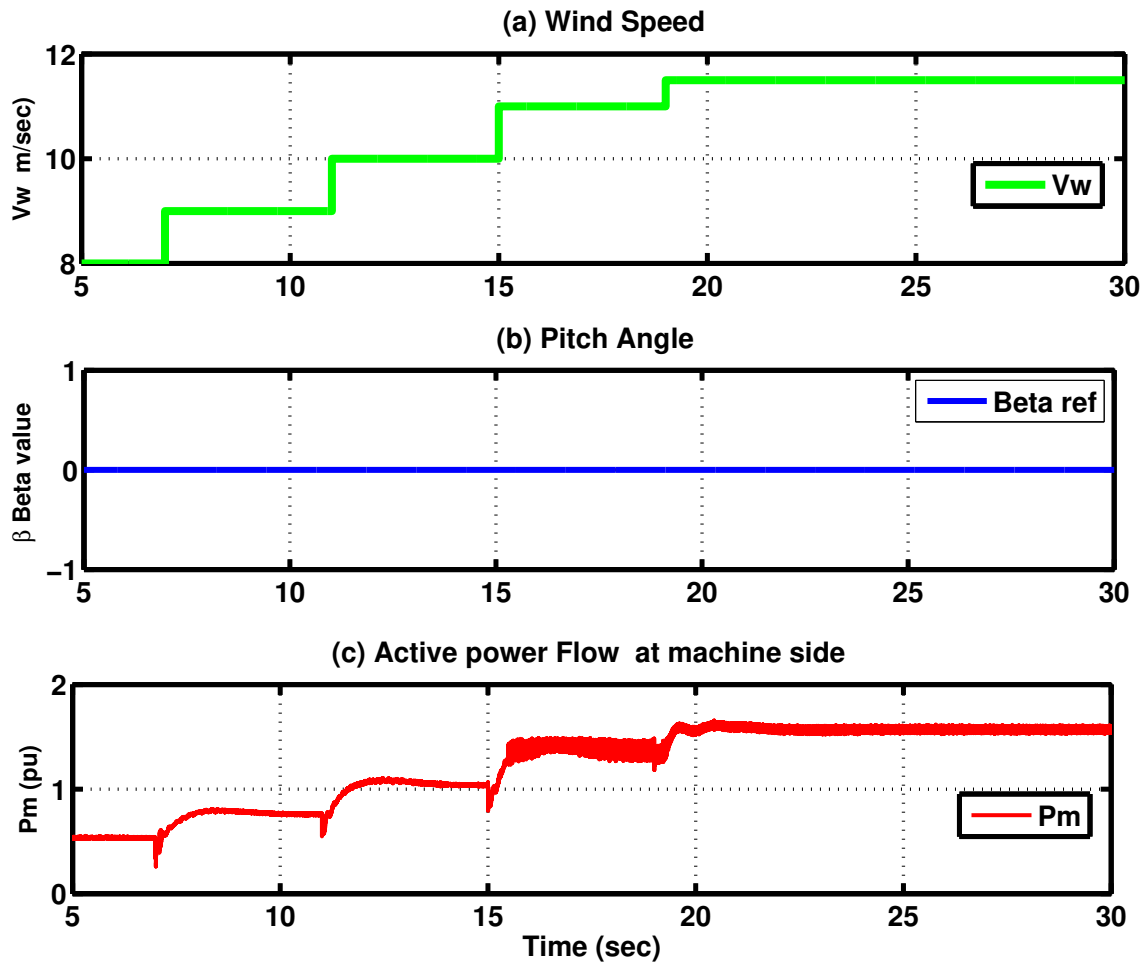
Figure 3.4: Wind speed and Power dynamics: Tip speed ratio (MPPT Control and Beta $(\beta) = 0$)

code is used to create a data table in this algorithm and is listed in Appendix(A). The table contains two parameters, wind speed and the optimum TSR value at the given wind speed. The given table is used in PSCAD to get the optimum TSR value for a given wind speed. As shown in Figure 3.3, the MPPT block finds the optimum TSR value for a given wind speed using the data table. Then the optimum rotational speed of the PMSG is calculated using the respective optimum TSR value.

Using the EMTP-based test case, the MPPT tracking algorithm is tested. In this case, the pitch angle (β) is kept at zero value as the wind power extracted is kept below rated power. As shown in Figure 3.4, the wind speed increases from 8 m/s to 11.5 m/s in steps, and the corresponding PMSG output power increases. As the wind speed changes, the MPPT algorithm tracks the optimum TSR value, and the controller calculates the corresponding optimum machine speed. The PMSG rotates at this optimum speed, ensuring maximum power extraction from the wind generator.
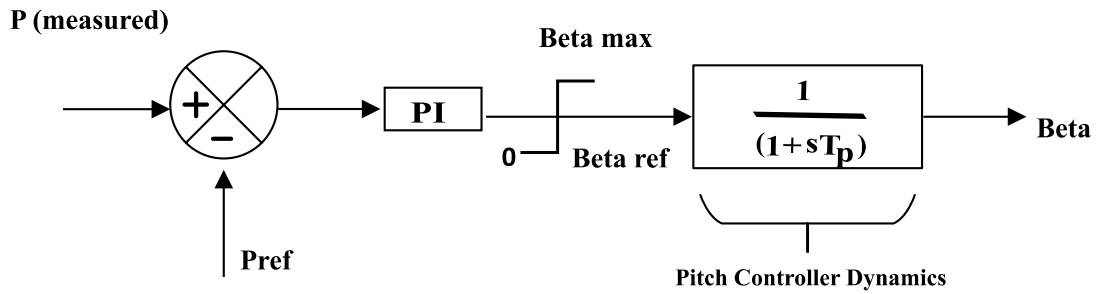
Figure 3.5: Pitch angle controller

3.3 Pitch Angle Controller

A pitch angle controller is a controller which can adjust the blade angle as per wind speed variations. It provides a reduced area for capturing less aerodynamic power during medium wind speed to operate the converter and wind generator within their rated power. C_p curve as mentioned in Equation 3.2, is the function of pitch angle, TSR etc. Equation 3.3 shows that power extraction from wind depends on the C_p curve, an area captured by wind and wind speed.

As the wind speed rises, the amount of power the wind generator generates also increases. The turbine's output reaches its maximum rated power when the wind speed reaches a specific level known as the "rated wind speed." If the wind speed continues to increase beyond this point, the turbine's power output will exceed its

maximum capacity. To address this, a pitch angle controller is activated when the wind speed exceeds the rated wind speed. This controller adjusts the pitch angle of the turbine's blades to ensure the turbine operates at its rated power level even at higher wind speeds. The adjustment in the pitch angle is achieved using a pitch angle
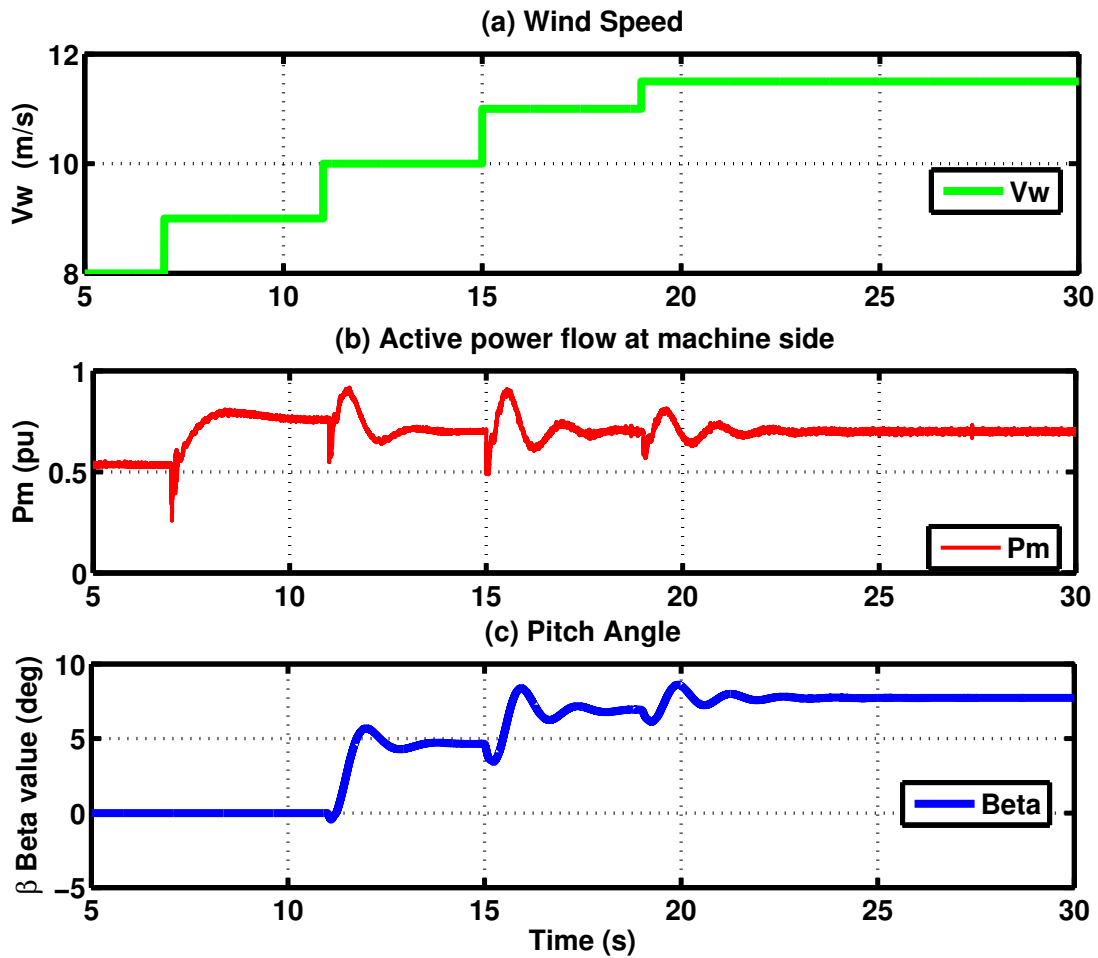
Figure 3.6: Pitch angle controller dynamics with MPPT

controller, as depicted in Figure 3.6. It compares the wind generator's power output with the reference power (rated power) and passes the error through a PI controller. Pitch angle change is a slow operation. The dynamics of the pitch angle change is modelled as a first-order transfer function with gain $K_p = 1.0$ and time constant $T_p = 1$ s. The test system is used to check the operation of the pitch controller. As

shown in Figure 3.6(a), the wind speed changes from 9 m/s to 11.5 m/s. As depicted in Figure 3.6(b), the wind power output increases as the wind speed increases. The pitch controller is enabled when wind speed V_w is greater than 10 m/s, where the rated wind speed is set to 10 m/s. The pitch controller power reference is set to 0.75 pu. As shown in Figure 3.6(c), the pitch controller is activated for $V_w \geq 10$ pu, causing pitch angle β to increase. Consequently, the wind generator's output power is maintained at 0.75 pu. The pitch controller remains active for V_w greater than 10 m/s and V_w less than the cutout speed.

3.4   Dc chopper with Hysteresis Control

In the Type-4 wind generator, a dc chopper is employed in the dc link of the BTB VSC converter. Its purpose is to prevent over-voltage in the dc-link capacitor when grid-side disturbances such as faults occur. It consists of an insulated gate bipolar transistor (IGBT) controlled resistance. This resistor dissipates the power mismatch if the wind generator output power exceeds the output power to the grid or vice-versa. As discussed in Chapter 2, by controlling the switching on and off duration of the IGBT switch, the effective resistance of the dc-chopper is changed, and so does the corresponding power dissipation. The chopper activates when the dc-link voltage V_{dc} hits $[V_{dc-min}, V_{dc-max}]$ range while riding through the fault. A voltage hysteresis controller is used to issue the chopper firing pulses.

The test system is used to check the operation of the dc chopper. A 10-cycle, 3-phase line to ground fault is applied at the PCC bus at $t = 6$ sec. During the fault, the grid-side converter output power becomes zero. During this period, the MSC converter continuously feeds active power, which causes a power imbalance at the dc link. As a result, the dc capacitor voltage rises. With the dc chopper disabled, the dc link voltage rises to 11 pu, as shown in Figure 3.7. Such a high dc link voltage will damage converter components, and the wind generator will be tripped to save the system from the rise in dc link voltage. As shown in Figure 3.7, with the dc chopper enabled, the dc link voltage is controlled with a band of [3.1 pu, 3.3 pu] within the safe operating range of dc-link voltage.

The dc chopper power and energy consumption are shown in Figure 3.8(a) and (b), respectively. The energy consumed by the dc chopper during the fault-ride through

operation is 0.3 MJoule. The chopper switches off at $t = 6.35$ s once V_{ac} reaches the nominal value and after complete active power recovery of the GSC converter.
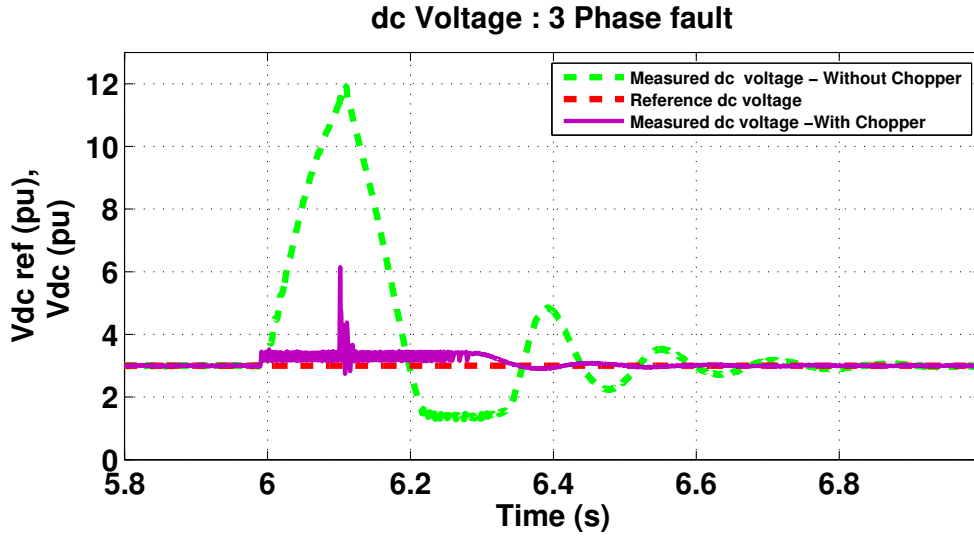
Figure 3.7: Response of V_{dc} (Dc chopper activated)

3.5 Step response Transient behaviour of PMSG connected to the Grid

To investigate the wind generator's response, step changes are applied to three different controller references, namely wind speed (V_w), dc voltage(V_{dc}), and grid-side ac voltage, and their effects are observed.

3.5.1 Step Change in Wind Speed Reference

In this section, the wind speed reference is changed, and the TSR-based MPPT control, as explained in Section 3.1, will make the converter change its power order to ensure that the PMSG runs at the optimum speed for extracting maximum power.
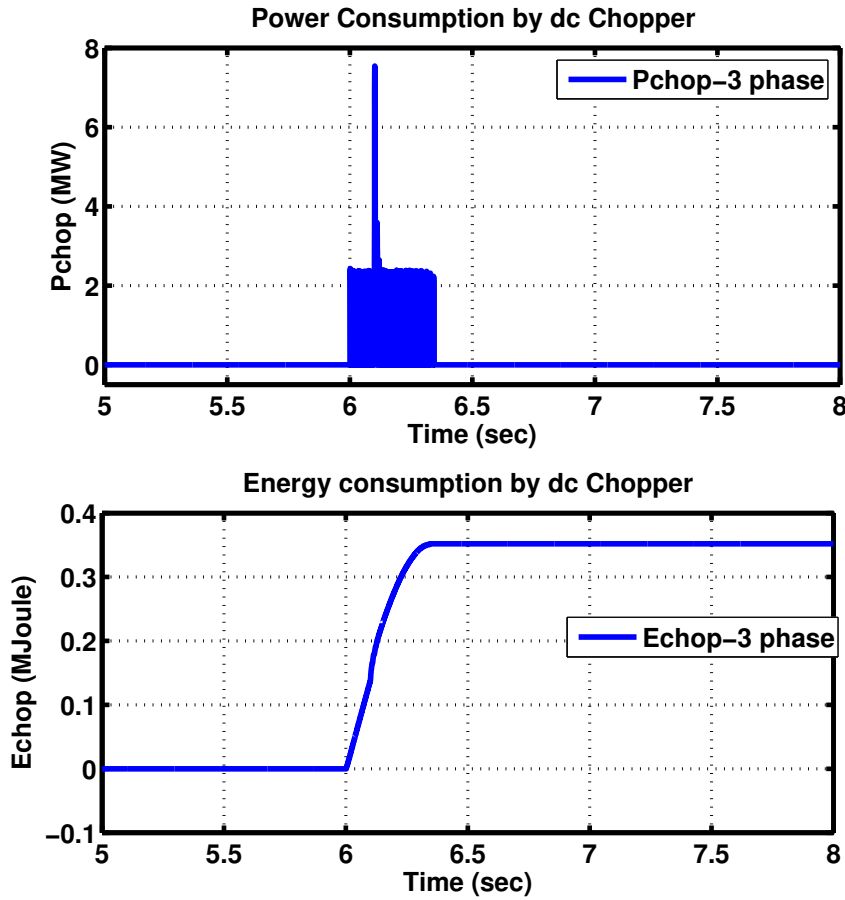
Figure 3.8: Power and energy consumed by dc-chopper

The performance of the outer control loop is observed, which is responsible for managing active and reactive power flow, and the inner decoupled control loop regulates current references coming from the outer controller for both the MSC and GSC. The control diagram is shown in Figure 3.9.It is the same figure from Chapter 2 (Figure 2.6) but is repeated for convenience.

When the speed of the wind changes, the speed reference, which controls active power flow at the MSC side, also changes, resulting in the generator generating respective active power. The wind speed changes from 9 m/s to 8 m/s at 11 s and back to 9 m/s at 18 s, as shown in Figure 3.10. According to the MPPT algorithm, the optimum rotational speed of PMSG varies with wind speed. It can be observed in Figure 3.10(a) that the optimum speed reference changes from around 0.91 pu for
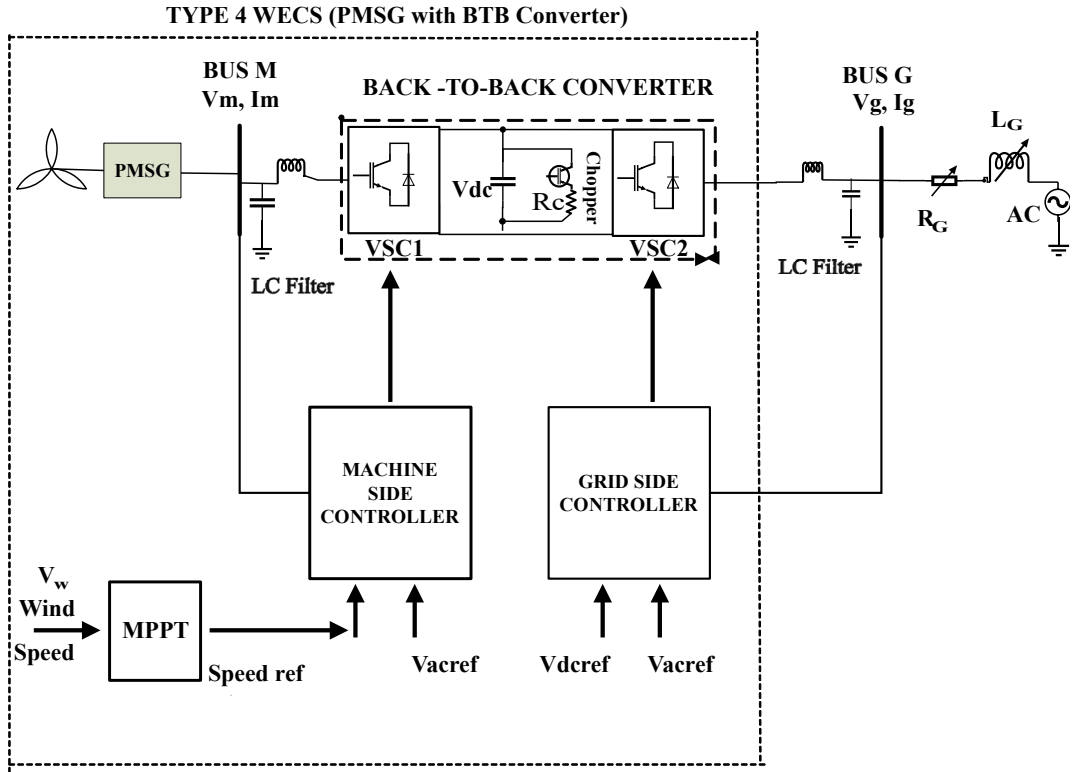
Figure 3.9: PMSG-based wind generator connected to the grid
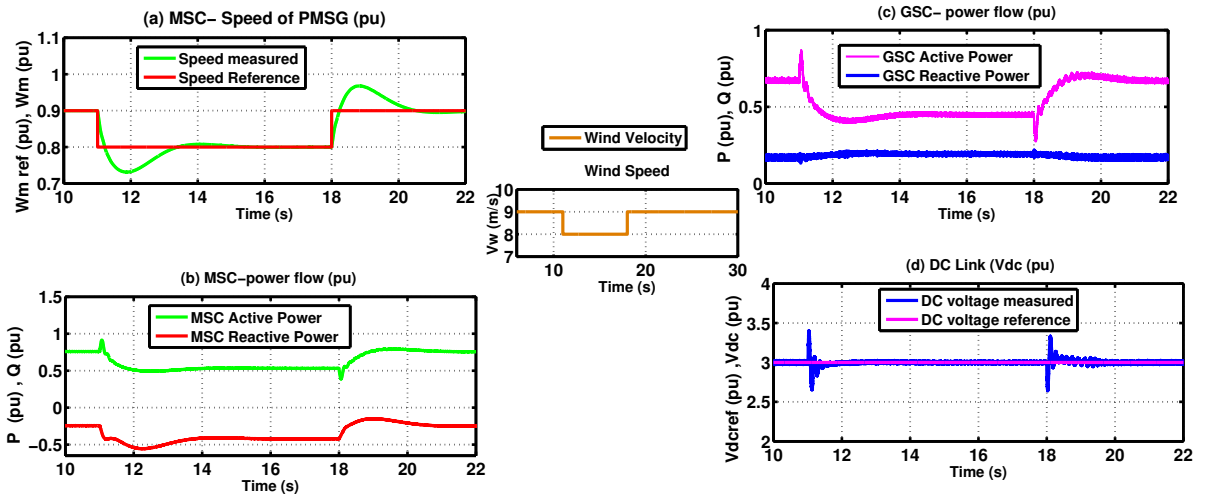
Figure 3.10: Response of MSC and GSC due to step change in wind speed

the wind speed of 9 m/s to 0.82 pu for the wind speed 8 m/s around 18 s and the
rotational speed of PMSG accurately follows the MPPT optimal speed reference due

to action of speed controller at MSC side. Figure 3.10(b) shows the change in the active power flow due to rotational speed variation as the MPPT dictates. That is, at the lower wind speed, the MPPT orders a power reduction in both the MSC and GSC, as can be observed in Figure 3.10(b) and (c). Due to the change in active power value, dc-link will observe the power imbalance during the transition and the transients are observed during the changing wind speed as shown in Figure 3.10(d).
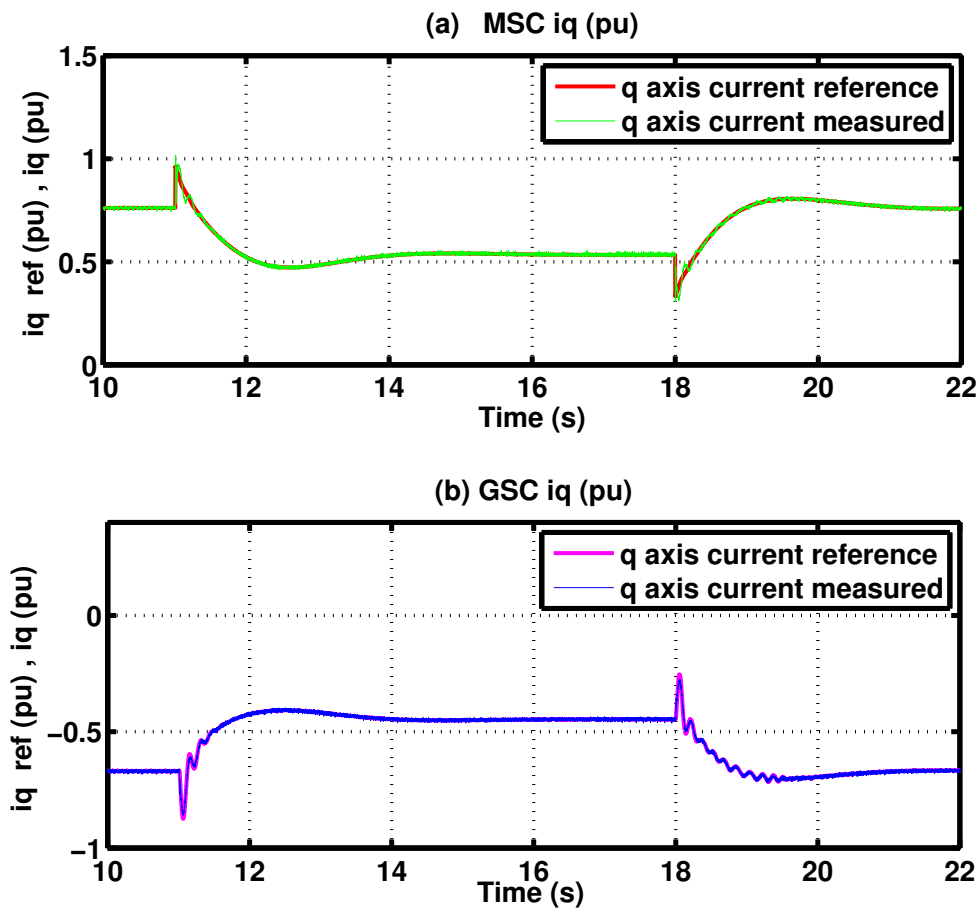
Figure 3.11: q - axis current references at MSC and GSC sides

Figure 3.11(a) and Figure 3.11(b) shows the variation of q-axis current reference as active power flow order changes. The decrease and increase of active power flow due to a change in wind speed are coordinated with the corresponding decrease and
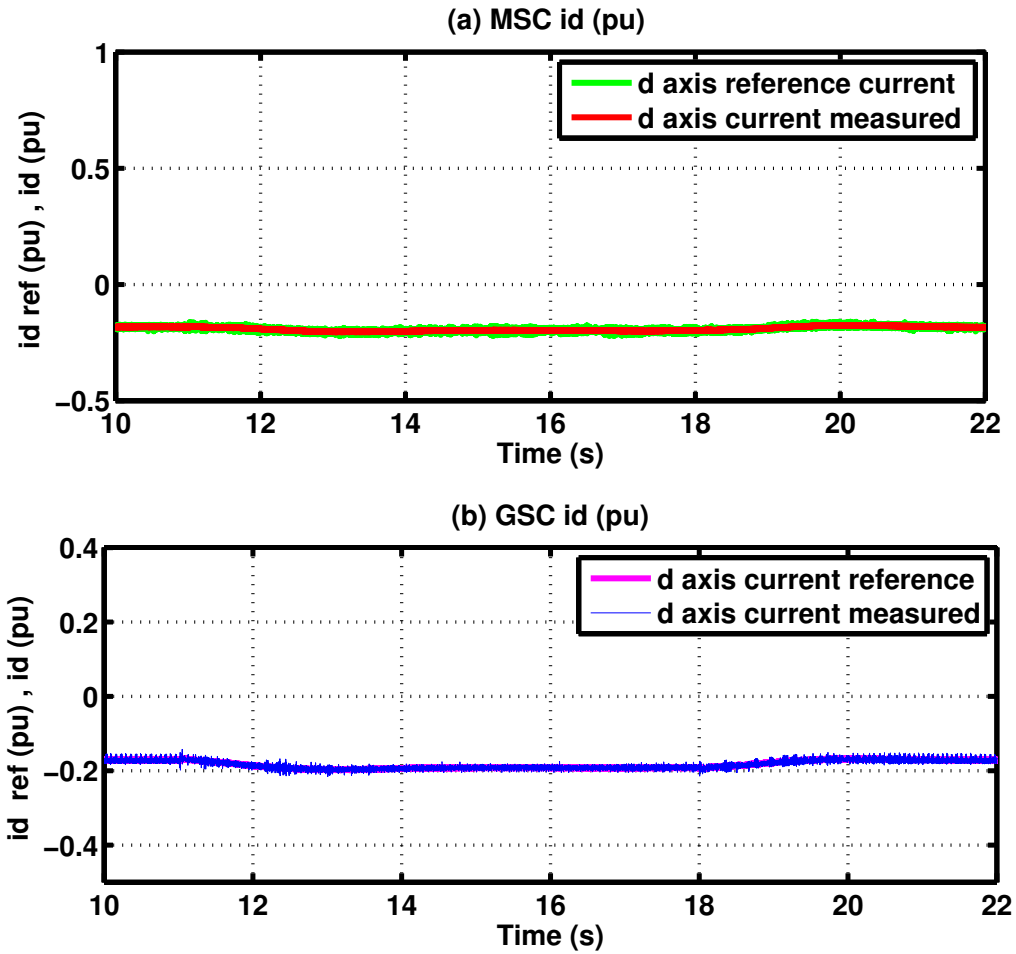
Figure 3.12: d - axis current references at MSC and GSC sides

increase in q-axis current at both MSC and GSC sides. The increase in active power flow is manifested as an increase in q-axis current and vice versa. Also, MSC and GSC side q-axis currents follow the respective q-axis current references generated by the corresponding upper-level controllers.

In Figure 3.12 (a,b), a marginal change is observed in the d-axis currents of the MSC and GSC sides as the change in wind speed directly affects active power flow. This shows that the decoupled current controller is working correctly, and variation in wind speed does not significantly affect the working of ac controllers in MSC and GSC.

3.5.2 Step Change in Dc Voltage Reference

Figure 3.13 shows the converter controller's dynamics in the machine and grid side. In Figure 3.13(a), (V_{dcref}) value has been changed to $2.8pu$ from $3pu$ at $11s$ and changed back to $3pu$ at $15s$. The dc chopper operation is turned off to study the system response without the chopper control.
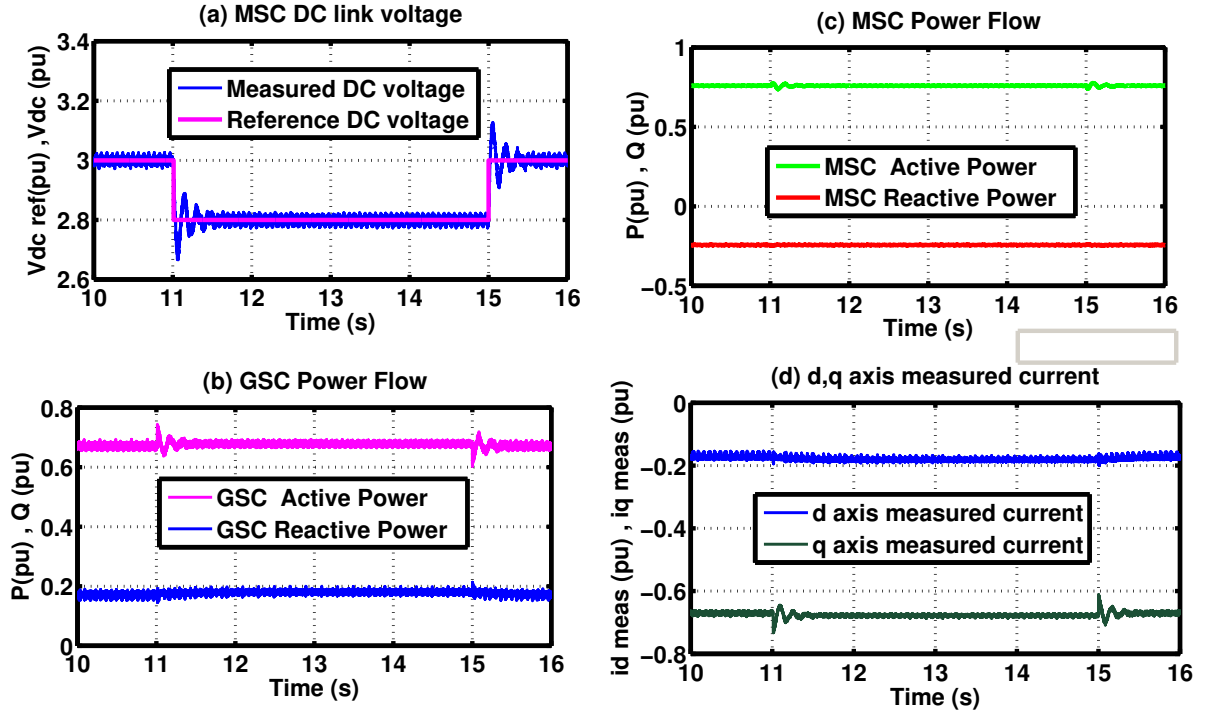
Figure 3.13: Response of MSC and GSC due to a step change in (V_{dcref})

As shown in Figure 3.13(b), at the instant when the dc voltage reference changes, there is a difference between measured dc-link voltage and (V_{dcref}), which results in error detection at the (V_{dc}) controller. To regulate the dc voltage to its set point, the V_{dc} controller transiently changes the active power flow at the GSC side as shown in Figure 3.13(a).

As the references for the MSC converter controller do not change, the active and reactive power flow remains constant in this step change operation, as shown in Figure 3.13(c). As V_{dc} controller affects the q-axis current of GSC, a more significant transient is observed in q-axis current as shown in Figure 3.13(d). The d-axis current reference remains unaffected, so the reactive power flow remains unchanged.

3.5.3   Step Change in Grid Side Ac Voltage Reference
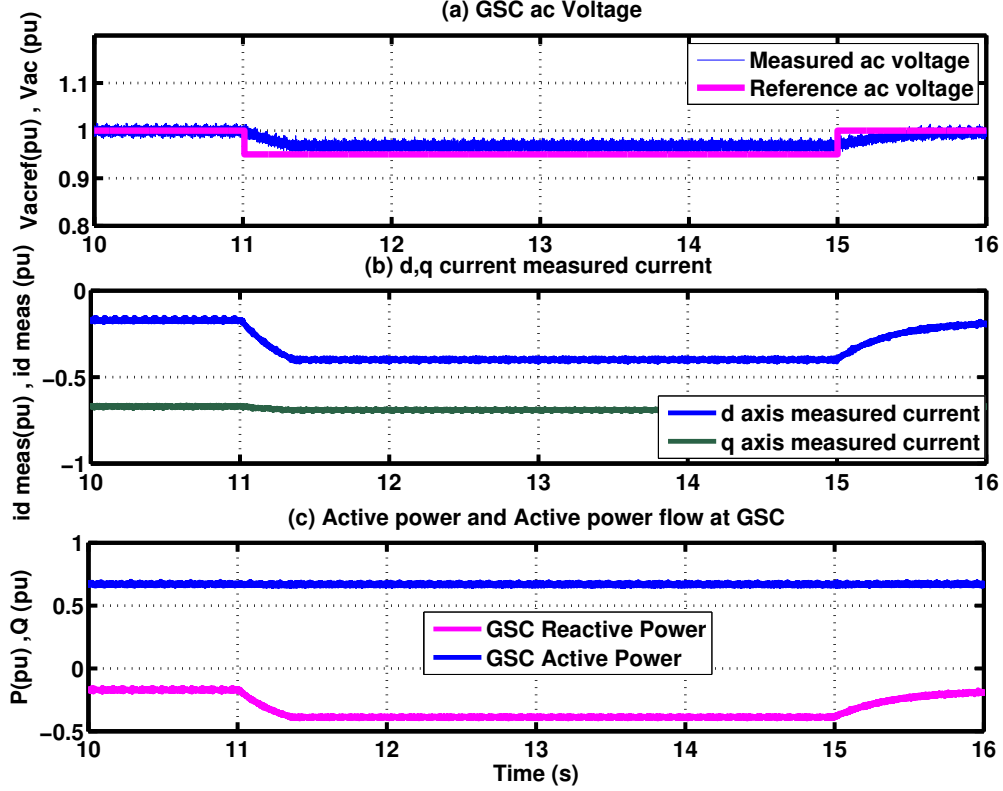
Figure 3.14: Step change in V_{acref}: (a) Grid side ac voltage variation (b) d-q current reference at GSC (c) Active power and Reactive power at GSC

At the time $t = 11$ s, the grid-side ac voltage reference (V_{acref}) is decreased by 5%, and subsequently, it returns to its initial value of 1 pu at $t = 15$ s as seen in Figure 3.14(a). When the (V_{acref}) at the GSC side is decreased, the ac controller observes the negative error and produces a decreased d-axis current reference (i_{dref}) (Figure 3.14(b)), resulting in the decrease of the reactive power value as shown in Figure 3.14(c). Figure 3.14c) proves the decoupled current controller action, which shows the independent working of inner loop controllers. Only i_{dref} is changed due to variation in V_{acref}, and no significant change in the q-axis current reference is observed.

3.6 Fault Behaviour of PMSG-based Wind Generator

A 3-phase line to ground fault is applied at the point of connection (POC), i.e. at BUS G as shown in Figure 2.6 around $t = 6$ s for six cycles. This section will show the importance of the dc chopper across the dc link.

As shown in Figure 3.15(a), as the MSC side has an active power controller, the fault does not affect the machine side power, and the rotational speed remains at its reference value of 1 pu. Due to the fault, the grid-side power (P_{grid}) approaches zero as depicted in 3.15(b).
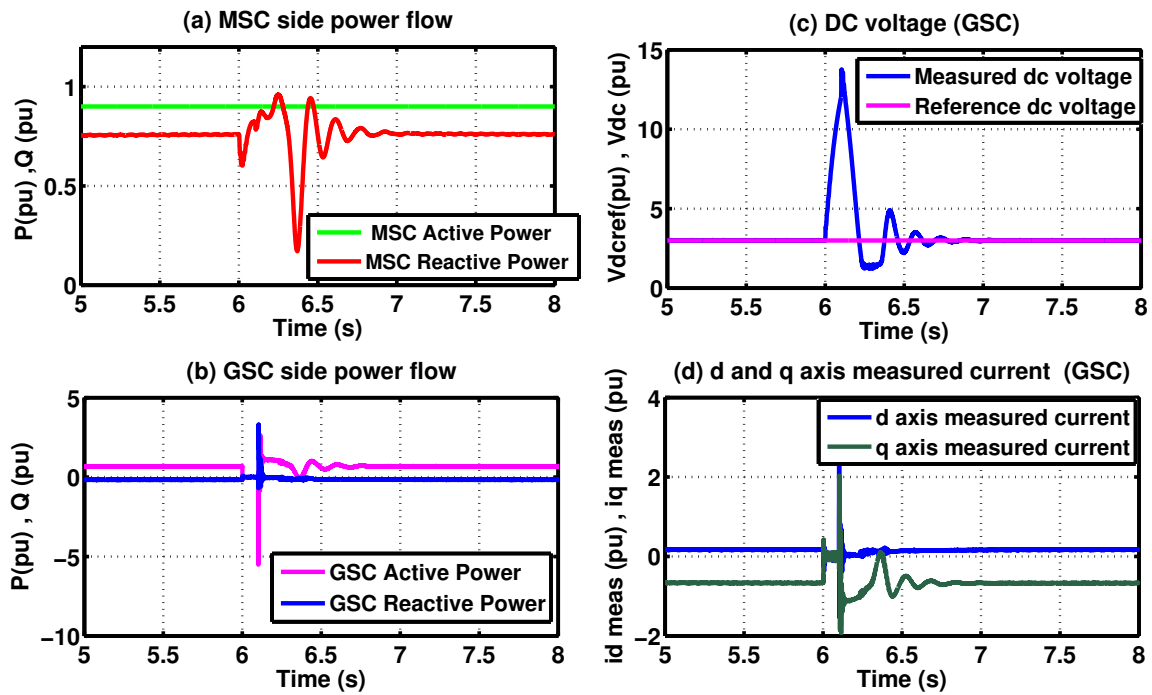
Figure 3.15: Active power and Reactive power at MSC and GSC; Speed control, dc control in GSC for active power control

As there is no change in power generation on the machine side, this creates a power imbalance. The chopper has been turned off to observe the severe effect. Figure 3.15(c) illustrates that as the power imbalance increases during the fault, all the extra power is dumped across the dc-link capacitor, increasing the voltage to around 11 pu.

This would cause the capacitor to burn out, and the generator would shut down. As the fault persists, the d-axis and q-axis references, representing the desired current components, reach their limit. A current limiter is employed to avoid exceeding safe levels and prevent damage. As soon as the fault gets cleared, active power, reactive power and the current references return to the original value, and PMSG successfully recovers. However, it should be noted that this recovery process is slower than the generator with fault ride-through capabilities, which will be discussed in Chapter 4.

3.7 Summary

This chapter has provided an overview of the characteristics of the Type 4 wind generator, the VSC-based BTB converter transmission, and the main components of a VSC transmission system in a PMSG-based wind generator. It has also delved into the signal generation, control system, and additional controllers used in a Type 4 wind generator.

The essential wind characteristics of the wind generator, the basic operating principles of VSC-based BTB transmission, and the main components of a back-to-back converter system in Type 4 wind generators have been presented. The generation of the signal through the Sinusoidal Pulse Width Modulation (SPWM) method and the control system of the BTB converter for a Type 4 wind generator have also been discussed. The chapter has further examined the workings of additional controllers, such as the maximum power point tracking (MPPT) controller. MPPT is a control algorithm that maximizes the wind generator's power output by continuously adjusting the rotor speed or blade pitch angle. In case studies, we have observed the use of a chopper across the dc link, a device that limits the dc link overvoltage during abnormal grid conditions.

Chapter 4

Implementation of Fault Ride-through Requirements in Simulation Model

4.1 Introduction

Vendors and system operators follow well-established grid codes[1] for the electric power system to maintain uniformity, economical maintenance and safe operation. Grid codes may differ based on geographic location and grid operators. A widely followed standard is the IEEE Std $1547 - 2018$, whose suggestions for fault ride-through capability are adhered to in this thesis. Hereafter IEEE Std $1547 - 2018$ is addressed as "IEEE 1547" [1]. The IEEE 1547 applies to all DER technologies in the electric power system (EPS). The electric power system may include one or more Distributed energy source (DER) units, supplemental DER devices and loads. DERs are small-scale generation and energy storage units which export power to the grid at typical primary or secondary distribution voltage levels. Resources like renewable energy like solar photo-voltaic, wind generators, electric vehicles, energy storage, fuel cells, and diesel or natural gas generators come under distributed energy resources.

---

[1]A technical document which suggests different settings for the electric power system's operation, maintenance, and development.

4.2 Assignment of Performance Categories of DER

IEEE 1547 [1] recommends the required operational capabilities of a DER during normal and abnormal operating conditions. The IEEE 1547 helps to specify the control mechanisms of DER performance during contingencies and to decide whether the DER will remain connected or disconnected from the grid [42] [43]. The DER's operation is categorized into two types of performance categories.

The first is the normal operating performance category[2], where the DER terminal voltage is between 0.88 pu and 1.1 pu. The grid frequency lies between 0.98 pu to 1.02 pu. During normal operating conditions, the operating regions for a DER continuous operation [3], are categorized as Category A and Category B. Categories A and B dictate standard operating characteristics of a DER, such as voltage regulation and reactive power capability requirements. Generally, a DER with performance Category A capability is not subjected to frequent disturbances and has a lower penetration level into the power grid. A DER, which comes under performance Category B, has all the operational capabilities of Category A. Additionally, it has supplementary capabilities that allow a higher penetration into the distributed system.

Any deviation from the continuous operation is considered an abnormal operating performance category. This second performance category dictates the capabilities of DERs in response to contingencies and is categorized as Category I, II, and III. All the categories are explained below.

The governing authorities assign performance categories I, II and III to DERs based on the primary power source type, power technology, DER application purpose, and integration level with the grid. Examples of abnormal performance Category I are Synchronous generators (hydro and engine/turbine-driven and fuel cell-based inverter sources). DERs such as inverters sourced by solar panels, wind generators and energy storage come under Category II, providing directions for stability/reliability over a broader range of contingencies. Category III settings for fault ride-through are assigned to the DER with a higher penetration level. This equips the DER with the capability to address concerns like system overloads, power quality, and operational reliability.

---

[2]Specified operational settings and technical capabilities during continuous operation.

[3]Continuous operation is when there is a prescribed active power flow between the DER and the grid while the voltage and system frequency is within a specified range

All performance categories specify designated limiting requirements for ranges of allowable settings of control with respect to nameplate ratings, i.e., nominal voltage, current, maximum active power, apparent power, reactive power, and trip parameter values and specify the minimum equipment capability requirements. Figure 4.1 summarizes a DER operation's performance categories.
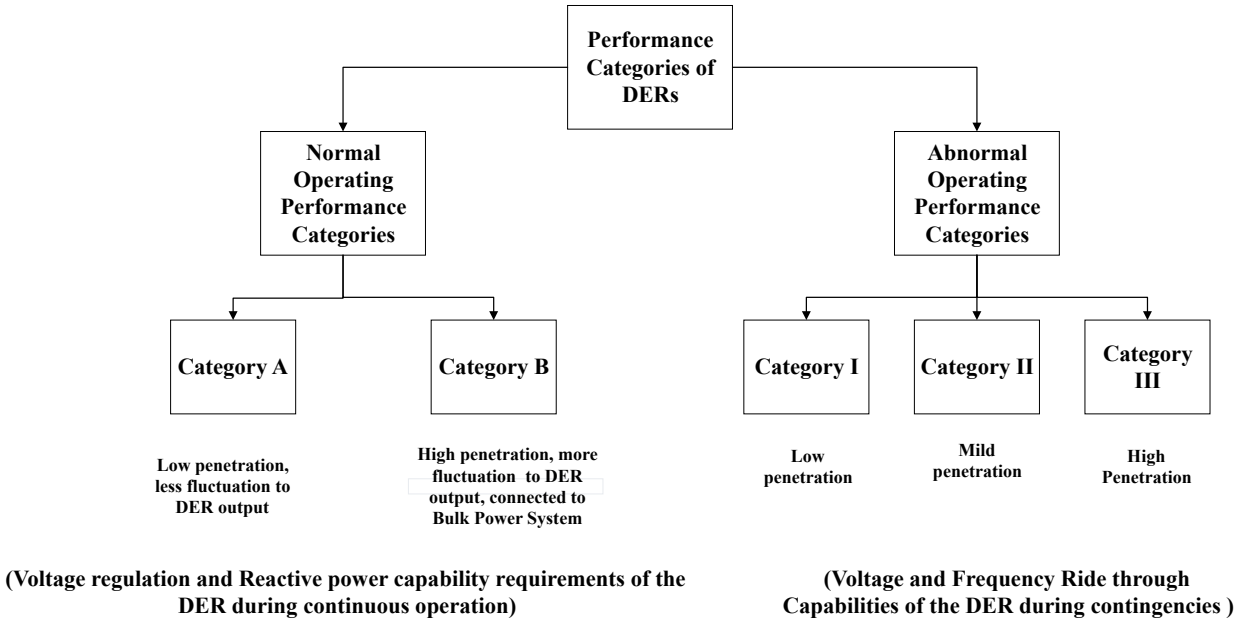
Figure 4.1: Types of Performance Categories as per the IEEE 1547

As there has been a significant increase in the contribution of renewable sources to power systems, integration of Type 4 wind generators comes under Category B during normal operating conditions, and wind energy follows fault ride-through requirements of Category II and Category III for abnormal conditions.

The assignment of the Category II and III requirements for wind energy depends upon the area electric power system (EPS) operator[4] [5][6] and authority governing interconnection requirements. In this thesis, we implement fault ride-through requirements for Category II in a 50 Hz system for the Type 4 wind energy generators.

---

[4]A responsible authority to design, build, operate and maintain the electric power system which consists of Local EPS(5) and Area EPS(6)

[5]a. Local EPS is an entity which may contain DER units, loads and supplemental DER devices.

[6]b. Area EPS is an entity which serves Local EPSs.

4.3 Voltage Ride Through

In the normal mode of operations, the DER is typically expected to operate at $+/-$ 10 percent of nominal voltage continuously. The power frequency variations should stay within the order of $+/-0.1Hz$ for less than $10s$. The accuracy of voltage regulation may also be specified, such as $+/-0.5$ percent of the set point value, i.e., the acceptable voltage range is usually $95-105$ percent. The power factor range is usually between -0.95 and 0.95. The active power is continuously supplied to the grid. [1]

During contingencies, voltage tends to deviate from its nominal value, creating an imbalance in power transfer between DER and connected loads. This often leads to instability. The IEEE 1547 has suggested two methods: (i) low voltage ride through (LVRT) and (ii) high voltage ride through (HVRT) to minimize voltage sag and voltage rise and maintain voltage during and after contingencies. The normal operating condition is where applicable voltage falls within the continuous operation range, i.e., where the DER must remain in operation and continue to deliver active power at the assigned pre-disturbance level of active power. Based on the applied voltage value during voltage disturbances, Tables 4.1, 4.2 and 4.3 specify the voltage range, minimum response, type of operation, and minimum ride-through time for Categories I, II, and III, respectively.

For example, in Category I (Table 4.1), when the terminal voltage (V) lies in the interval [0.88 pu, 1.1 pu], the DER performs as per normal operating condition, which is described above in this section. For a voltage (V) less than 0.50 pu and more than 1.20 pu, the DER is recommended to operate in 'cease to energize' mode up to the maximum specified time. It may imply disconnection, isolation, a temporary break, or a trip of the DER. Table 4.1 suggests the minimum ride-through times for the applied voltage (V) in the (1.175 pu, 1.20pu], (1.15 pu, 1.175pu], (1.10 pu, 1.15pu] as 0.2 s, 0.5 s and 0.16 s, respectively. When the applied voltage (V) is in the range of (0.88 pu, 0.7 pu], the minimum ride-through timer starts and follows the expression ($T_{lvrt}(s) = 0.7\,s + \frac{4.0\,s}{1\,pu}(V - 0.7\,pu)$). The detailed explanation of voltage ride through is explained in Section 4.5.1mm

Table 4.1: Voltage ride through requirements of abnormal operating performance Category I[1]

Voltage range (pu)	Operating mode/response	Minimum ride through time(s)(Design criteria)	Maximum response(s) (design criteria)
$V > 1.20$	Cease to Energize[7]	N/A	0.16
$1.175 < V \leq 1.20$	Permissive Operation[8]	0.2	N/A
$1.15 < V \leq 1.175$	Permissive Operation	0.5	N/A
$1.10 < V \leq 1.15$	Permissive Operation	1	N/A
$0.88 \leq V \leq 1.10$	**Continuous Operation**	**Infinite**	**N/A**
$0.70 \leq V < 0.88$	Mandatory Operation[9]	Linear slope of 4 s/1 p.u. voltage starting at 0.7 s @ 0.7 p.u. $T_{lvrt} = 0.7 + \frac{4s}{1pu}(V - 0.7pu)$	N/A
$0.50 \leq V < 0.70$	Permissive Operation	0.16	N/A
$V < 0.50$	Cease to Energize	N/A	0.16

Similarly, Table 4.2 and Table 4.3 give the voltage ride-through settings for Categories II and III. There are a few abnormal conditions where the above tables are not consulted, and the operator takes the corrective action, i.e. trip the DER or cease to energize it. The first instance is when the DER pre-disturbance power is below 10% of P_{rated}, and the local power system is intentionally islanded by disconnecting from the

---

[7]Active power delivery under steady-state conditions is halted. There is a limited reactive power exchange as specified, e.g., through inverter-based resources and filter banks.

[8]This operating mode responds to a disturbance of the applied voltages or the system frequency where the DER performs ride-through (voltage/frequency) either in mandatory operation or in momentary cessation.

[9]In this operating mode, there is a prescribed exchange of active and reactive current in response to a disturbance of the applied voltages or the system frequency.

[10]momentarily cessation means the DER is supposed to take a temporary break when faced with voltage/frequency disturbances. During the momentary cessation period, DER is still in connection with area EPS and can reinstate the operation immediately. Also, the voltage threshold between the mandatory and momentary operation can be set based on mutual agreements between the Area EPS and the DER operator.

Table 4.2: Voltage ride through requirements of abnormal operating performance Category II [1]

Voltage range (pu)	Operating mode/response	Minimum ride through time(s)(Design criteria)	Maximum response(s) (design criteria)
$V > 1.20$	Cease to Energize	N/A	0.16
$1.175 < V \leq 1.20$	Permissive Operation	0.2	N/A
$1.15 < V \leq 1.175$	Permissive Operation	0.5	N/A
$1.10 < V \leq 1.15$	Permissive Operation	1	N/A
$0.88 \leq V \leq 1.10$	**Continuous Operation**	**Infinite**	**N/A**
$0.65 \leq V < 0.88$	Mandatory Operation	Linear slope of 8.7 s/1 p.u. voltage starting at 3 s @ 0.65 p.u.: $T_{lvrt} = 3 + \frac{8.7}{1pu}(V-0.65)$	N/A
$0.45 \leq V < 0.65$	Permissive Operation	0.32	N/A
$0.30 \leq V < 0.45$	Permissive Operation	0.16	N/A
$V < 0.30$	Cease to Energize	N/A	0.16

Table 4.3: Voltage ride through requirements of abnormal operating performance Category III [1]

Voltage range (pu)	Operating mode/response	Minimum ride through time(s)(Design criteria)	Maximum response(s) (design criteria)
$V > 1.20$	Cease to Energize	N/A	0.16
$1.10 < V \leq 1.20$	Momentary Cessations[10]	12	0.083
$0.88 \leq V \leq 1.10$	**Continuous Operation**	**Infinite**	**N/A**
$0.70 \leq V < 0.88$	Mandatory Operation	20	N/A
$0.50 \leq V < 0.70$	Mandatory Operation	10	N/A
$V < 0.50$	Momentary Cessations	1	0.083

larger grid. The second instance is when within 0.1 seconds of the Distributed Energy Resources (DER) discontinuing their power supply to the Area Electrical Power System (EPS) and tripping, and the Local EPS load that demands active power equal

to or exceeding 90% of the pre-disturbance total active power output of the DER is shed.

4.3.1 LVRT Mode of Operation

In the early days, when wind energy resources were new, it was recommended to disconnect the wind energy system from the ac grid during a fault. As there has been a significant increase in the contribution of renewable sources to power systems, wind generators are equipped with voltage and frequency ride-through abilities, as discussed earlier. In such a case, the wind generators go to LVRT mode during grid-side disturbances and remain connected to the grid. Depending upon grid conditions, grid operators can set the exchange of active and reactive power values in the LVRT mode operation. The dynamic reactive power support is provided to the EPS by injecting reactive current to support fast voltage recovery. This mode also ensures rapid active power recovery after the fault. Section 4.6 presents detailed modelling and explanation of LVRT in the Type 4 wind generators. As discussed, this thesis implements Category II default settings for voltage ride-through for low and high-voltage disturbances in a 50Hz system. [1]

4.3.2 HVRT Mode of Operation

Overvoltage conditions occur due to contingencies like sudden load change, tripping of heavily loaded lines, lightning, etc., which can cause excessive current flow and damage the connected equipment. Overvoltage can be transient (e.g., a voltage spike) or permanent.

During overvoltage conditions, IEEE 1547 suggests following Table 4.1 for the abnormal operating performance of Category I [1]. Table 4.1 suggests that the voltage (V) falling in between 1.175 pu to 1.20 pu; 1.15 pu to 1.175 pu must operate within the minimum ride through time, which is 0.2 s, 0.5 s respectively. Similarly, Table 4.2 and Table 4.3 specify high voltage ride-through times for the abnormal operating performance of Category II and III, respectively. When the voltage exceeds 1.20 pu, DER ceases to energize afterwards for all the categories. The maximum response time given to trip in HVRT mode is 0.16 s.

4.4 Frequency Ride Through

Frequency Ride through (FRT) refers to the capability of the DER to maintain stable operation and ride through during contingencies which cause variations in grid frequency. The grid frequency may deviate from its intended value following disruptions such as faults or abrupt load changes, generation trips, etc. FRT capability improves the grid's stability by ensuring that the DERs can effectively adapt to changes in frequency as an immediate frequency control mechanism. It aids in maintaining a reliable and balanced power supply.

In a nominally 50 Hz ac grid, the continuous frequency operation range typically falls in $48.8 \leq f \leq 51.2$ (i.e., a dead band[11] of $+/-1.2$ Hz around the nominal frequency).DER of Category II and III must provide the frequency power operation for low-frequency conditions, whereas Category I based DER will have the choice to provide the frequency power operation or not. Table 4.4. provides the details for frequency ride-through requirements for the abnormal performance categories I, II and III. It suggests the DER's frequency range and operating modes during under-frequency or over-frequency deviations. For low-frequency conditions (47.0 Hz $\leq f < 48.8$ Hz), DER must follow the Eqn 4.1. During high-frequency conditions (51.2 Hz $< f \leq 51.8$ Hz), the DER shall have the capability to provide power-frequency droop operation as per Eqn 4.2. The DER should trip for frequency values above 52.0 Hz and below 47.0 Hz. [1]

The FRT action will be discussed in detail in Section 4.5.2. To activate the FRT ability in the DER connected to the local EPS, the voltage at PCC must be within the ride-through range, which is given in Tables 4.1, 4.2 and 4.3.

$$p = min_{f<50-db_{UF}} \left[\ p_{pre} + \frac{(50-db_{UF})-f}{50.k_{UF}}; p_{avl} \ \right] \qquad (4.1)$$

$$p = min_{f<50+db_{OF}} \left[\ p_{pre} + \frac{f-(50+db_{OF})}{50.k_{OF}}; p_{min} \ \right] \qquad (4.2)$$

Where,

p is the active power output of the DER, per unitized using the nameplate rating

f is the system frequency during a disturbance in Hz

p_{avl} is the available active power per unitized using the DER rating.

---

[11]Dead band is the frequency/voltage range in which DER is in continuous operation.

Table 4.4: Frequency ride through of abnormal operating performance Category I, II, III [1]

Frequency range (Hz)	Operating mode	Minimum time(s)(Design criteria)
$f > 52.0$	No ride-through requirements apply to this range	
$51.2 < f \leq 51.8$	Mandatory Operation	299
48.8 ≤ f ≤ 51.2	**Continuous Operation**	**Infinite**
$47.0 \leq f < 48.8$	Mandatory Operation	299
$f < 47.0$	No ride-through requirements apply to this range	

p_{pre} is the pre-disturbance active power output (pu) at the instant just before the frequency exceeds the dead band.

p_{min} is the minimum active power below which the DER is not connected to the EPS.

db_{OF} and db_{UF} are the single-sided dead band limits for low-frequency and high-frequency, respectively, in Hz

k_{OF} is the per-unit slope of the power-frequency droop characteristic when the frequency is low

k_{UF} is the per-unit slope of the power-frequency droop characteristic when the frequency is high.

4.5 Fault Ride-Through Capabilities of Type 4 Wind Generators

This section evaluates the voltage and frequency ride-through capability of a Type 4 wind generator using a PSCAD test case. IEEE 1547 suggests having fault ride-through capabilities in the DER to ensure the reliable and secure integration of renewable energy sources into the power grid. By actively participating in grid support, wind generators with FRT capabilities contribute to grid stability, increase the reliability of the overall power system, and facilitate the integration of more renewable energy generation. In this section, fault ride-through techniques outlined in IEEE 1547, such as low/high voltage ride-through and frequency ride-through capabilities,

are incorporated in the Type 4 permanent magnet synchronous generator (PMSG) based wind energy conversion system. A Type 4 wind generator is a popular wind energy conversion system connected to the grid through power electronic converters. These converters enable the turbines to efficiently convert the wind generator's variable speed and variable frequency output into a stable ac power output that matches the grid frequency. By employing fault-ride through control strategies, wind generators can adjust their converter operation to support the grid and actively mitigate voltage and frequency deviations. Chapters 1 and 2 explain all the details of PMSG-based Type 4 wind generators.

The section 4.5.1 explores the voltage instability, system operation with different short circuit ratios, and operation of the dc chopper in a Type 4 wind generator during the abnormal condition. Electromagnetic transient simulations are used to assess the voltage ride-through modes. The chapter describes how the control method of wind generators is adapted to ensure grid-code adherence.

Next, the effect of frequency-based power modulation on grid stability is also investigated in section 4.5.2. The primary purpose of fault ride-through operation is to maintain voltage by providing sufficient reactive power support and to achieve grid frequency through the frequency droop method during and after the fault.

4.5.1   Voltage Disturbance Ride Through Capability Test (LV RT and HVRT)

This section investigates the wind generator's voltage ride-through capability during grid disturbances and its impact on the voltage of the weak grid. The behaviour of the machine and grid side converter, dc chopper operation, etc., are analyzed during voltage ride-through operation. Table 4.2 is incorporated for LVRT and HVRT operation. The LVRT and HVRT operation logic is implemented using a FORTRAN-based customized model in PSCAD (Appendix B and C).

4.5.1.1   Case Study Details

Figure 4.2 shows the Type 4 wind generator test system used for the case study. The wind generator generates a 1 kV voltage, and a step-up transformer steps the voltage to 11 kV for the medium voltage transmission. The transformer's High Voltage (HV) side is connected to the 69 kV grid via a 40 Km long-distance transmission line. A

single wind generator is rated at 2 MW, and five wind generators contribute 10 MW of active power. As shown in Figure 4.2, an aggregate model of the modelled wind generator is simulated, equivalent to assuming five identical wind generators with the same prime mover powers. The grid impedance is represented as a series R-L circuit.

Type 4 Wind Generator
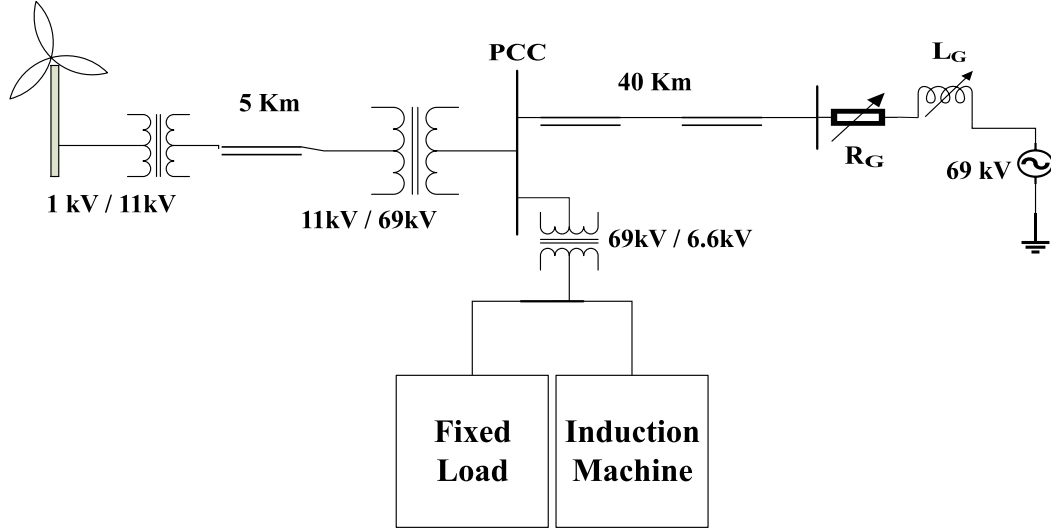
Figure 4.2: System 1: Type 4 wind generator connected with grid

The wind generator parameters are shown in Table 4.5. A total load of 14 MW is connected to the PCC bus. The total load consists of an induction motor load of 11 MW and a constant impedance load of 3 MW. Table 4.6 shows the induction motor load parameters. This simulates a practical situation with a mix of static and motor loads. The motor also creates a more challenging voltage control scenario, as after a fault, the voltage can be depressed for a longer duration[44].

The details of the controller structure are discussed in Chapter 3. The wind generator is a PMSG-based Type 4 wind generator, and the schematic diagram for the controller is shown in Figure 4.3. It is a similar figure from Chapters 2 and 3 but is repeated for convenience. The ac grid is represented by a simple voltage source behind the impedance model. The grid impedance is a series R_G and L_G circuit. The values of R_G and L_G are changed to generate different Short Circuit Ratios (SCR) of the grid to create strong and weak grid scenarios [45] [46]. The SCR value is calculated as per Equation 4.3, where V_{base} is the nominal grid voltage and Z_{grid} is

TYPE 4 WECS (PMSG with BTB Converter)
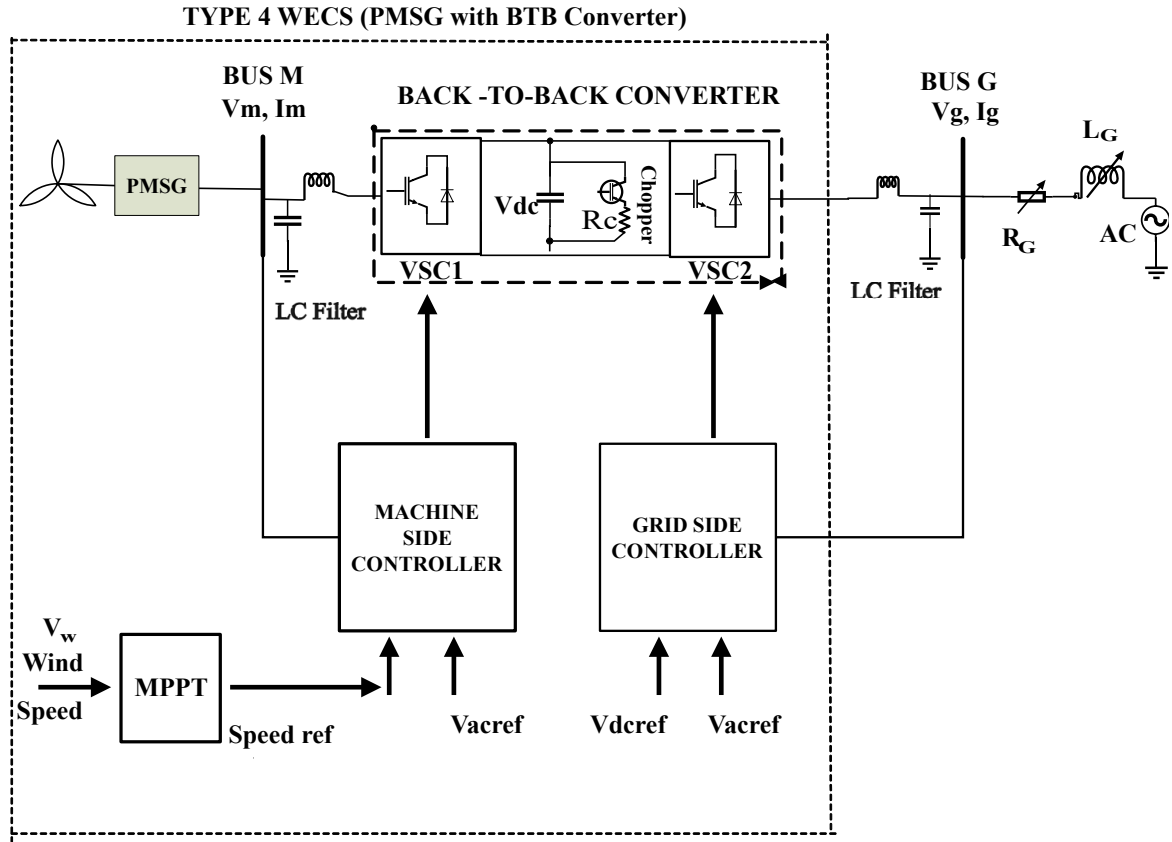
Figure 4.3: Basic design of converter based wind generator with PMSG

the grid impedance, and S_{base} is the rated MVA of the grid. So, by changing the grid impedance value, the SCR of the grid can be changed. In this case study, the grid is rated at 80 MVA and $V = 69$ kV is used. The X/R ratio of 10.0 is used to calculate the R_G and L_G grid impedance circuit. Note that transmission line impedance is included with grid impedance for SCR calculation.

$$SCR = \frac{\frac{V_{base}^2}{|Z_{grid}|}}{S_{base}} \tag{4.3}$$

where $|Z_{grid}| = \sqrt{(R_G^2 + X_G^2)}$, R_G and X_G represents resistance and reactance of the grid impedance respectively.

56

Table 4.5: The wind generator parameters (K_p:Proportional Constant, T_i:Integral Time Constant)

MSC Controller	ac Voltage controller : Kp=1 pu/pu, Ti=0.1 pu/pu-sec
	Speed Controller : Kp=2 pu/pu, Ti=0.07 pu/pu-sec
	PLL parameter : Kp=50 pu/pu, Ti=0.002 pu/pu-sec
GSC Controller	ac Voltage controller : Kp=0.66 , Ti=30.23 pu/pu-sec
	dc link Voltage Controller : Kp=0.321 , Ti=0.1097 pu/pu-sec
	PLL parameter : Kp=50 , Ti=0.002 pu/pu-sec
PMSG parameters	Rated Voltage : 1 kV
	Rated MVA : 2 MVA
	Rated frequency : 50 Hz
	Stator Winding Resistance : 0.017 pu
	Stator Leakage Reactance : 0.064 pu
	D axis reactance (Xd) : 0.55 pu
	Q axis reactance (Xq) : 0.11 pu
	D-Damper winding resistance : 0.055 pu
	D-Damper winding reactance : 0.62 pu
	Q-Damper winding resistance : 0.183 pu
	Q-Damper winding reactance : 0.175 pu
	Angular Moment of Inertia : 0.7267 sec

Table 4.6: Induction Motor Data

Induction Motor	Rated Voltage : 6.6 kV
	Rated MVA : 3.73 MVA
	Rated frequency : 50 Hz
	Stator/rotor turn ratio : 2.637687
	Angular Moment on inertia : 2.6 sec
	Mechanical Damping : 0.01 pu
	Stator resistance : 0.0054 pu
	Wound rotor resistance : 0.00607 pu
	Magnetizing Reactance : 4.362 pu
	Stator leakage reactance : 0.102 pu
	Wound rotor leakage reactance : 0.11 pu

4.5.1.2 LVRT Capability Test

a. Control of Type 4 wind generator During LVRT

Due to the high penetration of Type 4 wind generators into the grid, the capa-

bilities of the Type 4 wind generator fall under Category B for normal performance operation and Category II for abnormal performance. The voltage ride-through requirements for a Category II system are given in Table 4.2, and details are discussed in Section 4.3. A detailed flow chart representation can be developed from Table 4.2 and is shown in Figure 4.4. This algorithm makes decisions based on the RMS voltage of the PCC bus.

According to the flow chart, the system is in its normal operation region when the PCC voltage is in the nominal range of (0.88 pu $\leq Vpcc \leq$ 1.1 pu). The contingencies such as faults and load change lead to voltage sag. If the PCC voltage goes below 0.88 pu, the LVRT control mode is triggered. It helps to improve the PCC voltage and causes quick voltage recovery. This is achieved by modifying the functionality of the grid side converter (GSC) to prioritize the reactive power as soon as LVRT mode is detected. The GSC is responsible for the reactive power exchange between the wind and grid systems. To do this, the outputs of upper-level controllers (i.e.,V_{dc} controller and V_{ac} controller) are frozen at their values just before the fault. As mentioned in Chapter 2, the dq transform convention is used here. With the orientation of the dq frame, the active power is controlled by q-axis current reference (i_{qref}), and reactive power by the d-axis reference current (i_{dref}). In some implementations, i_{dref} can be set as per the system's requirement, and then i_{qref} is computed as (i_{qref})= $\sqrt{(i_{max})^2 - (i_{dref})^2}$). However, the LVRT model in the thesis gives importance to reactive power support during LVRT mode. (i_{qref}) is set to 0.0 pu, and the reactive current order (i_{dref}) is set proportional to the RMS ac voltage error, i.e.,

$$i_{dref} = K(V_{ac-ref} - V_{ac}) \tag{4.4}$$

so that a larger voltage deviation results in more reactive power generation, to restore the voltage. Giving more importance to reactive power during LVRT will help in faster recovery from voltage sag.

During LVRT mode operation, only the GSC control is prioritized as above, but the machine-side converter's (MSC) control remains in the ac voltage and wind speed control mode. The control algorithm also calculates a time delay (T_{LVRT}) which depends on the PCC voltage level. If the system does not recover within this time (T_{LVRT}), the controller sends a trip signal to the main breaker of the wind generators. The time delay decreases as PCC voltage increases. If the PCC voltage goes to 0.2 pu or below, (T_{LVRT}) is set to zero, and the controller instantly sends the trip
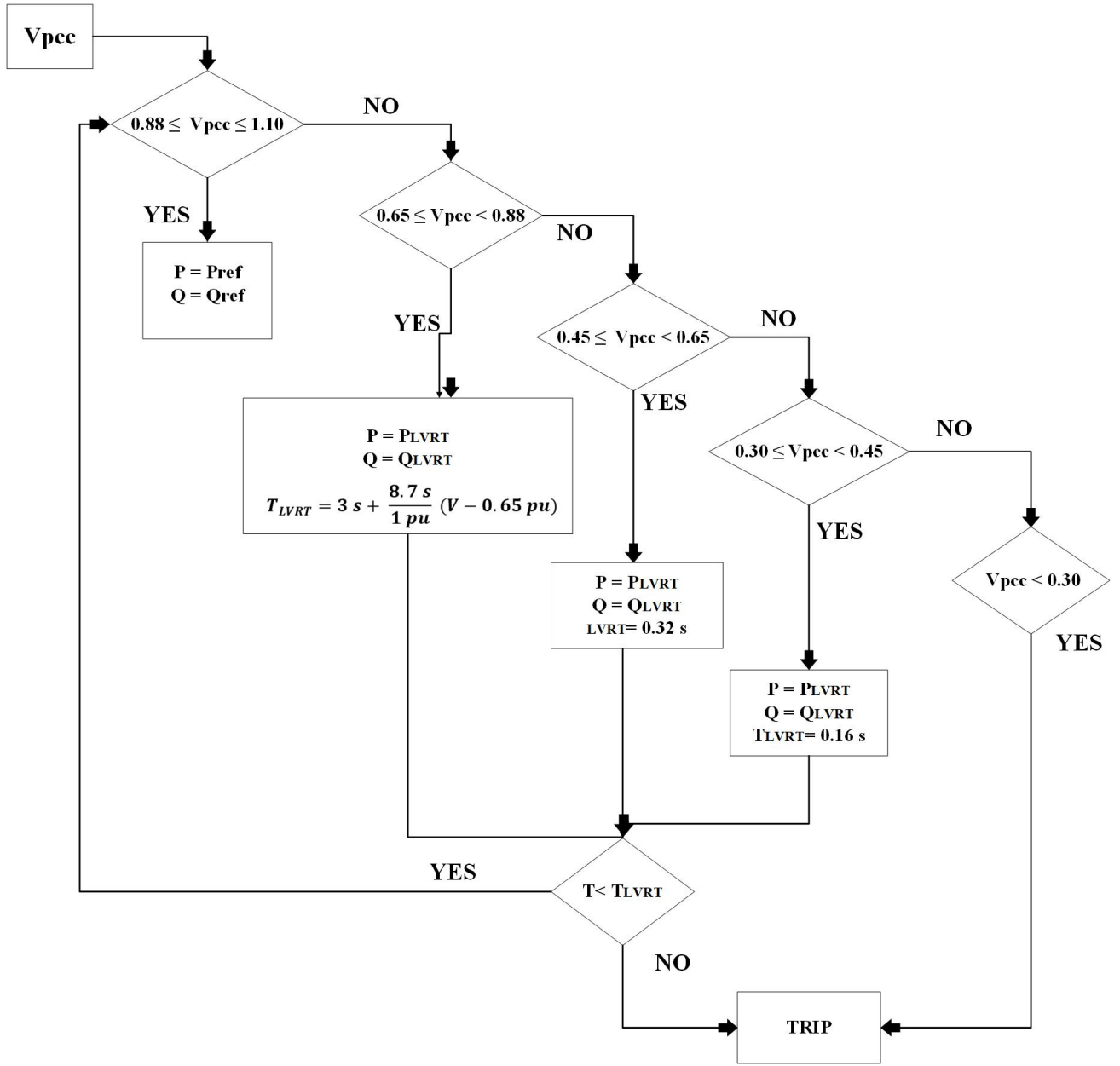
Figure 4.4: Flow chart for LVRT mode detection in Category II

signal. To conduct the LVRT studies, the author developed a Category II-based customized LVRT controller component specific to the Type 4 wind generator. It calculates the voltage-dependant time delay (T_{LVRT}) and sets the priority d and q current orders described in the previous paragraph. A counter counts the elapsed time (T) to generate the trip signal if T exceeds T_{LVRT}. The counter is reset to

59

zero when the wind generator comes out of the LVRT mode. The code is listed in Appendix B.

b. Study and analysis of the LVRT mode

The models for the LVRT controllers were discussed in the previous sections. This section discusses how they can be effectively used for riding through faults. The test system shown in Figure 4.2 is simulated in PSCAD. A disturbance of a two-phase to ground (AB-G) fault of 12 cycle duration is applied at $t = 7$ s at the midpoint of the grid side 69 kV transmission line. The reason for selecting this particular type of disturbance is to create a voltage sag at the PCC bus of the wind generator, which will trigger LVRT and also allow the wind generator to stay and ride through the fault.

i. Scenario 1: Effectiveness of special control of GSC during LVRT

As discussed in Section 4.5.1.2, during LVRT, the GSC goes to a reactive power priority control mode where the GSC is ordered to provide zero active power and controlled reactive power during the LVRT event. The test system is simulated with a grid SCR of 2.1 with normal operational GSC control and LVRT mode with reactive power priority control.

As shown in Figure 4.5, the PCC voltage plot indicates that without LVRT control, the PCC voltage (V_{pcc}) remains in a low voltage condition and fails to recover to its normal operating range of [0.88 pu,1.1 pu] after the fault. On the other hand, with LVRT mode, the system successfully recovers from the fault in about 1.575 s. This shows the benefit of LVRT reactive power priority control, which helps voltage recover in weak systems. As soon as the fault is cleared, the induction motor draws a large amount of reactive power, which is the cause of the voltage dip during fault recovery. With LVRT mode with reactive power priority control, the wind generator provides reactive power support, which helps to bring the system back to normal operation. The operation of the LVRT mode when connected to an ac network of different SCRs is studied in subsequent scenarios.

ii. Scenario 2 : Relatively Strong System

Scenario 2 uses the test system with an SCR value of 3.2. Figure 4.6 shows the LVRT response of the wind generator in a relatively stronger system, (a) ac voltage of the PCC, (b) LVRT enable signal and (c) active and reactive powers.

60
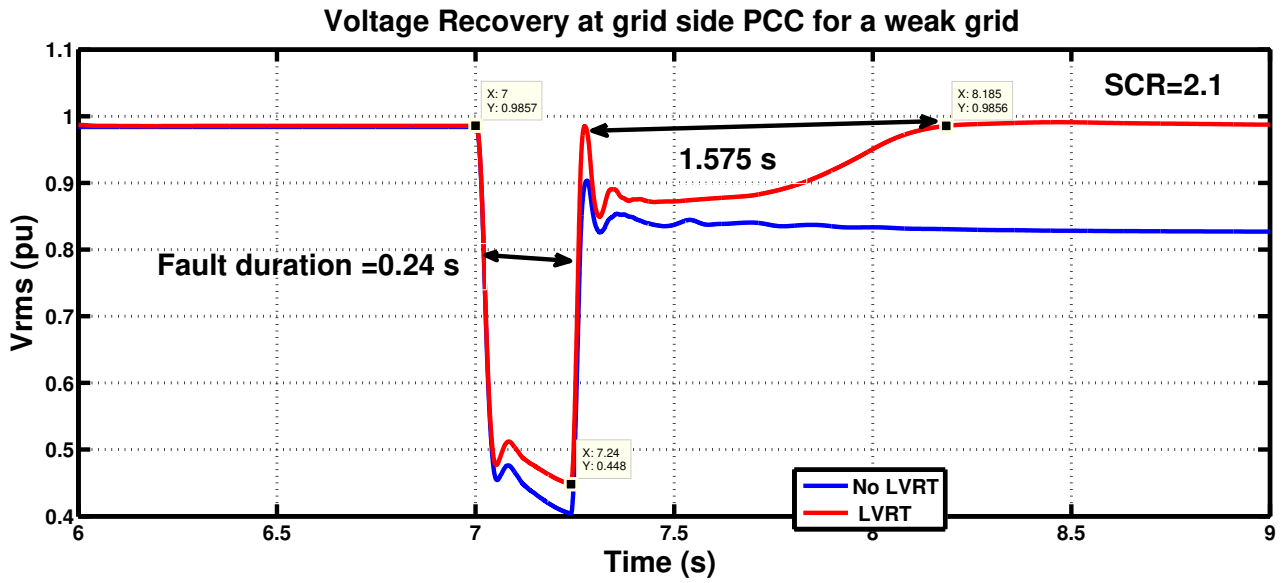
Figure 4.5: Voltage Recovery at PCC (Weak grid) with without LVRT control
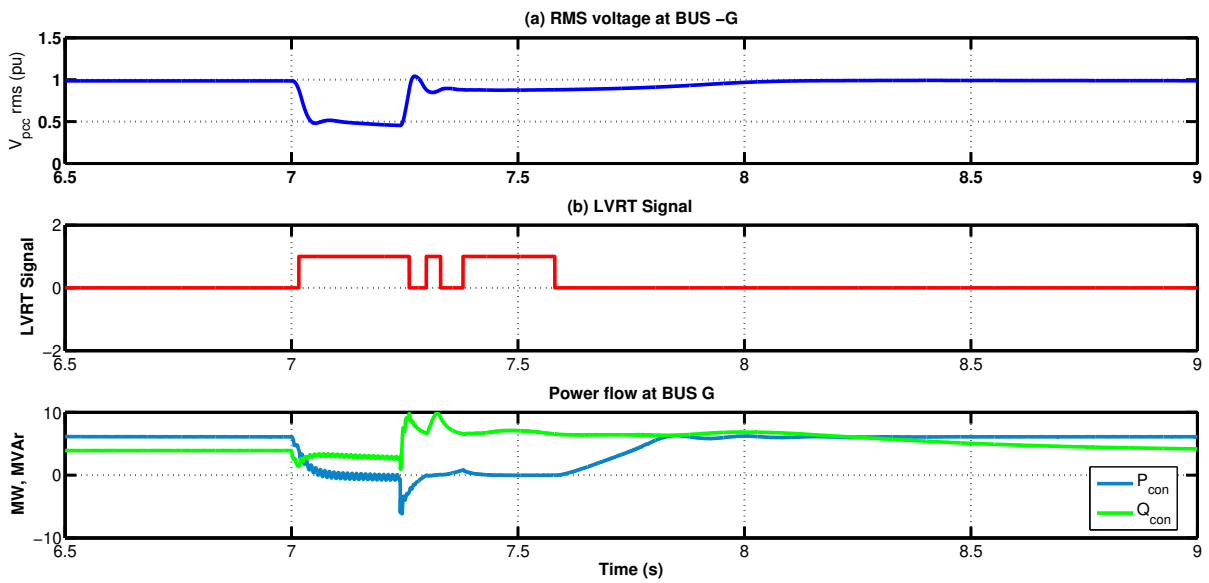
Figure 4.6: Plot for LVRT operation (Scenario 2)

Due to the fault at $t = 7$ s, the PCC voltage value drops to around 0.5 pu, triggering the LVRT mode. During the fault, the grid side converter remains in LVRT mode, and as soon as the fault is cleared at $t = 7.24$ s, the PCC voltage

quickly returns to about 0.9 pu and then to 1 pu in about 1.3 s. During the fault, due to the low voltage condition, power consumption of the induction motor and constant impedance loads decreases; hence, the induction motor speed also decreases. As soon as the fault is cleared and the PCC voltage reverts to normal, the induction motor speed increases and the power consumption of the motor and fixed impedance load increases. During this time, the induction motor draws a lot of reactive power, which causes the PCC voltage to decrease below 0.88 pu. This drop in PCC voltage activates the LVRT mode for a specific time per the voltage ride-through criteria as mentioned in Section 4.2, and the system slowly returns to normal operation.

As seen in Figure. 4.6 (c), during LVRT mode, the wind generator GSC controller goes into a different control mode, reduces the active power to zero and provides reactive power support to the grid. This reactive power flow is decreased as PCC voltage improves. This confirms the ability of the LVRT controller response to ensure that the wind generator successfully rides through and recovers from the fault. On fault clearance, there is a momentary reversal of power which causes the dc capacitor to overcharge, resulting in a transitory spike. This is likely due to the fact that the PLL is incorrectly tracking the phase at the instant of fault removal. Generally, a surge arrestor would be present, limiting this spike, but this was not included in the model.
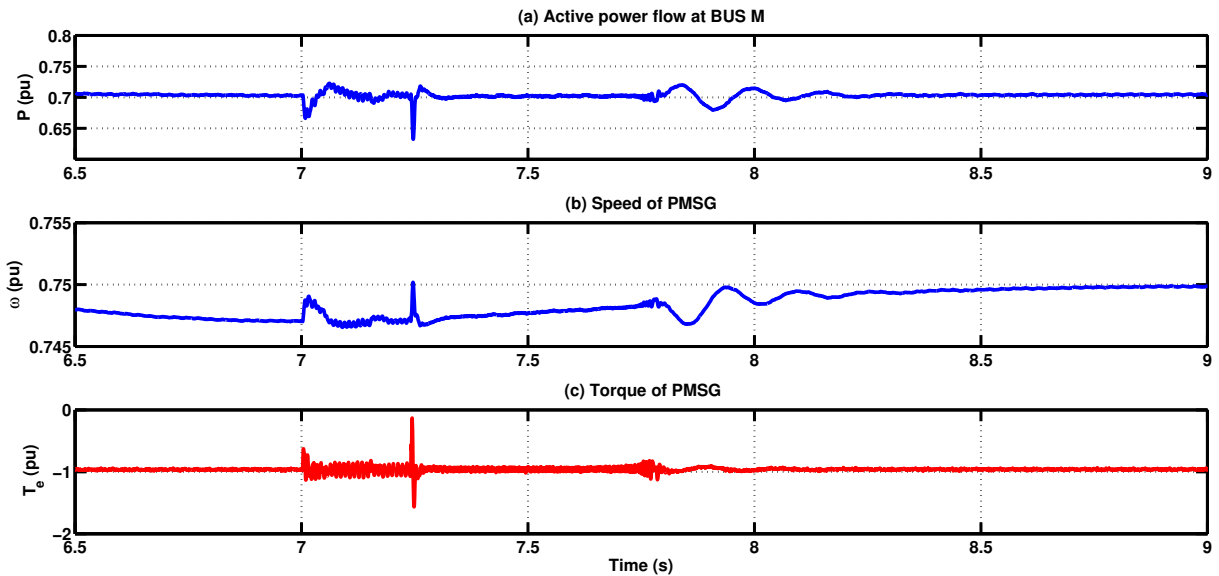
Figure 4.7: MSC response plot for LVRT operation (Scenario 2)

Figure 4.7 shows the plots of the response of the machine side converter, (a) active power flow from MSC, (b) speed of PMSG, and (c) torque of PMSG. The response plot in Figure 4.7(c) shows that the grid side disturbance does not create any significant transients in the operation of the machine side converter in the Type 4 wind generator. As discussed in Chapter 2, this is due to the dc link voltage, which remains within the maximum limit of 3.45 pu during fault and LVRT operation. This operation can be explained as follows. In a Type 4 wind generator, MSC and GSC are coupled via a dc link capacitor. During the fault and the subsequent period of LVRT mode operation, the active power output of the grid side converter is zero. The dc capacitor absorbs the total power coming from the MSC, which causes the rise in the dc link voltage, as shown in Figure 4.8 (a).
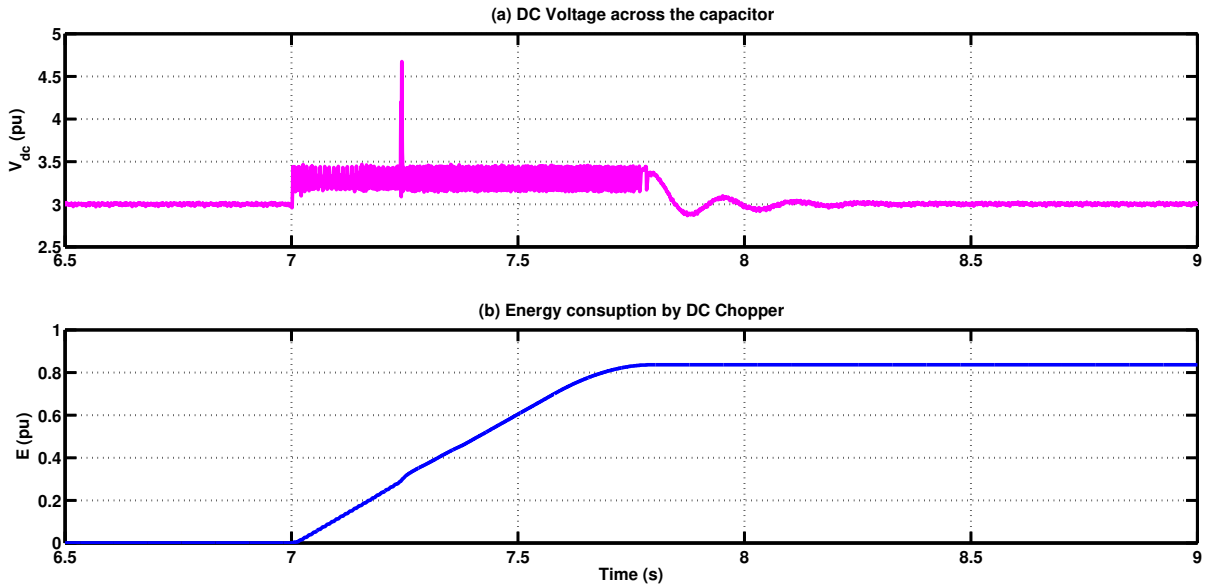
Figure 4.8: Dc link voltage and dc chopper energy response for LVRT operation (Scenario 2)

As the dc link voltage goes above 3.1 pu, the dc chopper gets activated and limits the dc link voltage rise by dissipating power coming from the MSC, as can be seen from the plot showing the energy consumed by the dc chopper. In this scenario, the wind generator does not trip even though the wind generator enters the LVRT mode multiple times. This is because the time duration in which the wind generator remains in LVRT mode does not exceed the tripping time for the LVRT operation,

as given in Table 4.2

iii. Scenario 3: Relatively Weak System

The grid side SCR is changed to 1.8 to create a weak system. The test system is simulated using PSCAD, and a similar 12-cycle fault (AB to ground) is applied at $t = 7$ s at the midpoint of the 69 kV transmission line. The PCC voltage and GSC response plots are shown in Figure 4.9. Due to the weak system behaviour, the voltage remains below 0.85 pu even after the fault is cleared, as shown in Figure 4.9 (a). As per Table 4.2, the LVRT tripping time for the voltage 0.85 pu is 4.74 s. This is validated by Figure 4.9(b), where the wind generator enters LVRT mode at $t = 7.2$ s and gets tripped at time $t = 11.9$ s.
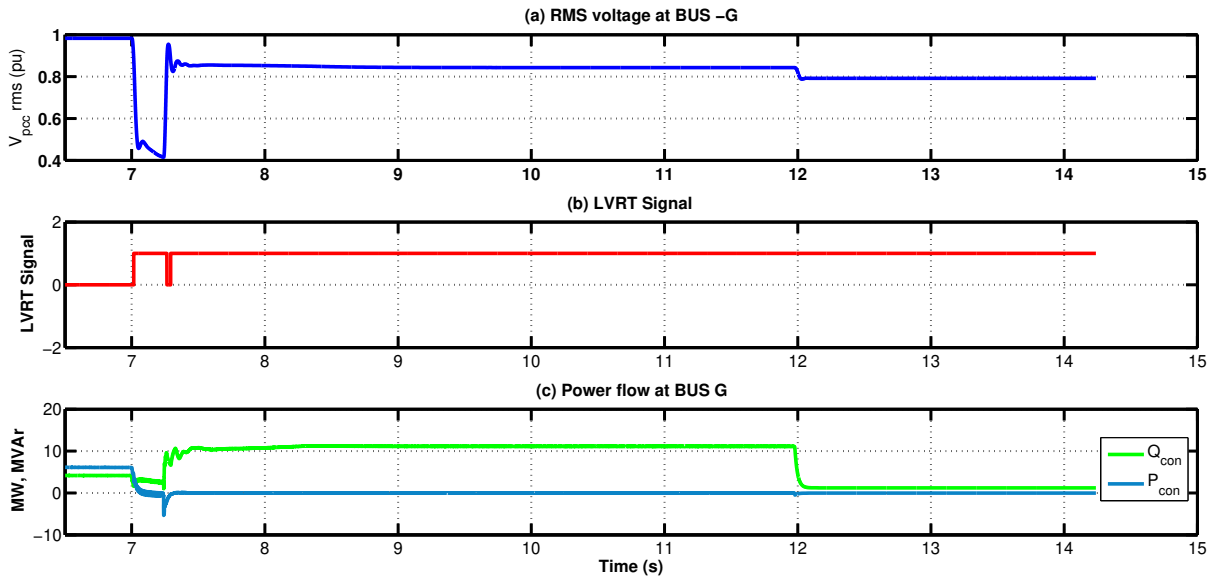
Figure 4.9: wind generator response for LVRT operation (Scenario 3)

iv. Scenario 4: wind generator behaviour during LVRT for different SCR conditions of the grid

In scenario 4, the SCR of the grid is varied from 3.5 to 1.8 (from relatively strong to weak). The SCR is achieved by choosing an appropriate grid impedance ($Z_{grid} = R_G +jX_G$) as mentioned in Equation 4.3. A similar kind of fault (AB-G for 12 cycles) is applied at $t = 7$ s for each SCR condition, and wind generator behaviour is observed. The PCC voltage plot is shown in Figure 4.10. Figure 4.10 shows that as the system
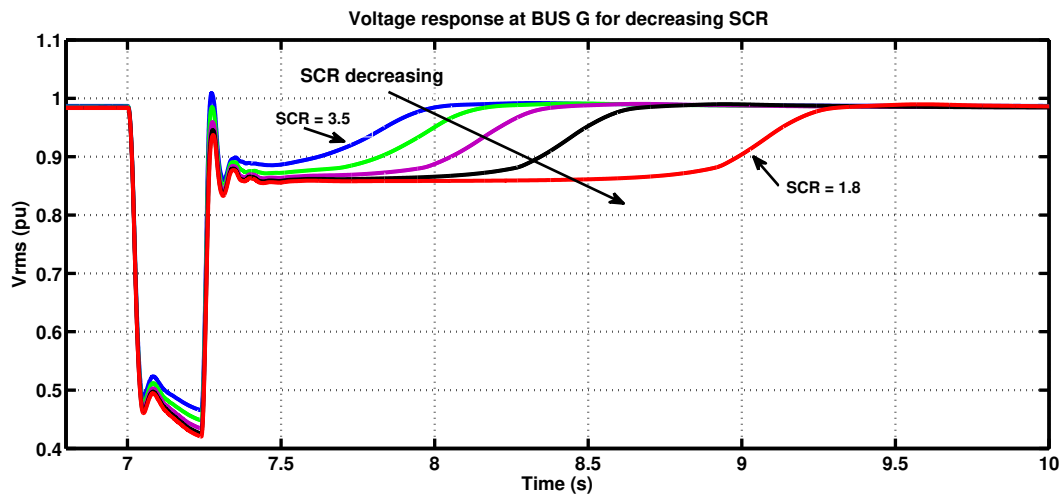
Figure 4.10: Voltage response at PCC for decreasing SCR.
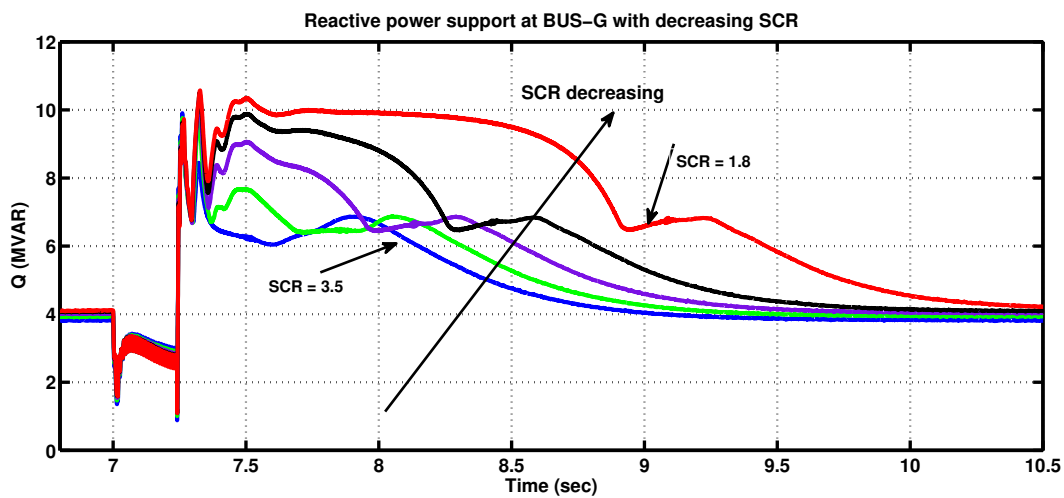
Figure 4.11: Reactive power support at PCC with decreasing SCR

weakens, fault recovery and the voltage sag at the PCC last longer, and the wind generator remains in LVRT mode for more time. As mentioned before, during LVRT, the GSC's active power order is reduced to zero, and the GSC only provides reactive power support. This can be seen from the GSC converter's plot responses to reactive and active power flow, as shown in Figure 4.11 and Figure 4.12, respectively. The lower the SCR value, the more reactive power is generated by the GSC of the wind generator. Due to sluggish fault recovery of the system as the grid becomes weak, the larger the time for which the wind generator remains in the LVRT mode and

65
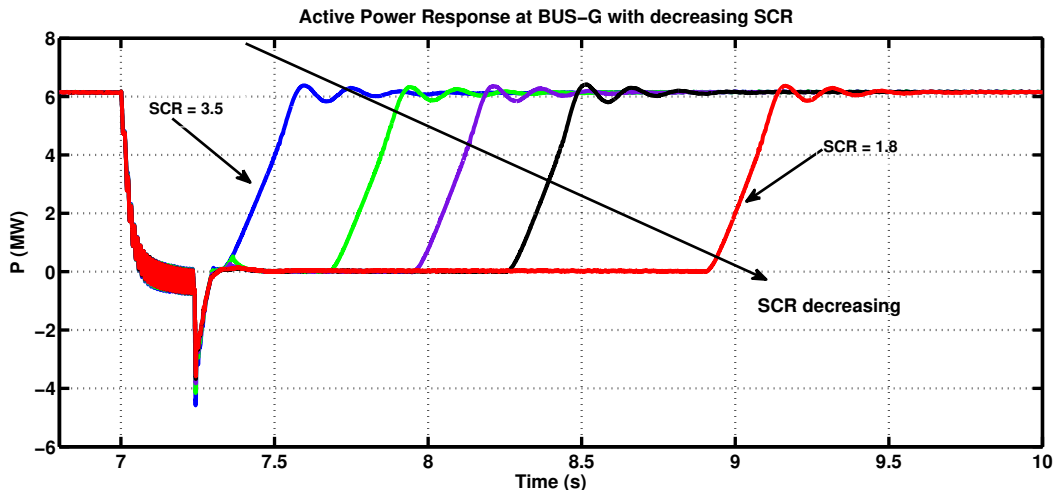
Figure 4.12: Active power Response of wind generator with decreasing SCR
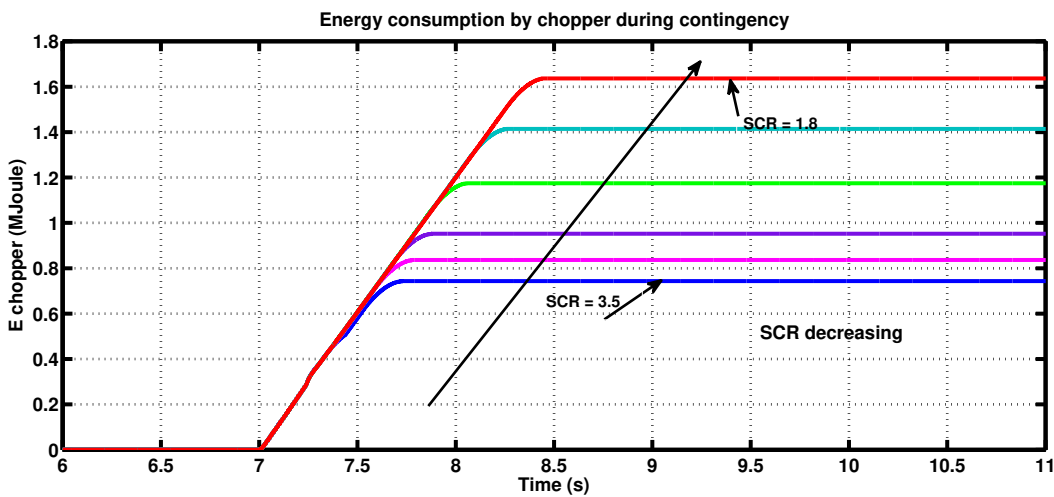
Figure 4.13: Energy consumption by chopper during contingency

subsequently in zero active power mode. This adds more stress to the dc chopper due to the additional heating as it dissipates the energy imbalance between MSC and GSC. This can be seen from the dc chopper energy plot as shown in Figure 4.13 as SCR decreases, the energy dissipation by the dc chopper increases.

4.5.1.3 HVRT Study Result and Analysis

IEEE 1547 recommended HVRT default settings are implemented in a custom model for the Type 4 wind generator. During HVRT mode, the GSC stays in its normal control mode and does not go into reactive priority control. As the PCC voltage exceeds 1.2 pu, the wind generator enters HVRT mode. Similar to LVRT mode, if the time duration in HVRT mode exceeds a voltage-dependent timing threshold, as given in Table 4.2, an appropriate signal is generated to trip the GSC side ac breaker. Two scenarios are used to show the HVRT capability of the wind generator. In one scenario, less severe voltage disturbance is considered, and the wind plant successfully rides through the disturbance, whereas in another scenario, the plant tripped due to HVRT threshold time.

i. Scenario 1: Short duration HVRT condition with mild overvoltage)

To simulate the HVRT condition, the same test system as shown in Figure 4.2 is used. The SCR of the grid is 2.1. A similar line-line-ground fault is applied at $t = 7$ s for 12 cycles.The induction motor load was tripped just before the fault cleared at $t = 7.24$ s. This situation will assist in evaluating the functionality of the high-voltage ride-through controller. Figure 4.14 shows the PCC voltage and GSC responses.
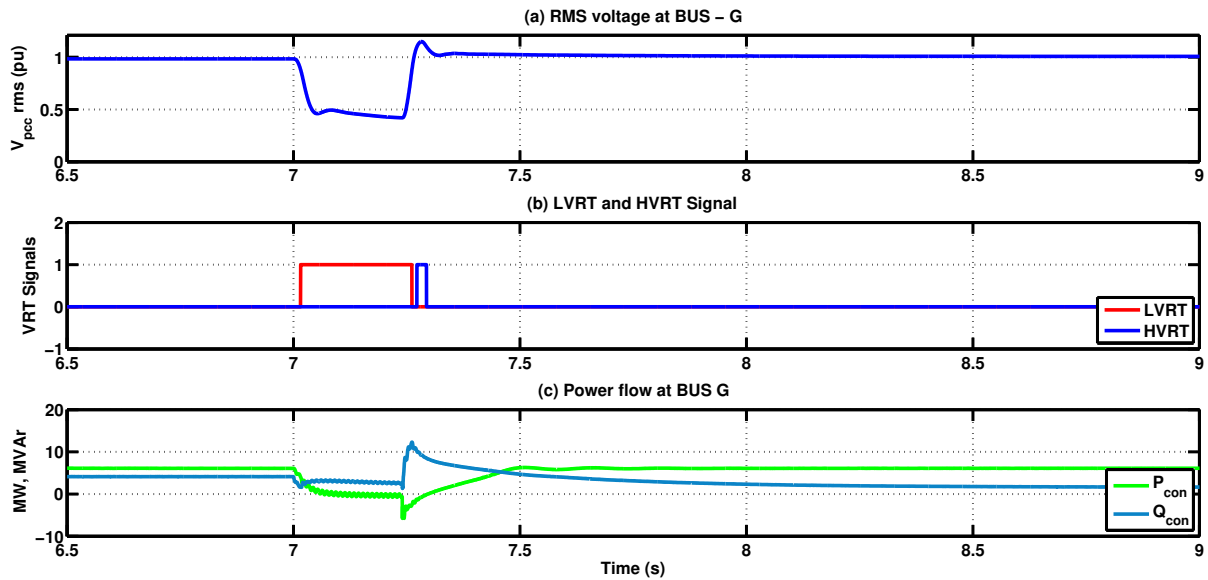
Figure 4.14: HVRT case study result (No tripping)

67

Figure 4.14 shows that when the PCC voltage goes below 0.88 pu due to fault, the wind generator goes to LVRT mode, and the LVRT signal becomes high. As the fault is cleared at $t = 7.24$ s and the induction motor is tripped, the PCC bus voltage rises above 1.1 pu, the wind generator goes to HVRT mode, and the HVRT signal is set to 1, as shown in Figure 4.14 (b). The plant does not trip as the rise in voltage is below 1.2 pu, and the time duration of the plant remains in HVRT mode is less than the HVRT threshold time (t_{HVRT}), as mentioned in Table 4.2. The plant gradually recovers from HVRT mode and returns to normal operation due to ac controller of GSC.

This overvoltage in Figure 4.14 (a) can be explained as follows. While experiencing a fault, the wind generator operates in Low Voltage Ride-Through (LVRT) mode, and the Grid-Side Converter (GSC) supplies reactive power support by injecting additional reactive power into the grid. An induction motor load utilizes most of this reactive power, as shown in 4.14 (c). As the induction motor trip following the fault clearing around $t = 7.24$ s, a high reactive current from a wind generator flows to a grid. As a grid is relatively weak, this extra reactive current suddenly increases the grid's voltage and the PCC bus.

ii. Scenario 2: HVRT in wind generator during severe overvoltage conditions

In this scenario, the test system consists of a total load comprised of an induction motor and a constant impedance. Similar to the previous example, an SCR of 2.1 is used, and a line-to-line fault is applied at time $t = 7$ s.

The total load (induction motor and constant impedance load) was tripped just before the fault cleared at $t = 7.24$ s. As illustrated in Figure 4.15(a, b), the PCC voltage surpasses 1.2 pu just after the fault is cleared at $t = 7.24$ s, leading to the tripping of the plant at $t = 7.27$ s due to HVRT criteria. The induction motor tripping causes a surge in reactive current from the wind generator to the grid. The relatively weak grid experiences a rapid voltage rise around $t = 7.25$ s at the PCC bus due to this sudden influx of reactive current, as shown in Figure 4.15 (c).

4.5.2 Frequency Ride Through (FRT) Capability of Type 4 Wind Generators

This section examines the Frequency Ride-Through (FRT) capability of a Type 4 wind generator and its impact on grid stability during contingencies. FRT holds particular

68
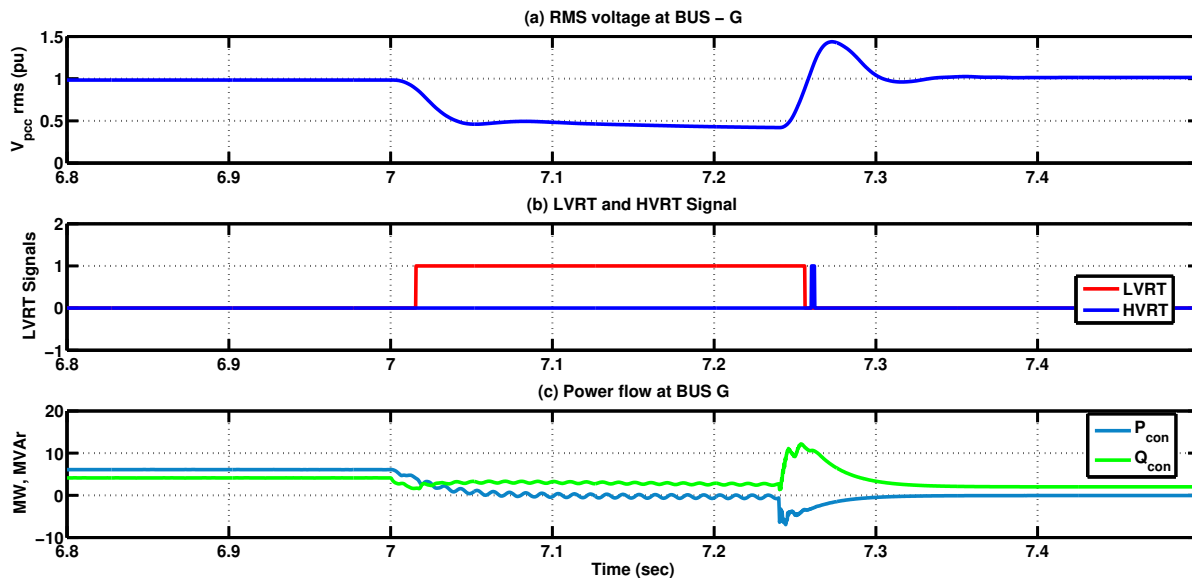
Figure 4.15: HVRT case study result (wind tripping)

significance for renewable energy systems such as wind generators that connect to the grid via power electronic converters. These converters are crucial in converting the wind generator's variable speed and frequency output into a steady ac power output that aligns with the grid frequency. By implementing FRT control strategies, wind generators can dynamically regulate their converter operation to assist the grid and minimize frequency deviations actively.

To demonstrate the effect of FRT, a modified version of Dr. Prabha Kundur's two-area and four-machine system, referred to as Kundur's system, is used [47]. The system configuration is shown in Figure 4.16. The system is modified by replacing the second 900 MVA synchronous generator (G2) with a single aggregated wind generator with the same rating. This system example allows for observing frequency variations following disturbances, enabling an evaluation of the frequency-dependent behaviour as outlined in Table 4.4. The grid frequency is measured using a Phase-Locked Loop (PLL) at the Grid-Side Converter (GSC) ac side, and it is low pass filtered to eliminate noise and pollution caused by harmonics. This filtered measurement serves as the reference signal for the FRT application.

The frequency ride-through capability is implemented per Table 4.4 in the Type 4 wind generator. Figure 4.17 shows the speed controller. Table 4.4 shows that IEEE 1547 recommends using frequency droop-based active power modulation in

69
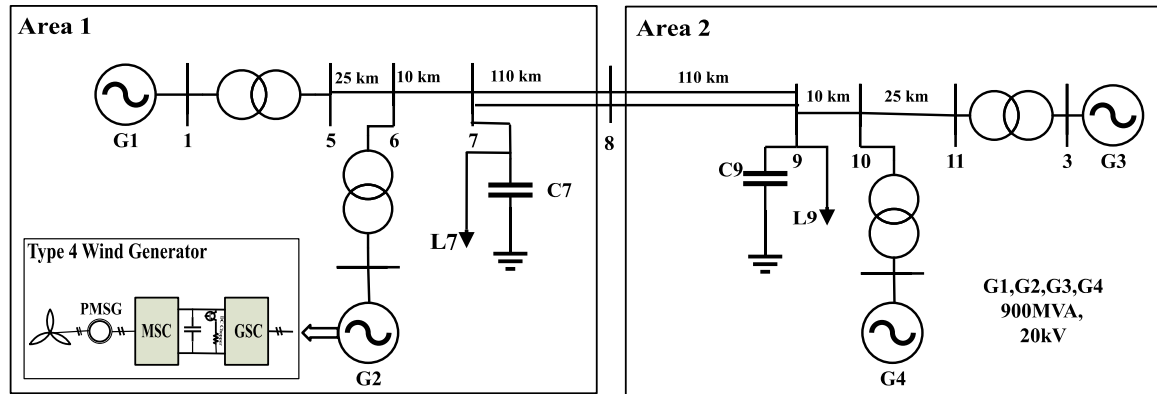
Figure 4.16: Kundur 2- Area and 4-Machine System .Machine 2 is replaced by a similarly rated (900 MVA) Type 4 wind generator.

wind generators. To implement this capability in the Type-4 wind generator, the speed controller of the MSC converter is modified as shown in Figure 4.17. The measured grid frequency within the dead band will not pass through. The speed reference of the MSC controller is modulated using a speed signal ($\Delta\omega$). At first, the modulating power p is calculated using Equation 4.1 and 4.2 depending upon the frequency value. The Gain (K_f) is calculated such that ($\Delta\omega$) = (K_f . p), where ($\Delta\omega$) is equivalent modulation speed signal. The speed is adjusted by controlling the active power reference current i_{qref}. This ($\Delta\omega$) is added to the speed controller. The optimal reference speed (Speed opt) is generated by looking up an MPPT characteristic as was discussed in Section 2.5.2. To create a range for power modulation, the MPPT speed order is reduced by a small margin so that the wind generators operate at 90% of maximum available power, and a 10% reserve is available for the power modulation. Two distinct scenarios assess the wind generator's frequency ride-through capability.

    i. Scenario 1 (FRT with no tripping of wind plant)

    a. Operation with Active Power Modulation

The test system shown in Figure 4.16 is used for this case study. Initially, the load L7 is at 85%. Then at $t = 21s$, it is re-connected and restored to 100%. The sudden re-connection of the load creates a transient imbalance between total generation and load which causes a decrease in grid frequency and initiates an electro-mechanical oscillation. This can be seen in Figure 4.18 (a) from the GSC's grid side frequency plot. As the grid frequency decreases below $48.80Hz$ around $t = 23.5s$, an FRT signal is triggered according to the requirement of Table 4.4, also can be seen from Figure

70
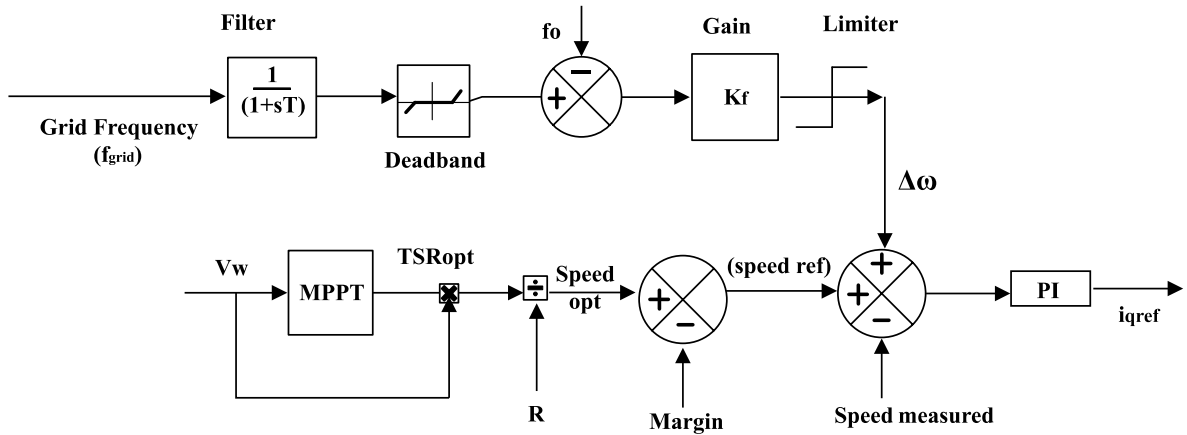
Figure 4.17: Speed controller modification for Active power modulation in FRT

4.18 (b). The grid side controller modulates the active power order per Equation 4.1 based on the wind generator's response to the measured grid frequency. Figure 4.18 (c) shows the wind generator's active power flow response. The active power of the wind generator is modulated and settles at a steady state of 739 MW. Figure 4.18 (d) shows the reactive power flow.
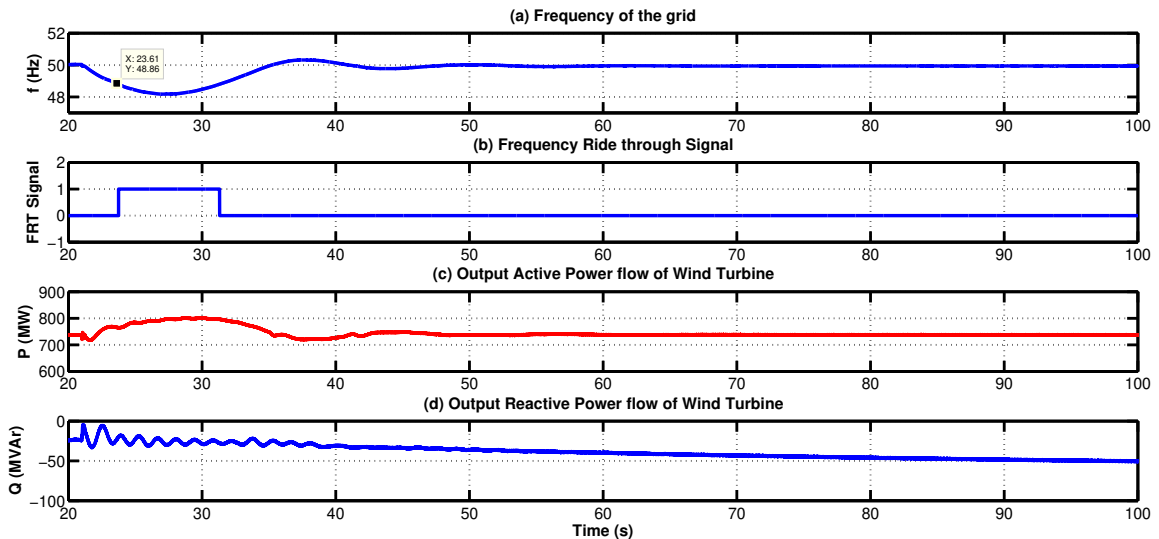
Figure 4.18: wind generator plot for FRT operation (no tripping of wind plant)

In this scenario, the wind power system remains connected to the grid and does not experience a tripping event. This is because the grid frequency does not drop below the tripping frequency threshold of 47 Hz, as stated in Table 4.4. This allows the wind

71

power system to ride through the disturbance and continue operating. During the disturbance, the system frequency experiences oscillations for a while but eventually dampens out and returns close to the nominal frequency of 50 Hz within 40 s. This indicates the system successfully recovers from the disturbance without significant frequency deviations.

Furthermore, the FRT controller implemented in the wind power system takes action to improve the transient stability of the overall system. The generator speed responses of the other generators connected to the system also exhibit well-damped behaviour. This indicates that the FRT control strategy effectively enhances system stability by providing high damping to electromechanical oscillations, as shown in Figure 4.19. From the above test, it is clear that the FRT control strategy with wind power modulation improves the transient stability of the system by providing high damping.
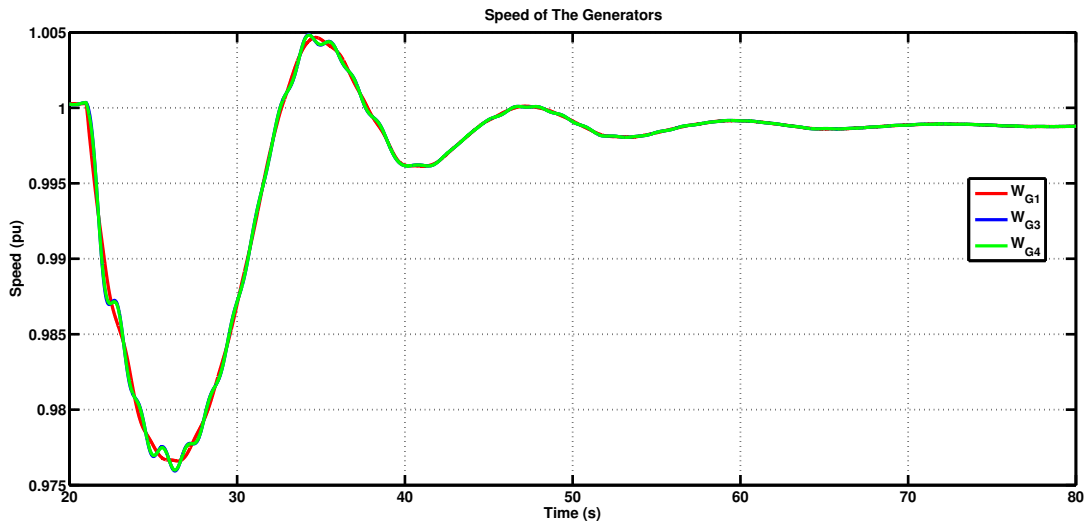
Figure 4.19: Speed response of generators

b. Operation without Active Power Modulation

To prove this advantage of frequency droop-based power modulation, the same system is simulated with the power modulation disabled during FRT operation. In this case, as shown in Figure 4.20 (a), in the absence of active power modulation, the grid frequency decreases and falls below 48.8 Hz during the disturbance. The recovery is slower than the scenario with active power modulation, where the lowest frequency

recorded was 48.0 Hz as well (Figure 4.18 (a)). This implies the system experiences a larger frequency drop and takes longer to settle during FRT operation without power modulation. The settling time refers to the duration for the system to stabilize after a disturbance. A longer settling time implies that it takes more time for the system to recover and return to its nominal operating conditions. As shown in Figure 4.20 (b,c), the simulation result indicates that the wind plant output remains constant after a load change. This means that wind power generation does not respond to the system disturbance and continues to inject the same amount of power into the grid.
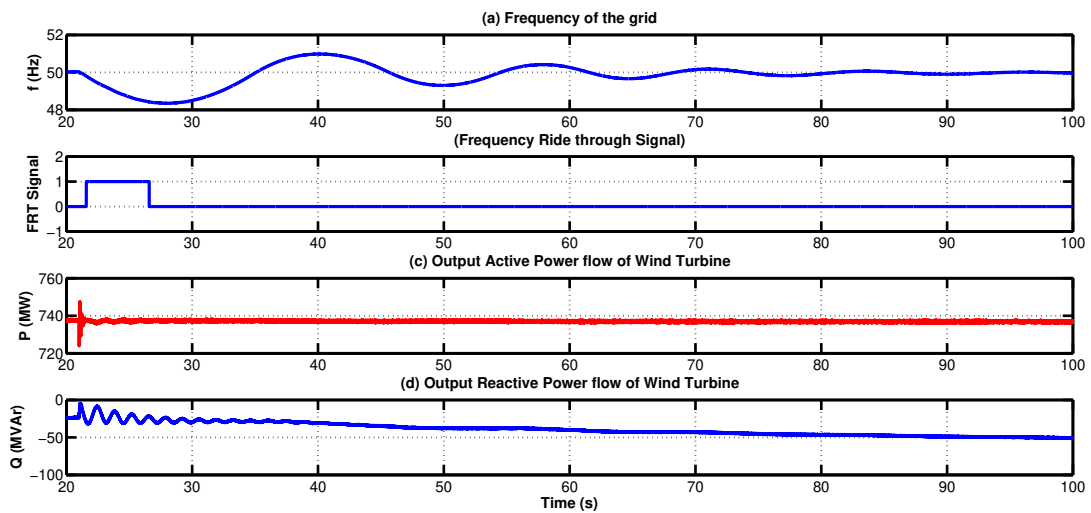
Figure 4.20: Wind plant response during FRT (power modulation is disabled)

Figure 4.21 displays the generator speed responses of G1, G3, and G4 with disabled active power-based FRT. In this case, without active power modulation, the system's settling time is significantly higher (> 80 s) than the scenario with active power modulation. These results highlight the positive impact of power modulation concerning frequency during fault ride-through events. With power modulation enabled, the wind power system can actively respond to changes in grid frequency, helping to stabilize the system more rapidly and efficiently. By modulating the power output in coordination with the grid frequency, the wind power system contributes to the restoration of grid stability and reduces the settling time following a disturbance.

ii. Scenario 2: Severe frequency variation

A simulation was conducted, replicating the scenario described in the previous section, with the initial load L7 set at 40%. The load is restored to 100% at $t = 21$

73
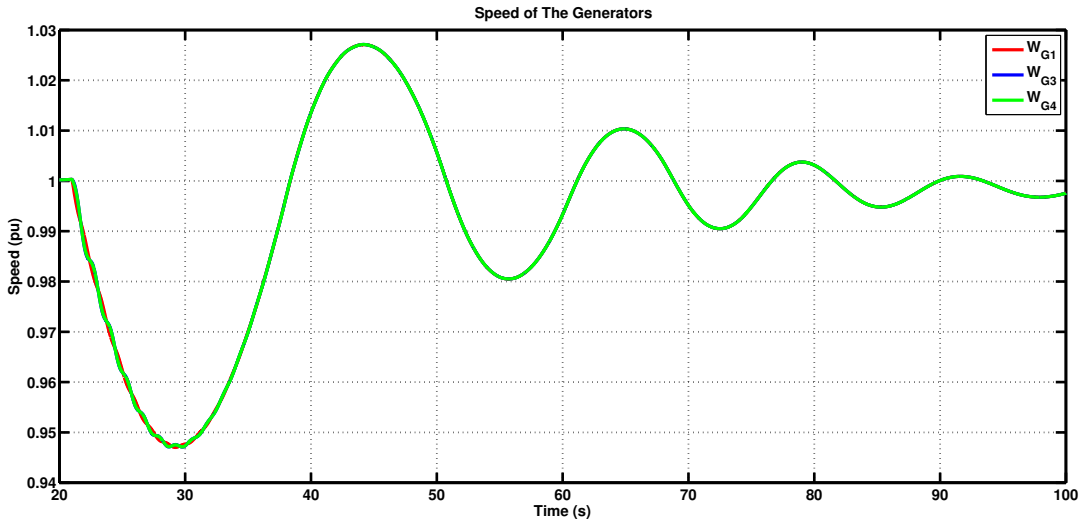
Figure 4.21: Generator speed responses during FRT (power modulation is disabled)

s. Due to large load increases, initially, the grid frequency decreases below 48.8 Hz at $t = 22$ s as shown in Figure 4.22 (a).
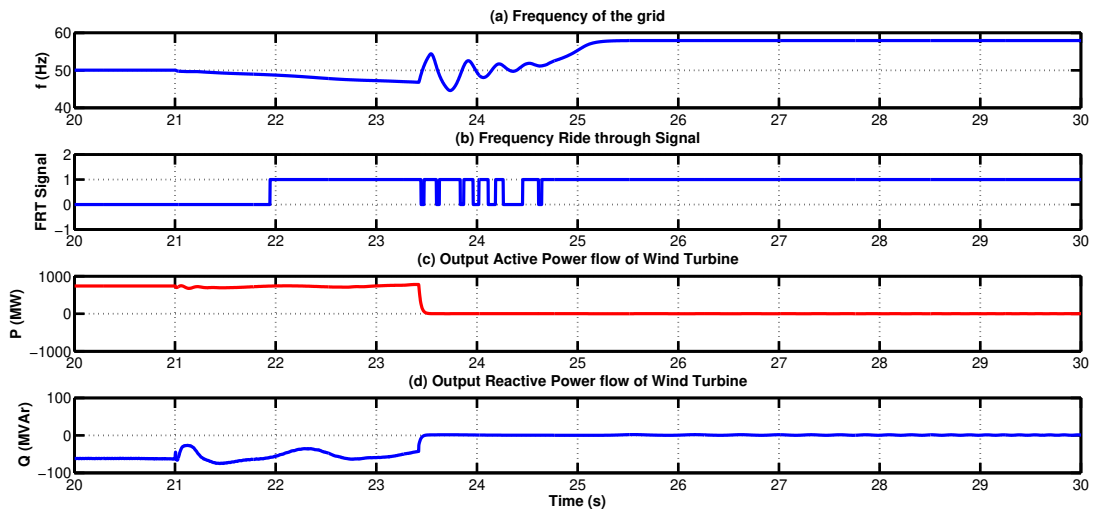
Figure 4.22: wind generator response during FRT (wind plant tripped)

At this point, the FRT signal is set as HIGH, as shown in Figure 4.22(b). After 3.5 seconds of the disturbance, the frequency drops below 47 Hz, which according to the IEEE 1547 FRT strategy in Table 4.4, initiates a trip to the wind plant at $t = 23.5$ s. The reduction in power output from the wind generators to zero, approximately around $t = 23.5$ s, is evident in Figure 4.22(c), confirming the trip occurrence. Figure

4.22(d) illustrated the reactive power flow transients during the disturbance.

4.6   Summary

This chapter has developed simulation models for the voltage and frequency ride-through mechanisms based on the IEEE 1547 Std for the modelled Type 4 wind generators (Chapter 2). The IEEE 1547 Std specifies the requirements for interconnecting distributed energy resources (DERs). Default settings have been selected for fault ride-through models. Type 4 wind generators have full-power conversion capability and can control active and reactive power output. These systems are crucial in modern renewable energy integration and have required effective control strategies to ensure grid stability and reliability.

The simulation models developed in this chapter have captured the behaviour of the Type 4 wind generators during voltage and frequency disturbances. The LVRT mech-anism, as defined by the IEEE Std, has enabled the wind generators to ride through low-voltage events without tripping. The wind generators can actively support the grid voltage during these events by implementing appropriate control strategies, such as reactive power injection or curtailment. Similarly, the fault ride-through capability has helped in the over-voltage conditions.

Furthermore, the simulation models have also showcased the Type 4 wind generators' capability to modulate their power output based on frequency changes in the grid. This frequency ride-through capability allows wind generators to maintain grid frequency during disturbances. This suggests that power electronics-based power generators, such as wind generators, can help to balance the supply-demand dynamics and improve system performance.

Chapter 5

Improvement Of Power System Oscillation Stability Using Dc Chopper-Based Active Power Modulation in Type-4 Wind System

5.1   Introduction

Factors such as loss of generation, change in load and fault etc., can cause variations in the grid frequency. Such disturbances in the power grid cause the load and generation imbalance which subsequently causes the deviation in grid frequency. There is a limit to the change in grid frequency due to operational constraints [1]. The IEEE 1547 suggests providing frequency response support to maintain grid frequency within operational limits during disturbances. Frequency response support means generating systems can adjust the power output according to changes in grid frequency [48]. Synchronous machines dominate the traditional power system, so frequency response support from synchronous generators is inherent. Those frequency responses can be classified as primary and secondary frequency responses. Primary frequency response is where the active power flow of generators changes due to the inertia of the rotating masses of synchronous generators by changing the rotational speed of the machine. The primary frequency response can be specific to the technology. After the primary

frequency response of the synchronous generator, governor action is considered the secondary frequency response, where the machines' active power input is changed. Due to the mechanical nature of the governor, the secondary frequency response is relatively slow.

Renewable energy sources such as wind generators, batteries, and photovoltaic panels of large capacity are getting integrated into the conventional grid. Many of the old synchronous generators are retiring, and new synchronous machine generators are getting installed in smaller numbers. There is a net decrease in synchronous generators in the modern grid. The Wind generators are controlled by fast-power electronic controllers, which have faster response time than synchronous generators. Unlike synchronous generators, frequency response support is not an integral capability of typical grid-following wind generators. The controllers are primarily operating in constant power mode. As a result, frequency response support has diminished in the grid.

Usually, in a Type 4 wind generator, the pitch controller mechanism or changing the wind generator speed or both techniques are used to achieve the required change in the active power, to get the frequency support. The overall process of the control and recovery in both methods is slow due to the mechanical nature of the pitch and wind generator speed control. There is a limitation to the fast change in the output power of wind generators. This can be explained as follows. In Type-4 wind generators, the machine side converter regulates the active power flow, and the grid side converter controls the dc-link voltage. To get fast frequency support, the machine-side converter tries to regulate the active power value, and this causes a significant change in wind generator speed. There is a limitation to the maximum change in wind generator speed due to the mechanical stability of the wind generator. During frequency support, the wind generator operates at a different speed. Due to its mechanical nature, the generator takes some time to return to the pre-disturbance speed.

To improve the frequency response support in the grid, it is recommended in the IEEE 1547 to use distributed energy resources like wind energy. The goal is to maintain a steady frequency following the disturbance. According to the IEEE 1547, as discussed in Chapter 4, the active power output of the wind generators is modulated using a frequency-power droop-based controller. Wind generators use special con-

trollers to provide frequency ride-through support during abnormal conditions. It uses active power modulation to regulate the ac grid frequency.

A dc chopper is often installed between the machine and grid-side inverters to facilitate a temporary imbalance between the generator output power and grid demand by absorbing the imbalance of active power. A dc chopper is a fast-acting power electronic-based controlled resistor. By controlling the energy consumed by the dc chopper, the output power of the wind generator can be reduced in a controlled way. A hysteresis-based control mechanism is used to control the dc chopper, and more details about the operation and control of the dc chopper are discussed in Chapter 2 and Chapter 3 of the thesis. This chapter proposes the ancillary function of the dc chopper controller using active power modulation to damp electromechanical oscillations in the wider network [49].

The idea is to obtain a fast control response from the dc-chopper control as a primary frequency response for the Type 4 wind generator. During disturbances, when there is more generation in the grid compared to load, this causes an increase in grid frequency. A fast reduction in the wind power output can be achieved using a dc chopper controller, which will reduce the rise in grid frequency and control grid frequency changes as per IEEE 1547. In addition to the fast power reduction, dc chopper control dampens electromechanical oscillation. Using Electromagnetic transient simulations, the effectiveness of dc-chopper control is studied using a realistic case study of a modified Kundur 2-area and 4-machine system.

5.2   Power Imbalance and Frequency Change

Consider an ac grid consisting of several synchronous generators, buses, loads, inverter-based generators, etc. The ac grid can be equivalently modelled as a single generator with equivalent inertia constant (H_{eq}) and generating power (P_G), which is the net generation of the grid. This equivalent generator sees a load (P_L), which is the net load of the grid. The overall frequency of the grid is directly related to the speed (W_{eq}) of the equivalent generator. The speed dynamics of the equivalent generator can be represented in Equation 5.1 (damping terms are neglected for simplicity).

$$\frac{2H_{eq}}{W_b} \cdot \frac{\partial W_{eq}}{\partial t} = P_G - P_L \tag{5.1}$$

where, P_G is the net generation, including all generation from traditional synchronous machines and all renewable sources like PV, wind, etc. W_b is the base frequency in radian/second. For a 50 Hz system,W_b =314.14 rad/sec.

Generation and load power imbalance can be expressed as $P_{im} = P_G - P_L$. As seen from Equation 5.1, there is a change in grid frequency only if $P_{im} \neq 0$. The grid frequency increases if the net generation exceeds the net load, $P_{im} > 0$. Similarly, grid frequency decreases if there is more load consumption than power generation. It is important to note that while grid voltage is a local variable, grid frequency is a global concept. The total power generated and consumed throughout the grid is influenced by it. Generators and loads are typically distributed across a wide area within the grid. Therefore, any disturbance that leads to a generation loss or load tripping can affect the grid's frequency. The frequency change resulting from such disturbances can be felt at locations that are electrically distant from the actual disturbance.

The following sections will explain using the dc chopper in the Type 4 wind generator as an active power modulation controller. This modulation helps mitigate frequency deviations caused by load changes or generator disturbances, improving the overall stability and performance of the power system.

5.3 Active Power Modulation Control Mechanism Using Dc Chopper

Figure 5.1 shows the typical dc chopper. During disturbance in the grid, the power output at the grid side converter (GSC) decreases due to the voltage sag at the POI bus of the wind system. This decrease in power flow causes a power imbalance at the dc link of the Type-4 wind generator as the power fed by the machine side converter (MSC) remains unchanged. This power imbalance causes dc voltage to increase, and if the dc link voltage rise is not controlled, the wind system will be tripped to avoid any damage to different components due to dc link overvoltage. The dc chopper limits the dc link voltage rise by absorbing the power imbalance.

The chopper consists of a resistor and an IGBT switch connected in series. By controlling the on and off time duration of the IGBT switch, the effective resistance of the dc chopper can be varied, and subsequently, the power consumed by the dc chopper can be changed. The wind generator GSC output power can be modulated by controlling dc chopper power consumption. This can be achieved by controlling

the dc chopper's effective resistance (R_{eff}) using proper IGBT switching. This can be explained as follows:

If $'T'$ is the IGBT switching period, where $'T'$ is the sum of the switch-on duration (T_{on}) and switch-off duration (T_{off}). With this switching of IGBT, the effective resistance of the dc chopper:
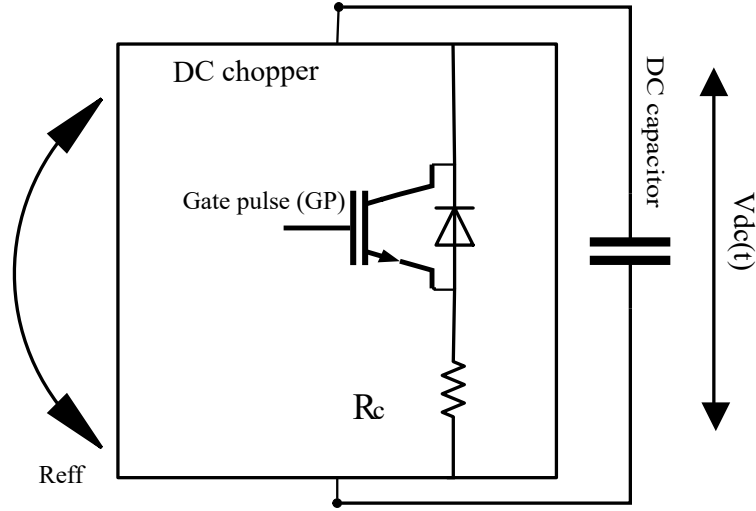
Figure 5.1: A typical Type 4 wind generator with Typical dc Chopper

$$R_{eff} = R_c \cdot \frac{T_{on}}{T_{on} + T_{off}} \tag{5.2}$$

The effective dc chopper resistance can be changed by adjusting the duty cycle(T_D $= \frac{T_{on}}{T_{on}+T_{off}}$). Subsequently, the active power absorption by the dc chopper can be controlled. As shown in Figure 5.2 (a), the chopper power is compared with an active power modulation signal $delP$ and the corresponding error is passed through a PI controller to produce the duty cycle (T_D). The controller objective is to adjust the IGBT switch's switch-on duty cycle period so that the dc chopper's power matches the modulating signal $delP$. The dc chopper can only consume power, so the wind generator output power can only be reduced from the current operating power by using dc chopper control. The signal is produced by a damping controller discussed below.

80

a. Damping Controller

b. Chopper Controller
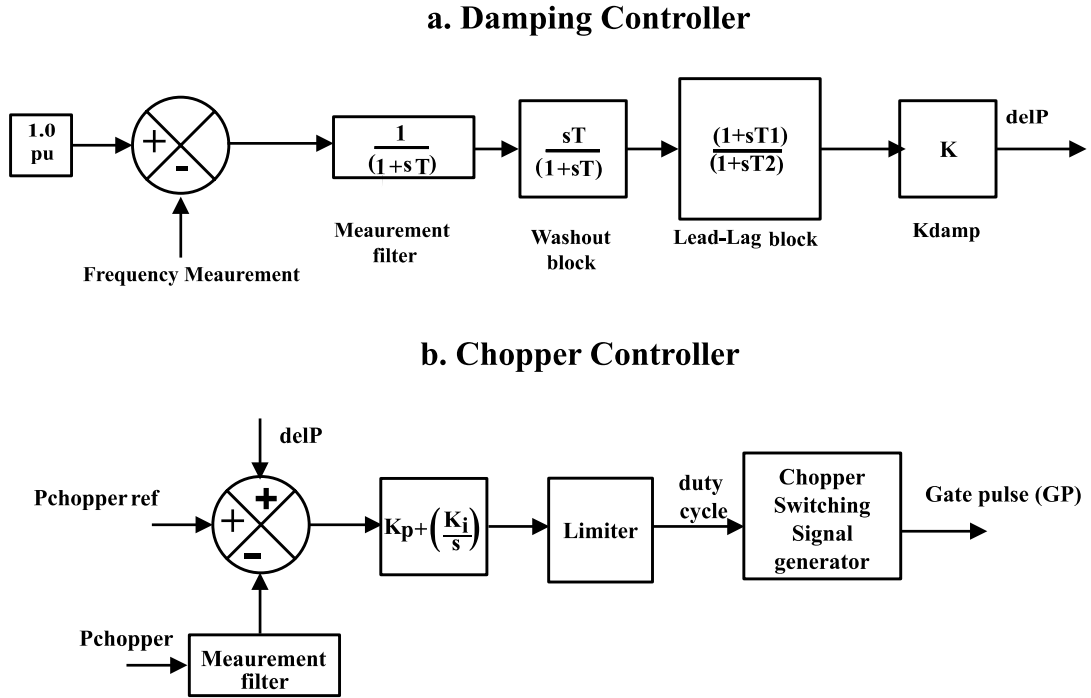
Figure 5.2: a. Damping Controller b. Chopper Controller

5.3.1 Damping Controller

This section proposes using an additional control function, damping control with the dc chopper. The main objective of the damping controller is to provide a fast reduction of wind generator output power by absorbing the extra power due to grid disturbance. Additionally, it aids in damping electromechanical oscillations in the grid frequency and reduces the rise in the grid frequency. The damping controller generates the active power modulation signal '$delP$' to achieve electromagnetic oscillations damping, as depicted in Figure 5.2(a). The input to the damping controller is the measured grid frequency. The typical damping controller structure consists of a measurement filter block, a gain block, a washout filter and a lead-lag block is used [47]. A measurement filter removes high-frequency noise in the measured grid frequency signal. The washout block acts as a high pass filter, which ensures that the damping controller only operates during transient conditions. The parameters for the lead-lag block are adjusted to provide the required phase lead or lags to the input signal to maximize the damping effect. The gain block makes the controller a fast or slow response. Enable signal is used to turn the damping controller on or off.

5.3.2 Wind Power Modulation Analysis through Dc Chopper Control: A Simple Test

To demonstrate the active power modulation using a dc chopper, consider a Type-4 wind system connected to a $69kV$ grid, as depicted in Figure 5.3. In this setup, the grid is represented as an ideal voltage source. The wind plant has a power rating of $150MW$.
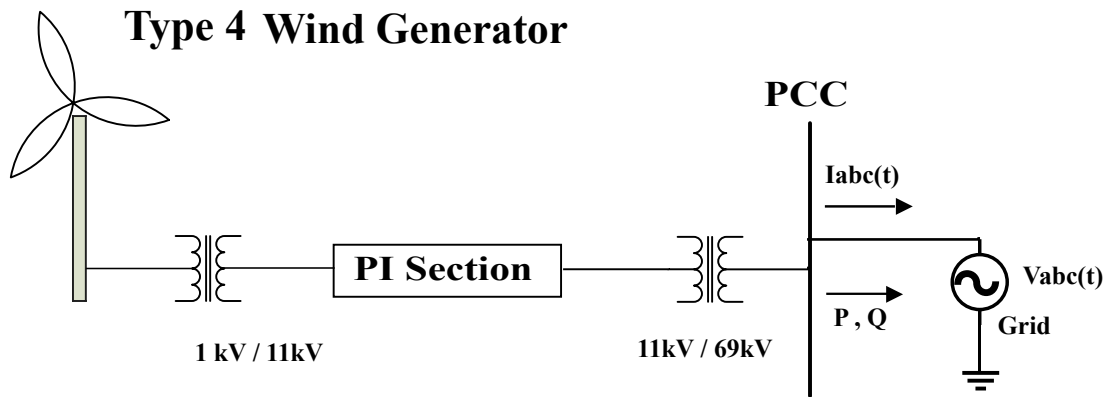
Figure 5.3: Example of Type 4 wind generator connected to the grid
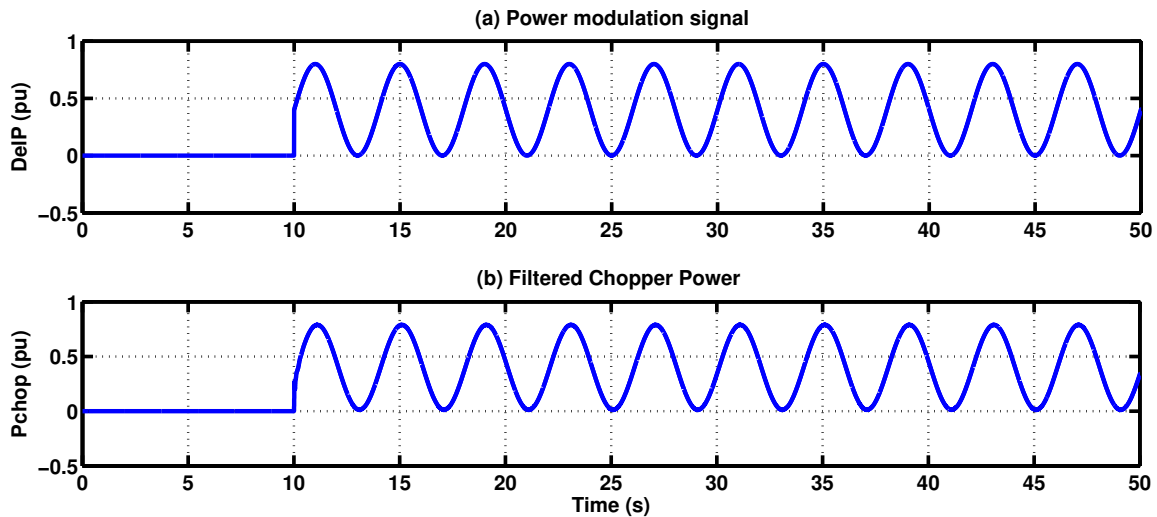
Figure 5.4: Power Modulation Signal ($delP$) and dc Chopper Power

The controllers described in Chapters 2 and 3 are used in the Type-4 wind system. As shown in Figure 5.3(b), to test the system, a $delP$ signal is given by
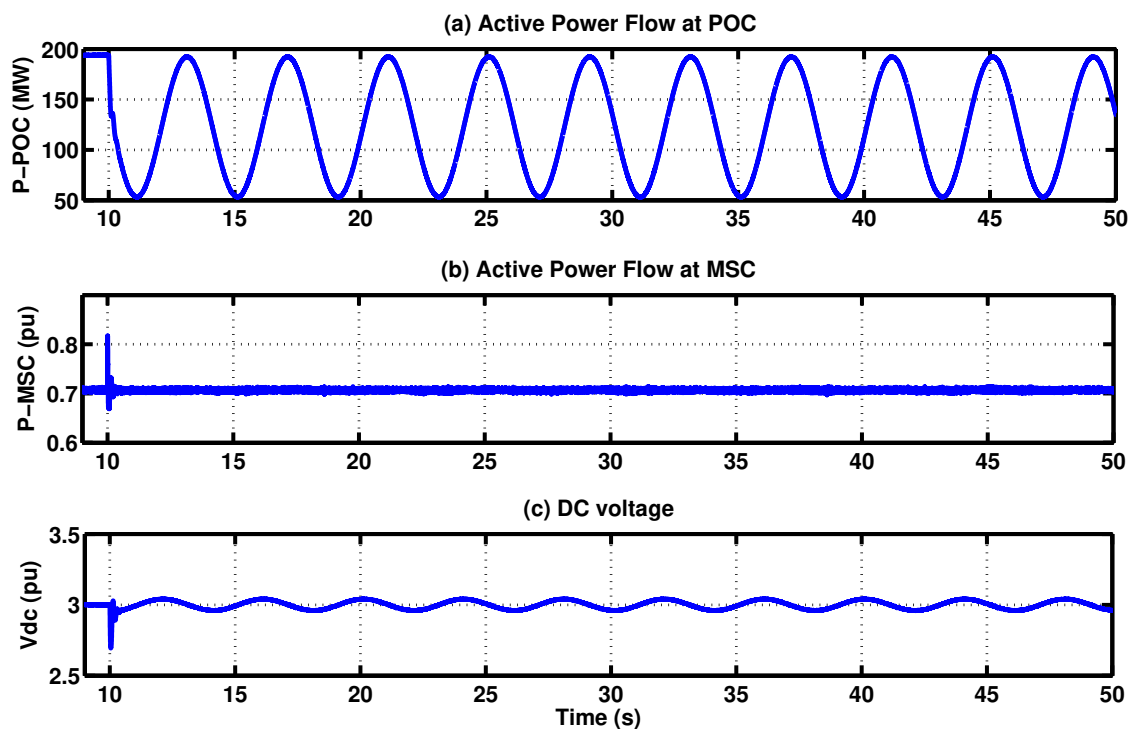
Figure 5.5: Grid side Power Output; Rotor side Power, dc chopper voltage

$-0.4 + 0.4sin(wt)$ is applied at the dc chopper controller input. As dc-chopper can only consume power, the $delP$ signal is selected to be positive over the selected time. At $t = 10$ s, the damping controller is enabled. Figure 5.4 shows the power modulation signal $delP$ and the corresponding filtered dc chopper active power, showing that the chopper power follows the power modulation signal $delP$. Figure 5.5 shows the response plot for (a) the grid side wind power output, (b) the output of the machine side converter and (c) the dc-link voltage. As expected, the output power of the wind plant (at the grid side) is also modulated according to the dc-chopper power modulation signal $delP$, as shown in Figure 5.5(a). Also, the rotor side active power flow is almost constant, and the dc link capacitor voltage does not change significantly due to the presence of the dc-link voltage controller at the grid-side converter controller.

This simple test confirms that the dc-chopper could be used for wind system active power modulation. The following section discusses the application of this dc chopper controller in a realistic system consisting of many synchronous generators, loads etc. and the benefit of fast frequency support from the wind generator to the

grid by reducing the grid frequency rise and providing damping to electro-mechanical oscillations in the grid.

5.4 Case Study: Kundur Two-Area Four-Machine System

Kundur's two-area and four- machines system is shown in Figure 5.6, which is used to test the effectiveness of the dc chopper-based active power modulation for the fast frequency response. This system is commonly used in power system analysis and control studies to represent interconnected power systems with multiple generators and loads [47].
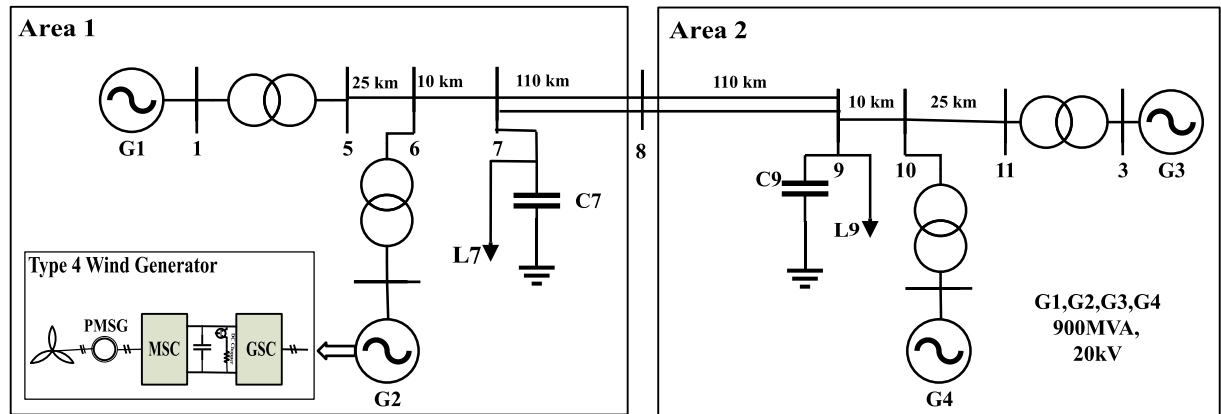
Figure 5.6: Kundur's Two Area and four machine System

The Kundur's system is modified to include a type-4 wind generator. The Generator G2 is replaced by a Type-4 wind system of a similar rating of 700 MW. All other parameters of the Kundur System are kept as they are. The slip speed of Generator G1 is used as input to the damping controller of the dc chopper. Table 5.1 mentions the dc chopper damping controller parameters. It consists of the settings and characteristics of the controller, such as gain, and time constants, to achieve the desired damping and stability performance in the system.

At steady state, 30% of load L7 is tripped at $t = 85$ s. This load trip is equivalent to 320 MW. Two simulations are performed using the same disturbance of load tripping with and without a dc-chopper active modulation controller. Considering both scenarios where the damping controller is enabled and disabled, the speeds of generators G1, G3 and G4 are plotted in Figure 5.7. The generator's speed responses

Table 5.1:   dc-chopper damping controller parameters

dc Chopper Damping Controller	$K_{gain} = 37.5$
	Measurement time constant = 0.01 sec
	Washout time constant = 10 sec
	Lead and lag time constant: 7 sec and 13 sec
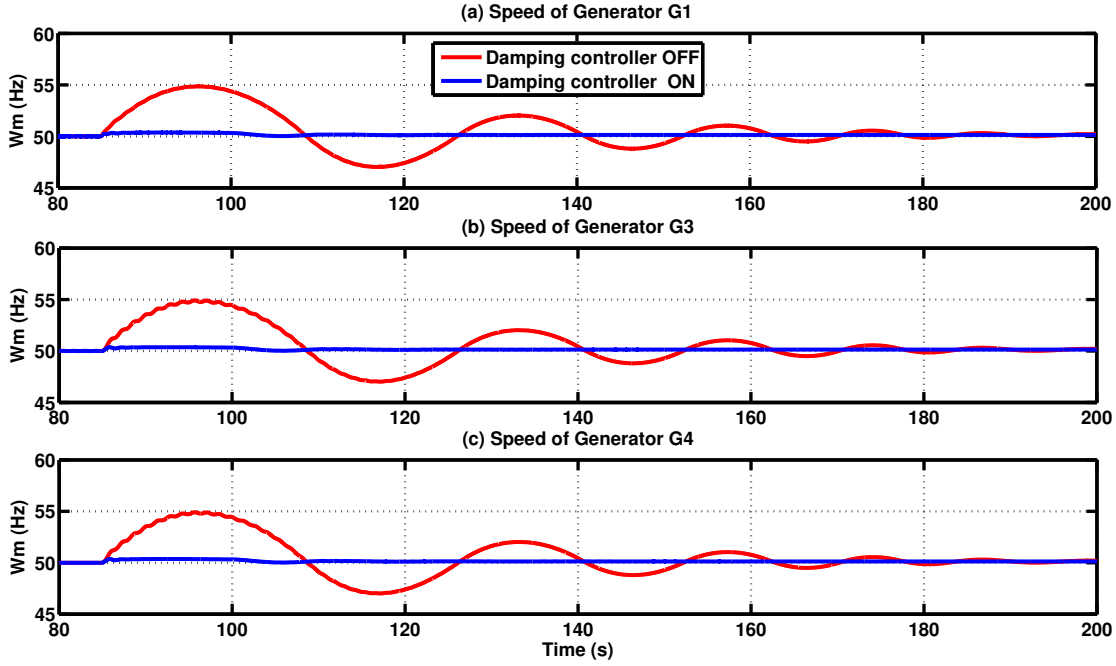
Figure 5.7: Speed of Three generators (pu)

show that the grid frequency increases due to sudden load trips due to net power imbalance. Without a dc chopper controller, the frequency increases to 5 Hz above the nominal frequency of 50 Hz, i.e. rise above 2 Hz, which will make the wind generator trip. With the subsequent action of the governor of synchronous generators, the grid frequency was restored to the nominal frequency after a long period of around t = 200 s. As discussed in Chapter 4, according to the IEEE 1547, wind generators will be tripped due to high grid frequency. Figure 5.7 shows the generator speed response with the dc-chopper modulation controller. Due to the sudden load trip, the maximum rise in speed (frequency) is 0.007 pu, i.e., 0.35 (50 Hz $system$) Hz, much lower than the case without the damping controller. Also, the grid frequency was restored to the nominal frequency very quickly (within 20 s) compared to the wind generator

without a dc chopper controller. Without dc chopper operation, the restoration of grid frequency mainly depends on the synchronous generators and the speed of their governor action. Governor action is a mechanical process which is relatively slow; the total restoration time after disturbance is 130 s as compared to 20 s for a wind system with an active power modulation, as shown in Figure 5.7.
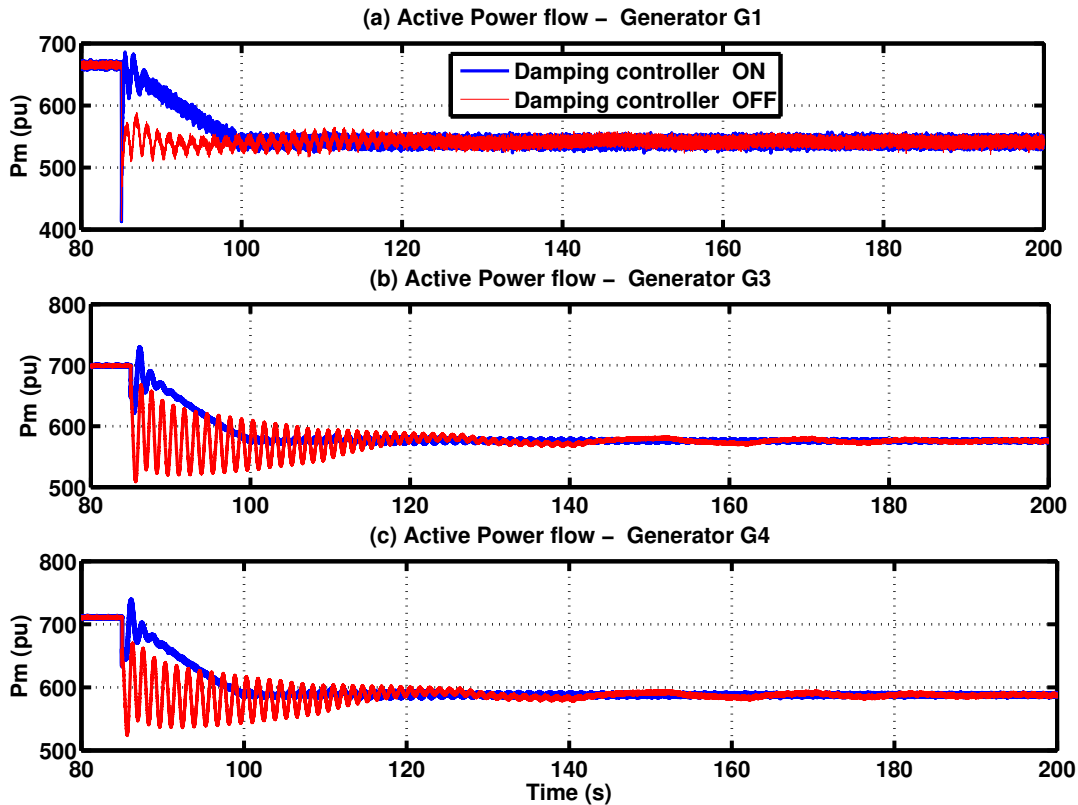
Figure 5.8: Output Power of Three Generators in (MW)

All generators' output power and input mechanical torque are shown in Figure 5.8 and Figure 5.9, respectively. Due to the load trip, there is more generation and less load in the grid leading to an increase in the grid frequency as shown in Figure 5.7. The output power of synchronous generators is reduced due to the governor action of synchronous generators by decreasing the input mechanical power, as shown in the output power and input torque plot of synchronous generators. In both scenarios, synchronous generator powers are reduced to the same steady-state output power with and without a dc chopper damping controller. The wind system POI voltage and power flow at the POI bus are shown in Figure 5.10 (a) and (b). In the wind system
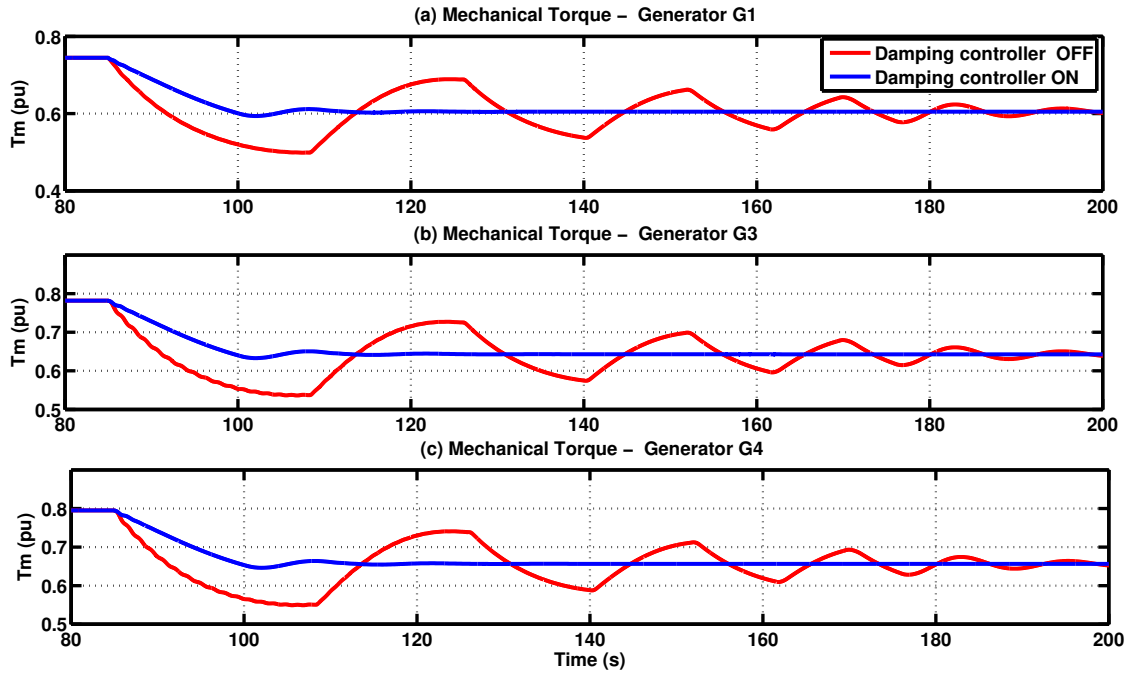
Figure 5.9: Mechanical input torque (Governor Output) (pu)

without a dc chopper damping controller, the output power of the wind generator remains constant at 700 MW. However, with the dc chopper damping controller, a fast reduction of the output power of the wind generator to 200 MW is observed due to an increase in grid frequency following the trip of the load. This reduction in power output is due to the energy absorbed by the dc chopper during this period, as shown in Figure 5.10 (b). As the grid frequency gradually returns to nominal frequency, the wind generator output returns to the pre-disturbance power of 700 MW.

Figure 5.10 (c) and (d) show the plot for the power modulation signal and the chopper energy, respectively. During FRT mode, the total energy consumed by the dc chopper of a single wind generator is 3.2 MJoule, much lower than the dc chopper's resistor rating for this wind system (i.e. for each 2MW wind generator, the 4-second rating is equivalent to 8 MJoule). Due to this sudden load trip, the wind system POI voltage does not change significantly, which does not trigger LVRT or HVRT operation. This means that the dc chopper remains idle, and the wind generator continuously operates in the pre-scheduled power during the disturbance. The above results show that using a dc chopper with active power modulation helps in the fast reduction of wind power, decreasing the rise in grid frequency, dampening

87
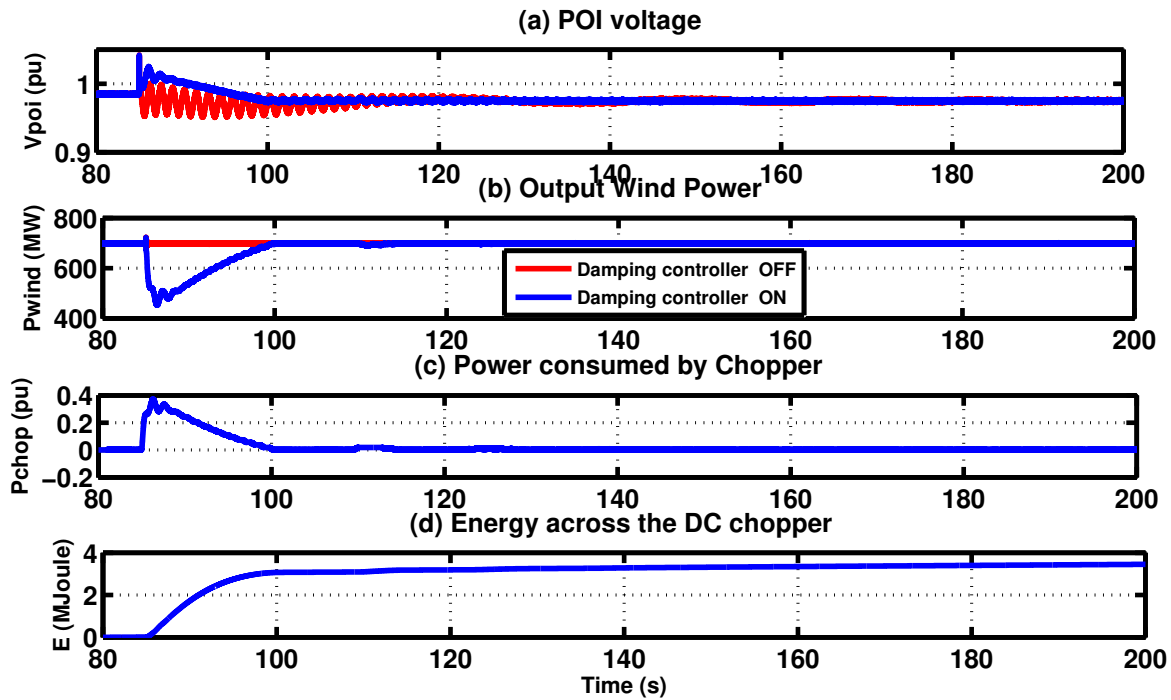
Figure 5.10: Response for the wind generator active power flow and POI voltage with dc chopper operation

electromechanical oscillation, and providing frequency support.

5.5 Summary

This chapter has discussed the benefits of employing a dc chopper with active power modulation. This technique has reduced the maximum change in frequency, effectively dampening frequency oscillations and leading to a more stable power system. It is crucial to highlight that the frequency damping feature has been an ancillary service, and priority has been given to LVRT or HVRT operation.

If LVRT or HVRT mode has been enabled in response to grid disturbances, the dc chopper could not have been employed for active power modulation during that phase. Instead, the dc chopper controller has reverted to its primary control mode, following pre-established control algorithms and strategies to meet the criteria set by LVRT and HVRT standards, as described in Chapter 4.

Chapter 6

Conclusion and Future Work

Power systems are continuously evolving, and with increasing awareness of global warming and the need to reduce carbon emissions, the use of renewable energy sources like solar and wind is increasing. This leads to the development of technologies of control systems, battery storage, and standards to manage various operating parameters effectively. These include controlling the flow of active and reactive power to maintain optimal operation.

1. This thesis has developed computer simulation models that enable the investigation of fault ride-through capabilities of a Type 4 wind generator, which has become the most widely used form of wind generator. The algorithms used for successful fault ride-through have been taken from the IEEE 1547-2018 standard and have used default values for the setting. The research has involved modelling a typical Type 4 wind generator using the PSCAD (Power System Computer-Aided Design) software. This modelling has allowed a detailed study of the converters used in the wind generator system. The research has comprehensively explained the converters' controller operation and significance within the Type 4 wind generator system.

   In Chapters 2 and 3, it has been shown that the utilization of back-to-back voltage source converter (VSC) converter technology has allowed the VSC to remain connected to a fixed-frequency grid, despite the variable and intermittent characteristics of wind. The research model has involved formulating a tip speed ratio-based algorithm to extract the maximum power from intermittent wind energy sources to optimize the operation and enhance efficiency. A dc

chopper with hysteresis loop control has been incorporated to maintain the power balance without overloading the dc bus capacitor.

2. Chapter 4 has demonstrated how electromagnetic transient (EMT) simulation can be effectively incorporated to design Voltage Ride Through (VRT) and Frequency Ride Through (FRT) strategies, allowing for the seamless integration of Type 4 wind generators into the grid. The LVRT mechanism, as specified in IEEE 1547, has allowed the Type 4 wind generator to endure most low-voltage events without shutting down. The wind generator has actively maintained grid voltage during such events by employing suitable control techniques like injecting reactive power or curtailing power output.

   Similarly, the HVRT technique has helped to ride through overvoltage conditions without excessive tripping of the wind generator. The frequency ride-through (FRT) capabilities have also been incorporated in the wind generator and discussed in detail in Chapter 4. The FRT has used active power modulation to ensure stable operation. It has been illustrated that the wind generator could withstand and continue operating within specific frequency deviation ranges without tripping or disconnecting from the grid. The specific ride-through requirements and limits vary depending on the application and grid regulations.

3. The thesis has also introduced a novel ancillary use of the dc chopper in the modelled Type 4 wind generator as a mechanism for power oscillation damping in Chapter 5. Traditionally, the primary purpose of the chopper has been to maintain the power balance between wind generation and load consumption. It has been observed that there has been a high rise in grid frequency during some fault conditions, and the electro-mechanical oscillation damping has also been poor.

   The proposed method, which uses a damping controller with the dc chopper in the Type 4 wind generator, has significantly reduced the grid frequency rise and improved electromechanical oscillation damping. The effectiveness of the dc chopper damping controller has been studied using a modified Kundur's two area four machine system, where one of the synchronous generators has been replaced with an equivalent rated Type 4 wind generator.

The proposed method has decreased the maximum frequency change from 5 Hz to 0.35 Hz (i.e. 0.1 pu to 0.007 pu) in the 50 Hz system. Also, the damping of frequency oscillations has been much faster, i.e. in 20 s instead of 130 s (without the damping controller). Thus, this has enhanced the frequency riding-through capability of the wind generator during severe faults and has contributed to a more stable power supply.

6.1 Suggestions for Future Work

The concepts and models studied in this thesis have great potential for understanding the basics of Type 4 wind generators and the need for fault ride-through techniques. This thesis can be used as a reference for the following future work :

1. The dc chopper control for fast active power reduction can be investigated for its efficacy in damping power oscillations in realistic large grids.

2. Recently, Grid Forming (GFM) Converters have been proposed as a new technology. The application of voltage and frequency ride-through can be investigated in GFM converter-based wind generators.

3. The thesis used an aggregated model where the whole wind power plant is modelled as a single aggregated converter. However, in a real wind power plant, each wind generator may be subject to different wind conditions; future investigations could investigate the IEEE 1547 capability (LVRT, HVRT, FRT, FFR) of such detailed wind models.

Appendix A

Tip Speed Ratio (TSR) based Maximum Power Point Tracking Algorithm

This MATLAB algorithm uses the Tip Speed Ratio (TSR) method to track the maximum power based on the wind speed for the Type 4 wind turbine. The "Wind Turbine Data" section defines the wind turbine parameters. Using the Equations 2.5 and 2.6, TSR and Power are calculated for the wind speed array. This code generates a text file which contains wind speed and respective optimum TSR. This text file will be used in the lookup table in the speed controller, which regulates active power in the Machine Side Converter. The section 3.2 explains the MPPT in detail.

```
-----------------------------------MATLAB CODE----------------------------
clc
clear all
close all
--------------------------------------------------------------------------
---------------------------- Wind Turbine Data----------------------------
Vw = [1 2 3 4 5 6 7 8 9 10 11 12 13 14 15];  % Wind Speed
Beta = 0;                                     % Pitch Angle
rho = 1.225;                                  % Air density
R = 50;                                       % Radius of the turbine
A = pi * R * R;                               % Area of the blade
GB = 150;                                              % Gear Box
---------------------------------First Loop-------------------------------
----Calculation of TSR and Power across the Turbine ----------------------
--------------------------------with Wind speed as Input------------------

k = 1;
for j = 1:15
```

```matlab
    Vw = j;
    for i = 1:100                                       % frequency
        w(j,i) = i * 2 * pi;
        TSR(:,i) = (R * 2 * pi * i) / (Vw * GB); % calculation of TSR
        Cp(:,i) = ((4.0/9.0) - (Beta/60.0)) * sin(0.5 * pi * 20.0 *
        (TSR(:,i) - 3.0) * (1.0) / (150.0 - 3.0 * Beta))
        - (2.0 * Beta / 1087.0) * (TSR(:,i) - 3.0);
        P(j,i) = 0.5 * Cp(:,i) * (Vw^3) * rho * A * 1e-6;
                                              % power present in wind
        k = k + 1;
    end
end
-------------------------Second Loop--------------------------------
------- Maximum power point, Optimum TSR via Matrix Index---------------
k = 1;
for i = 1:10
    Vw(k) = i;
    Power = P(i,:);                 % Power Matrix based on Wind speed
    Wbase = 2 * pi * 50;            % Base Rotation Speed
    W = (1:100) * 2 * pi / (Wbase);  % Rotational speed range (pu)
    [Pmax, Popt_index] = max(Power); % Finding the index at which P= Pmax
    wopt(k) = W(Popt_index);        % Storing the respective rotational speed
    TSRoptpu(k) = (wopt(k) * Ra) / Vw(k);% Calculation of optimum TSR
    k = k + 1;
    hold on
end

A = [Vw; TSRoptpu]';
save wind_curve.txt A;                      % Saving the data in text format
```

Appendix B

Low Voltage Ride Through Detection for Category II during abnormal conditions

Table 4.2 is used for implementation of voltage ride-through capability for abnormal performance Category II in Type 4 wind turbine as suggested in IEEE Std 1547-2018. This FORTRAN code detects voltage dip when a fault occurs and send the LVRT enable signal to the Grid side controller of wind turbine. Depending upon the terminal voltage, the algorithm calculates the appropriate time during which, the wind turbine will ride through and provide reactive power support. Section 4.5.1.2 uses the code and studies the LVRT capability of the wind turbine.

```
----------------------------FORTRAN--------------------------------
! Category II Low voltage ride through requirements for the
! Type 4 wind turbine
! Detecting LVRT Mode from the Vrms signal and issuing trip
! signal to breaker

#LOCAL REAL Slope
#LOCAL REAL Vmin
#LOCAL REAL Vmax
#LOCAL REAL Vmid
#LOCAl REAL T_h
#LOCAl REAL V_TEMP
#LOCAL REAL T_rem
#LOCAl INTEGER Trip_Temp
#LOCAL REAL Vmid1

IF (TIMEZERO) THEN
    $TRIP=0;
```

```
        $LVRT=0;
ENDIF
Trip_Temp=$TRIP


Vmax=0.88                !!!!! Level 1 voltage towards LOW voltage
Vmid=0.65                !!!! Level 2 voltage
Vmid1=0.45               !!!!! Level 3 voltage
Vmin=0.3                 !!!!! Level 4 voltage
Vh=1.1                   !!!!! Level 1 towards HIGH Volatge
T_h=0.625
SLOPE=1.0

$TRIP=0;
$LVRT=0; ! LVRT

IF ($ENAB .EQ. 1) THEN ! Enabling

    IF ($V .LT. Vmin) THEN                   ! Vpcc < 0.3volt
        $TRIP=1                      ! Trip when Vpcc < 0.3 volt
    ENDIF

    ! 0.65 < Vpcc < 0.88

    IF (($V .LE. Vmax) .AND. ($V .GE. Vmid)) THEN  ! 0.65 < Vpcc < 0.88
        $LVRT=1        ! LVRT mode -- ON
        IF ($tON1 .EQ. 0.0) THEN  ! tON = 0 and set LVRT value to time
                                  !at which ! LVRT enabled
            $tON1=TIME
        ENDIF
        Tlvrt=3 +(8.7*($V-0.65))   ! Tlvrt is calculated as per IEEE
        T_rem=TIME-$tON1           ! Check minimum ride through time value for
                                   ! respective Vpcc
        IF (T_rem .GT. Tlvrt) THEN  ! if Trem < Tlvrt
            $TRIP=1
        ENDIF
    ENDIF

    ! 0.45 <= Vpcc <0.65

    IF (($V .LT. Vmid) .AND. ($V .GE. Vmid1)) THEN   ! 0.45 <= Vpcc < 0.65
        $LVRT=1        ! LVRT mode -- ON
        IF ($tON2 .EQ. 0.0) THEN   ! LVRT_status = 0 and set LVRT value
                                   ! to time at which LVRT enabled
            $tON2=TIME
```

```
        ENDIF
        Tlvrt=0.32
        T_rem=TIME-$tON2            ! Check minimum ride through time value
                                   ! for respective Vpcc
        IF (T_rem .GT. Tlvrt) THEN  ! if Tres <Tlvrt =0.32
            $TRIP=1
        ENDIF
    ENDIF


! 0.30 <= Vpcc < 0.45

IF (($V \geq \text{Vmin}) \land ($V < \text{Vmid1})) THEN
    $LVRT = 1           ! LVRT mode -- ON
    IF ($tON6 = 0.0) THEN       ! LVRT_status = 0 and set LVRT value to
                                !  time at which LVRT enabled
        $tON6 = \text{TIME}
    END IF
    Tlvrt = 0.16
    T_rem = \text{TIME} - $tON6    ! Check minimum ride through time value
                                ! for respective Vpcc
    IF (T_rem > Tlvrt) THEN      ! if T_rem < Tlvrt = 0.16
        $TRIP = 1
    END IF
ENDIF


! 0.88 < Vpcc < 1.1         ! Dead Band- Normal Operation

IF (($V < \text{Vh}) \land ($V > \text{Vmax})) THEN  ! 0.88 < Vpcc < 1.1
    $LVRT = 0                           ! LVRT mode -- OFF
    $TRIP = 0
    $tON1 = 0.0
    $tON2 = 0.0
    $tON6 = 0.0
ENDIF


ELSE
    $tON1 = 0.0   ! LVRT_status = time instant when lvrt = 1 (first time),
                  !  no trip, no LVRT mode means continuous operation
    $tON2 = 0.0
    $tON6 = 0.0
    $TRIP = 0
    $LVRT = 0
```

```
ENDIF
IF (Trip_Temp = 1) THEN
    $TRIP = 1
ENDIF
```

Appendix C

High Voltage Ride Through Detection for Category II during abnormal conditions

Table 4.2

Table 4.2 is used for implementation of voltage ride-through capability for abnormal performance Category II in Type 4 wind turbine as suggested in IEEE Std 1547-2018. This FORTRAN code detects overvoltage when a fault occurs and send the LVRT enable signal to the Grid side controller of wind turbine. Depending upon the terminal voltage, the algorithm calculates the appropriate time during which, the wind turbine will ride through. Section 4.5.1.3 uses the code and studies the HVRT capability of the wind turbine.

```
!-------------------------FORTRAN-----------------------------------
! Category II High voltage ride through requirements
! for the Type 4 wind turbine
! Detecting hVRT Mode from the Vrms signal and
! issuing trip signal to breaker

#LOCAL REAL Slope
#LOCAL REAL Vh
#LOCAL REAL Vmax
#LOCAL REAL VmidA
#LOCAL REAL VmidB
#LOCAL REAL Thvrt

#LOCAL REAL T_rem

#LOCAl INTEGER Trip_Temp

IF (TIMEZERO) THEN
```

```
    $TRIP = 0;
    $HVRT = 0;
ENDIF
Trip_Temp = $TRIP


Vmax = 1.20
VmidA = 1.175
VmidB = 1.15
Vh = 1.1


$TRIP = 0;
$HVRT = 0; ! HVRT


IF ($ENAB = 1) THEN ! Enabling

    IF ($V > Vmax) THEN       ! Vpcc > 1.2 volt
        $TRIP = 1 ! Trip when Vpcc > 1.2 volt
    END IF

    ! 1.175 < Vpcc <= 1.20


    IF (($V \leq Vmax) \land ($V > VmidA)) THEN  ! 1.175 < Vpcc < 1.20
        $HVRT = 1  ! HVRT mode -- ON
        IF ($tON3 = 0.0) THEN    ! tON = 0 and set LVRT value to time at
                                 !which LVRT enabled
            $tON3 = \text{TIME}
        END IF
        Thvrt = 0.2                  ! Thvrt is calculated as per IEEE
        T_rem = \text{TIME} - $tON3  ! Check minimum ride through time
                                          value for respective Vpcc
        IF (T_rem > Thvrt) THEN      ! if T_rem < Thvrt
            $TRIP = 1
        END IF
    ENDIF

    ! 1.15 < Vpcc <= 1.175


    IF (($V \leq VmidA) \land ($V > VmidB)) THEN  ! 1.15 < Vpcc < 1.175
        $HVRT = 1      ! HVRT mode -- ON
        IF ($tON4 = 0.0) THEN    ! LVRT_status = 0 and set LVRT value
                                      to time at which LVRT enabled
            $tON4 = \text{TIME}
        END IF
        Thvrt = 0.5
        T_rem = \text{TIME} - $tON4    ! Check minimum ride through time
```

```
                                                    value for respective Vpcc
        IF (T_rem > Thvrt) THEN      ! if T_rem < Thvrt = 0.16
              $TRIP = 1
          END IF
      ENDIF


! 1.10 < Vpcc <= 1.15

IF (($V \leq VmidB) \land ($V > Vh)) THEN  ! 1.1 < Vpcc < 1.15
    $HVRT = 1       ! HVRT mode -- ON
    IF ($tON5 = 0.0) THEN     ! HVRT_status = 0 and set LVRT value
                                  to time at which LVRT enabled
        $tON5 = \text{TIME}
    END IF
    Thvrt = 1
    T_rem = \text{TIME} - $tON5      ! Check minimum ride through time
                                    value for respective Vpcc
    IF (T_rem > Thvrt) THEN      ! if T_rem < Tlvrt = 0.16
        $TRIP = 1
    END IF
ELSE
    $tON3 = 0.0   ! LVRT_status = time instant when lvrt = 1 (first time),
                  no trip, no lvrt mode means continuous operation
    $tON4 = 0.0
    $tON5 = 0.0
    $TRIP = 0
    $HVRT = 0
ENDIF
IF (Trip_Temp = 1) THEN
    $TRIP = 1
    $HVRT = 0
ENDIF
```

References

[1] "IEEE standard for interconnection and interoperability of distributed energy resources with associated electric power systems interfaces," *IEEE Std*, vol. 1547, pp. 1547–2018, 2018.

[2] S. Ellerbeck, "More than a third of the world's electricity will come from renewables in 2025," *World Economic Forum*, 2023 , [Online].

[3] Z. Shahan, "History of wind turbines," *Renewable Energy World*, 2014 , [Online].

[4] H. Li and Z. Chen, "Overview of different wind generator systems and their comparisons," *IET Digital Library*, vol. 2, no. 2, p. 123 – 138, June, 2008.

[5] C. Wu, X.-P. Zhang, and M. Sterling, "Wind power generation variations and aggregations," *CSEE Journal of Power and Energy Systems*, vol. 8, no. 1, pp. 17–38, 2022.

[6] R. Esterhuizen, "Comparative study between synchronous generator and doubly-fed induction generator in wind energy conversion systems," *IET Digital Library*, October, 2010.

[7] N. Demirovic, "The phasor simulation of wind turbines with double fed induction generator," *7th Mediterranean Conference and Exhibition on Power Generation, Trans-mission, Distribution and Energy Conversion*, January 2016.

[8] L. Fan and Z. Miao, *Modeling and analysis of doubly fed induction generator wind energy systems*. Academic Press, 2015.

[9] H. Matayoshi, A. M. Howlader, M. Datta, and T. Senjyu, "Control strategy of pmsg based wind energy conversion system under strong wind conditions," *Energy for Sustainable Development*, vol. 45, pp. 211–218, 2018.

[10] M. Yin, G. Li, M. Zhou, and C. Zhao, "Modeling of the wind turbine with a permanent magnet synchronous generator for integration," in *2007 IEEE Power Engineering Society General Meeting*. IEEE, 2007, pp. 1–6.

[11] T. Maguire and A. Gole, "Apparatus for supplying an isolated dc load from a variable-speed self-excited induction generator," *IEEE Transactions on Energy Conversion*, vol. 8, no. 3, pp. 468–475, 1993.

[12] F. Kanellos and N. Hatziargyriou, "Control of variable speed wind turbines equipped with synchronous or doubly fed induction generators supplying islanded power systems," *IET renewable power generation*, vol. 3, no. 1, pp. 96–108, 2009.

[13] H. Elaimani, A. Essadki, N. Elmouhi, and R. Chakib, "Comparative study of the grid side converter's control during a voltage dip," *Journal of Energy*, vol. 2020, pp. 1–11, 2020.

[14] S. Li and T. A. Haskew, "Transient and steady-state simulation study of decoupled dq vector control in pwm converter of variable speed wind turbines," in *IECON 2007-33rd Annual Conference of the IEEE Industrial Electronics Society*. IEEE, 2007, pp. 2079–2086.

[15] Z. Chen, J. M. Guerrero, and F. Blaabjerg, "A review of the state of the art of power electronics for wind turbines," *IEEE Transactions on power electronics*, vol. 24, no. 8, pp. 1859–1875, 2009.

[16] F. Blaabjerg, M. Liserre, and K. Ma, "Power electronics converters for wind turbine systems," *IEEE Transactions on industry applications*, vol. 48, no. 2, pp. 708–719, 2011.

[17] S. Fan, J. Yang, W. Ma, G. Liu, Z. Yang, and B. W. Williams, "A coordinated control scheme for power demand changes in a pmsg based multi-terminal dc wind farm," in *IECON 2013-39th Annual Conference of the IEEE Industrial Electronics Society*. IEEE, 2013, pp. 5224–5229.

[18] T. Ackermann, *Wind power in power systems*. John Wiley & Sons, 2012.

[19] M. Paolone, T. Gaunt, X. Guillaud, M. Liserre, S. Meliopoulos, A. Monti, T. Van Cutsem, V. Vittal, and C. Vournas, "Fundamentals of power systems modelling in the presence of converter-interfaced generation," *Electric Power Systems Research*, vol. 189, p. 106811, 2020.

[20] A. Murdoch, J. R. Winkelman, S. H. Javid, and R. S. Barton, "Control design and performance analysis of a 6 mw wind turbine-generator," *IEEE Transactions on Power Apparatus and Systems*, vol. PAS-102, no. 5, pp. 1340–1347, 1983.

[21] "Wind turbine equations," *PSCAD Help Document*.

[22] F. Blaabjerg, *Control of Power Electronic Converters and Systems: Volume 2*. Academic Press, 2018, vol. 2.

[23] J. Espinoza, G. Joos, and P. Ziogas, "Voltage controlled current source inverters," in *Proceedings of the 1992 International Conference on Industrial Electronics, Control, Instrumentation, and Automation*. IEEE, 1992, pp. 512–517.

[24] H. Chen, "Research on the control strategy of vsc based hvdc system supplying passive network," in *2009 IEEE Power & Energy Society General Meeting*. IEEE, 2009, pp. 1–4.

[25] Z. J. Zhou, *Co-ordination of converter controls and an analysis of converter operating limits in VSC-HVdc grids.* University of Manitoba (Canada), 2013.

[26] L. N. Raghuram and H. J. Suresh, "A critical study of modulation techniques for three level diode clamped voltage source inverter for grid connection of wecs," in *2011 1st International Conference on Electrical Energy Systems.* IEEE, 2011, pp. 221–226.

[27] S. Mukherjee and D. Kastha, "Transient performance of a double output induction generator driven by a pitch controlled horizontal axis wind turbine," in *2006 IEEE International Conference on Industrial Technology.* IEEE, 2006, pp. 927–932.

[28] F. Blaabjerg, *Grid Integration of Wind Generation.* CIGRE, 2011, vol. WG C6.08.

[29] D. Ramasubramanian, "Differentiating between plant level and inverter level voltage control to bring about operation of 100% inverter based resource grids," *Electric Power Systems Research*, vol. 205, p. 107739, 2022.

[30] J. Kauferle, "Using dc links to enhance ac system performance," *IEEE spectrum*, vol. 9, no. 6, pp. 31–37, 1972.

[31] G. Zhang and H. Wang, "A study based on dc chopper excitation system," in *International Conference on Computational Problem-Solving.* IEEE, 2010, pp. 402–405.

[32] J. S. Thongam, M. Tarbouchi, R. Beguenane, A. F. Okou, A. Merabet, and P. Bouchard, "An optimum speed mppt controller for variable speed pmsg wind energy conversion systems," in *IECON 2012-38th annual conference on IEEE industrial electronics society.* IEEE, 2012, pp. 4293–4297.

[33] J. S. Thongam and M. Ouhrouche, "Mppt control methods in wind energy conversion systems," *Fundamental and advanced topics in wind power*, vol. 15, pp. 339–360, 2011.

[34] E. H. Dursun and A. A. Kulaksiz, "Maximum power extraction from pmsg based vs-wecs by using variable step-size p&o method," in *2019 3rd International Symposium on Multidisciplinary Studies and Innovative Technologies (ISMSIT).* IEEE, 2019, pp. 1–5.

[35] A. Carlsson, "The back-to-back converter," *Lund: Department of Industrial Electrical Engineering and Automation Lund Institute of Technology*, vol. 7, pp. 1002–1016, 1998.

[36] F. Hassanzadeh, H. Sangrody, A. Hajizadeh, and S. Akhlaghi, "Back-to-back converter control of grid-connected wind turbine to mitigate voltage drop caused by faults," in *2017 North American Power Symposium (NAPS).* IEEE, 2017, pp. 1–6.

[37] A. Gole, "Validation and analysis of a grid control system using dqz transformation for static compensator systems," in *Proc. Can. Conf. Elect. Comput. Eng., Montreal, QC, Canada, 1989*, 1989, pp. 745–748.

[38] C. Schauder and H. Mehta, "Vector analysis and control of advanced static var compensators," in *IEE Proceedings C (Generation, Transmission and Distribution)*, vol. 140, no. 4. IET, 1993, pp. 299–306.

[39] S. Mukherjee and D. Kastha, "Transient performance of a double output induction generator driven by a pitch controlled horizontal axis wind turbine," in *2006 IEEE International Conference on Industrial Technology*. IEEE, 2006, pp. 927–932.

[40] S. B. Crary, "Two-reaction theory of synchronous machines," *Transactions of the American Institute of Electrical Engineers*, vol. 56, no. 1, pp. 27–36, 1937.

[41] M. Babu Narayanan, "Adaptive phase locked loops for vsc connected to weak ac systems," Master's thesis, 2015.

[42] "Grid integration of wind generation," in *WG C6.08*. CIGRE, 2011.

[43] M.-Y. Kim and D.-S. Rho, "Analysis of grid code requirements for wind power dynamic model," *International Journal of Control and Automation*, vol. 9, no. 5, pp. 45–54, 2016.

[44] V. Krishnan and J. D. McCalley, "Role of induction motors in voltage instability and coordinated reactive power planning," in *Induction Motors*, P. R. E. Araújo, Ed. Rijeka: IntechOpen, 2012, ch. 6.

[45] "Connection of wind farms to weak ac networks," in *WG B4.62*. CIGRE, 2016.

[46] Y. Zhang, S.-H. F. Huang, J. Schmall, J. Conto, J. Billo, and E. Rehman, "Evaluating system strength for large-scale wind plant integration," in *2014 IEEE PES General Meeting— Conference & Exposition*. IEEE, 2014, pp. 1–5.

[47] P. Kundur, "Power system analysis and control," McGraw-Hill Book Company, New York, 1994.

[48] N. I.-B. R. P. Task *et al.*, "Fast frequency response concepts and bulk power system reliability needs," *NERC*, p. 1, 2020.

[49] J. Zhu, Z. Deng, L. Yu, S. Li, C. Qu, W. Qiu, G. P. Adam, and C. Booth, "A dc chopper-based fast active power output reduction scheme for dfig wind turbine generators," *IET Renewable Power Generation*, vol. 15, no. 11, pp. 2480–2490, 2021.